EVALUATION OF GEOSTATISTICS AND WAVELETS FOR IDENTIFYING RELATIONS BETWEEN IMAGERY AND DIFFERENT SPATIAL RESOLUTIONS AND FOR DATA COMPRESSION

Final Report (RSSUSA - **4/3)**

Dr Margaret A. Oliver

July 1998 to September 1999

United States Army

ENVIRONMENTAL RESEARCH OFFICE OF THE U.S. ARMY

London, England

CONTRACT NUMBER - N68171 - 98 - M -5311

Contractor - Approved for Public Release; distribution unlimited

EVALUATION OF GEOSTATISTICS AND WAVELETS FOR IDENTIFYING RELATIONS BETWEEN IMAGERY AND DIFFERENT SPATIAL RESOLUTIONS AND FOR DATA COMPRESSION

Final Report (RSSUSA -   4/3)

Dr Margaret A. Oliver

July 1998 to September 1999

United States Army

ENVIRONMENTAL RESEARCH OFFICE OF THE U.S. ARMY

London, England

CONTRACT NUMBER - N68171 - 98 - M -5311

20000118 123

REPORT DOCUMENTATION PAGE

Form Approved
OMB No. 0704-0188

Public reporting burden for this collection of information is estimated to average 1 hour per response, including the time for reviewing instructions, searching existing data sources, gathering and maintaining the data needed, and completing and reviewing the collection of information. Send comments regarding this burden estimate or any other aspect of this collection of information, including suggestions for reducing this burden, to Washington Headquarters Services, Directorate for Information Operations and Reports, 1215 Jefferson Davis Highway, Suite 1204, Arlington, VA 22202-4302, and to the Office of Management and Budget, Paperwork Reduction Project (0704-0188), Washington, DC 20503.

1. AGENCY USE ONLY (Leave blank)	2. REPORT DATE	3. REPORT TYPE AND DATES COVERED
	01.08.99	Final July 1998-September 1999

4. TITLE AND SUBTITLE

Evaluation of geostatistics and wavelets for identifying relations between imagery and different spatial resolutions and for data compression

5. FUNDING NUMBERS

N68171
98-M-5311

6. AUTHOR(S)

Dr Margaret A. Oliver

7. PERFORMING ORGANIZATION NAME(S) AND ADDRESS(ES)

University of Reading, Whiteknights,
Reading, RG6 6DW, UK.

8. PERFORMING ORGANIZATION REPORT NUMBER

RSSUSA - 4/3

9. SPONSORING/MONITORING AGENCY NAME(S) AND ADDRESS(ES)

USARDSG-UK,Environmental Sciences Branch
Edison House, 233 Old Marylebone Road
London, NW1 5TH, UK.

10. SPONSORING/MONITORING AGENCY REPORT NUMBER

11. SUPPLEMENTARY NOTES

Final Report: Evaluation of geostatistics and wavelets for identifying relations between imagery and different spatial resolutions and for data compression.

12a. DISTRIBUTION/AVAILABILITY STATEMENT

No limitation on distribution/availability

12b. DISTRIBUTION CODE

13. ABSTRACT (Maximum 200 words)

This is the final report of the project to apply geostatistics and wavelet analysis to part of the area chosen at Fort A.P.Hill in northeastern Virginia. This report embraces several facets of the collaborative work starting with a summary of time spent at the US Topographic Engineering Center and of time spent by TEC personnel at the University of Reading. An analysis of cokriging of Korean temperature data with elevation has been done to assess whether the accuracy of estimates could be improved. The improvement was small compared with the temperature-estimates for the USA done previously. A comparison between geostatistics and wavelet analysis has been undertaken. It seems that wavelets provide a more accurate method for data reconstruction, but geostatistics is more appropriate for exploring different resolutions of spatial variation that have been identified by the variogram. A detailed analysis of ground cover at A.P.Hill has been done for three surveys (one was done in a previous report). The results show a relation between the scales of variation in certain ground cover attributes and the SPOT data. Cross variograms suggest that there are spatial relations among variables and the image data. The analysis of elevation data shows that the patterns in its variation correspond closely with those for the NIR waveband. Visually the relation is very strong, but statistically it is weaker.

14. SUBJECT TERMS

Keywords: cokriging,spatial resolution,wavelets,variogram, ground surveys,elevation

15. NUMBER OF PAGES

16. PRICE CODE

17. SECURITY CLASSIFICATION OF REPORT	18. SECURITY CLASSIFICATION OF THIS PAGE	19. SECURITY CLASSIFICATION OF ABSTRACT	20. LIMITATION OF ABSTRACT

NSN 7540-01-280-5500

Standard Form 298 (Rev. 2-89)
Prescribed by ANSI Std. Z39-18
298-102

TABLE OF CONTENTS

Contents **Page Number**

LIST OF TABLES

LIST OF FIGURES

Figure   **Page Number**

LIST OF FIGURES (continued)

LIST OF FIGURES (continued)

LIST OF FIGURES (continued)

LIST OF FIGURES (continued)

PREFACE

EXECUTIVE SUMMARY

This report contains most of the two earlier interim reports, together with the most recent results. In addition, there are three Appendices: a published paper, an abstract for the Geostatistics Congress in 2000, and some new computer programs that have been written for this project. The results of applying them will be provided in a possible new program of work. A cokriging analysis of Korean temperature data with elevation has been done to assess whether the accuracy of estimates of temperature could be improved using the elevation. The improvement was small compared with the temperature estimates for the USA done previously. The relation between temperature and elevation was strong after both variables had been detrended. The maps show slight differences as do the validation results.

A major aim of this project has been to examine the relation between geostatistics and wavelet analysis for exploring spatial variation in imagery at different spatial scales and data reconstruction. It seems that overall the wavelet analysis provides a more accurate method for data reconstruction. However, it is not straightforward because the reliability of the restored values when compared with the original data varies over the region. Kriging performs less well where there are marked changes in the reflectance values and they appear to be non-stationary. Kriging analysis, however, seems to be more appropriate for exploring different resolutions of spatial variation that have been identified by the variogram. The variogram could be used to make the wavelet analysis · for different resolutions more efficient because the relevant scales could be targeted at the outset. The results show that similar patterns of variation were retrieved by both analyses for the long range/low frequency component.

A detailed analysis of ground cover at A. P. Hill has been done on the information from three surveys (another survey was described in a previous report). The results show a relation between the scales of variation in certain ground cover attributes and the SPOT data: in particular grass, mixed woodland, forest and wetland. The multivariate variograms of the quantitative data and the categorical data confirm a relation between NIR and ground cover in terms of the spatial scales identified. Cross variograms between the ground cover types and also between each type and each waveband suggest that there are spatial relations among variables and the image data.

The analysis of the elevation data shows that the patterns in its variation correspond closely with those for the NIR waveband. These results confirm our earlier interpretation, in the previous project, that the observed changes in the long-scale component of the variation coincides with changes in the physiography. The raw data and detrended data were analysed, but there was little difference between the results. Visually the relation between elevation and NIR is very strong, but it is more difficult to show this statistically.

PART I: REPORT ON TIME SPENT WITH TEC PERSONNEL

This report embraces several different components and includes the material in the previous interim reports. It begins with a brief summary of the work that was done by Dr Oliver at TEC in February 1998 which was part of this contract (albeit slightly premature) and July 1999, and the work done while E. Bosch and E. Shine were working with Dr Oliver at Reading in September 1998 and May 1999, respectively. Part II of the report is a small piece of work for Dr Krause on cokriging, Part III focuses on a comparison between wavelet analysis and geostatistics, Part IV on the vegetation surveys and analysis of the digital elevation model for A. P. Hill. There are three appendices to the report. The first is a copy of the paper presented by Dr Oliver at the Geoenv'98 conference in Valencia last year, and which has subsequently been published (Oliver *et al.*, 1999). The second is the abstract submitted to the Geostatistics Congress, and the third a set of computer programs written by Professor Richard Webster to compute moving variograms, and moving averages and variances. These will be tested in the next phase of the work.

The work for the majority of this project has been based at Fort A. P. Hill in northeastern Virginia, about 75 miles from Washington, DC. The area is intensely dissected by many small waterways, and this appears to have contributed to the pattern of variation observed in the image.

Report of visit to TEC in February 1998

Much of the first day at TEC was spent discussing the results of the first analyses from Fort A. P. Hill, and what other work should be done. In addition the paper that has now been accepted by the International Journal of Remote Sensing was also discussed and suggestions for improvement considered and incorporated. Since Dr Oliver was to brief the senior management team at TEC including Dr Roper the contents of the briefing were also ratified at the outset. A further paper on this subject was considered for presentation at the Geoenv'98 conference in Valencia (Oliver *et al.* 1999) and this has now been published. (Appendix 1).

The main aim of this visit was to work with Jim Shine to enable him to make full use of Genstat. A set of programs was prepared to cover exploratory data analysis (histograms, box plots, summary statistics, trend detection and so on), variogram analysis and modelling and kriging. All of the programs were examined. They were eventually compiled as part of the aide memoire that formed an Appendix of the final report for the previous contract (Contract N68171-97-C-9029).

Jim Shine and Dr Oliver worked though all of the programs. A problem was identified with the kriging algorithm in Genstat which was eventually reported to the NAG library and corrected. TEC then received a new implementation of the package. At least half of the time at TEC was spent instructing Jim in the use of the programs and interpreting the results. In addition we had several discussions on geostatistics.

Half a day was spent on the briefing to Dr Roper and senior staff at TEC, and in answering questions arising from this. During the course of our collaboration we have covered a substantial amount of work and much of it was described briefly at this meeting. Dr Roper

showed considerable interest in what has been done and when he visited the University of Reading in November 1998 it was clear that he had a sound appreciation of the value of geostatistical analysis. The discussion that followed the briefing was stimulating and well considered.

Other discussions were held with Edward Bosch about comparing wavelets and geostatistics. This culminated with an arrangement for him to visit Reading in September 1998.

Visit by E. Bosch to University of Reading September 1998

Dr Oliver and E. Bosch worked together for a week. The time was used for analyses, interpreting results and discussion. Several analyses were undertaken - some of which feature in the report. Others have been done by both of us subsequently. The visit was very profitable to both of us. As a result of this investigation we have submitted an abstract to the Geostatistics Congress to be held in April 2000, and this has now been accepted for presentation and publication. The appendix is appended at the end of the report. The paper will acknowledge the support of US Army and of TEC in this work, and will be authored jointly by M. A. Oliver, E. Bosch and K. Slocum.

Visit by James Shine to University of Reading May 1999

Dr Oliver and Mr Shine worked together for a week in May 1999 when Mr Shine visited the University of Reading. This time was used for analyses, a draft outline of a proposed paper and discussion. Mr Shine wished to go over the analysis for computing the variogram from large sets of data. We experimented with some of the 1-m data for A. P. Hill using the program *ggrid3.f*, written for the project by Professor R. Webster. Mr Shine wanted to develop his experience in this so that he can compute variograms from large data sets within a short time. He left reading feeling confident about this. In addition we also fitted models to the variograms with Genstat and again this reinforced what we did together at TEC last year.

A considerable part of the week was spent discussing the results from the final report of contract No. N68171-97-C-9029 which we now wish to publish. We examined previous issues of the *International Journal of Remote Sensing* to see whether this was suitable for this work. We decided that it was, but that as the content will be small compared with the previous paper we shall submit it as a *Letter*. This is confusing because this form of publication is a short paper in essence and will suit our needs perfectly in this instance. An outline of the paper has been prepared and the introduction written. We shall continue with this when Dr Oliver visits TEC in July.

The remaining time was spent discussing the recent work on the ground survey data. Part of this work is included in this report. However, there is still some way to go on this. We also discussed future work. One idea is to compute a moving variogram to deal with the problems of local trends or non-stationarity in the data. This arises at A. P. Hill for

example where there are water bodies and areas of hard standing and buildings. The computer code for this will be written as part of the current contract, but any testing of it will have to be done in the future.

Report of visit to TEC in July 1999

Dr Oliver visited TEC in July 1999 for three days. On arriving she gave a short briefing to Mr W. Clarke (head of section) on the status of our current research, how this builds on work done in the past and where any future research is likely to develop. On the second day Dr Oliver had a meeting with Dr Roper together with Mr Shine. This was to discuss present work and also spatial investigations more generally. Dr Roper invited Dr Oliver to give a general briefing to TEC next year on the research to date.

Part of each day was spent with Mr E. Bosch. We have been exploring a one-dimensional set of radon values in soil where we know there are distinct boundaries. The aim is to see how wavelet analysis deals with this variation and also that of the residuals from the geological classes. We explored different levels of resolution for the raw data. This work is still to be completed.

The work with Mr Shine began by extracting part of the data from the SPOT image and the digital elevation model (DEM). We plan to explore the relations in this smaller file in more detail because statistically the relation between the wavebands and the DEM was weak, yet it was fairly strong for the NIR band visually. The weak relation might arise from the areas of hard standing and buildings which have no particular relation with the elevation. The program *ggrid.f* would not work with these small files - Mr Shine has since discovered that the zero origin has caused part of the problem.

We continued the discussion about the Letter for IJRS and have decided to use NDVI of subsets from the whole site covered by the 1 m data. The additional work to prepare the new variograms for this has now been completed.

Part II

Cokriging temperature data in Korea

The data for the analysis were provided by Dr P. Krause. They comprised temperature and elevation records at 100 sites irregularly scattered over Korea. In addition elevation had been measured at another 565 sites. Table 1 gives the summary statistics for these variables at places where they were both measured. Both have distributions that depart from normality, in particular. Although a geostatistical analysis does not assume that the data are normally distributed it is generally advisable to transform the data to a near-normal distribution for the variogram analysis to stabilize the variances.

Both variables were transformed to common logarithms and for elevation the skewness decreased markedly and the transformed data are close to normal. Temperature departs less so from a normal distribution, but after transformation to common logarithms the departure from normality increases.

Table 1: Summary statistics for Elevation and Temperature

	Elevation	Temperature	Log Elevation	Log Temperature
Number of observations	100	100	100	100
Mean	403.45	53.02	5.17	3.97
Minimum	8.00	33.00	2.08	3.50
Maximum	4546.00	62.00	8.42	4.13
Variance	574928.23	24.95	1.53	0.011
Standard deviation	758.24	4.99	1.24	0.103
Skewness	3.836	-1.45	0.21	-1.93

The data were also examined for trend as part of the exploratory data analysis. This would generally be normal practice when one of the variables is elevation because it can vary in a predictable way. However, in this case it was temperature not elevation whose variation comprised a large element of trend. For elevation linear trend counted for 13.8% of the variation, and quadratic trend for 21.0%. This is much less than expected. It is marginal as to whether this degree of trend should be removed, but it was to ensure that the analysis was reliable. For temperature the trend was much greater: a linear trend accounted for 74.9% of the variation and the quadratic one 77.9%. Clearly a linear trend model is adequate for describing the trend for temperature.

The aim of this analysis was to assess whether temperature could be estimated more reliably with the use of additional information from elevation. In geostatistics the method used is known as cokriging. The value of the method is that it can be used to estimate a property that is more expensive to measure using information from another variable with which it is coregionalized and that is cheaper to measure or that does not change with time. This is particularly true in general for temperature and elevation. There is a physical reason for their relation and elevation does not change substantially in the short term. Therefore, once a digital elevation model has been produced it is a source of inexpensive and reliable

information. Cokriging depends on the two (or more) variables being strongly correlated. From the correlation matrix below it is clear that the correlation between elevation and temperature is moderate.

Table 2: Correlation matrix for temperature and elevation in Korea.

*** Correlation matrix ***

Elevation   1   1.000
Temperature   2   -0.741 1.000

                   1   2

This level of correlation would suggest that it is worthwhile pursuing a coregionalization analysis. The classical correlation coefficient does not take spatial location into account, therefore the relation spatially could be either better or worse.

Cokriging: Theory

The cross variogram

This is the logical extension of ordinary kriging to situations where two or more variables are spatially interdependent or co-regionalized. The first stage is to model the coregionalization. The two regionalized variables, $Z_u(\mathbf{x})$ and $Z_v(\mathbf{x})$, denoted by u and v, both have an autovariogram defined by:

$$\gamma_u(\mathbf{h}) = \frac{1}{2}E[\{Z_u(\mathbf{x}) - Z_u(\mathbf{x}+\mathbf{h})\}^2]$$

and

$$\gamma_v(\mathbf{h}) = \frac{1}{2}E[\{Z_v(\mathbf{x}) - Z_v(\mathbf{x}+\mathbf{h})\}^2],$$

and a cross variogram defined as:

$$\gamma_{uv}(\mathbf{h}) = \frac{1}{2}E[\{Z_u(\mathbf{x}) - Z_u(\mathbf{x}+\mathbf{h})\}\{Z_v(\mathbf{x}) - Z_v(\mathbf{x}+\mathbf{h})\}].$$

The cross variogram function describes the way in which u is related spatially to v. Provided that there are sites where both properties have been measured $\gamma_{uv}(\mathbf{h})$ can be estimated by:

$$\hat{\gamma}_{uv}(\mathbf{h}) = \frac{1}{2m(\mathbf{h})}\sum_{i=1}^{m(\mathbf{h})}[\{z_u(\mathbf{x}) - z_u(\mathbf{x}+\mathbf{h})\}\{z_v(\mathbf{x}) - z_v(\mathbf{x}+\mathbf{h})\}].$$

which provides the experimental cross variogram for u and v.

The cross variogram can be modelled in the same way as the autovariogram, based on the linear model of coregionalization. Each variable is assumed to be a linear sum of orthogonal random variables $Y(\mathbf{x})$:

$$Z_u(\mathbf{x}) = \sum_{k=1}^{K} \sum_{j=1}^{2} a_{uj}^k Y_j^k(\mathbf{x}) + \mu_u.$$

in which

$$\mathrm{E}[Z_u(\mathbf{x})] = \mu_u.$$

$$\frac{1}{2} \mathrm{E}[\{Y_j^k(\mathbf{x}) - Y_j^k(\mathbf{x}+\mathbf{h})\}\{Y_{j'}^{k'}(\mathbf{x}) - Y_{j'}^{k'}(\mathbf{x}+\mathbf{h})\}]$$

$$= g_k(\mathbf{h}), \quad \text{positive for } k = k' \text{ and } j = j'$$

$$= 0 \quad \text{otherwise}$$

The variogram for any pair of variables u and v is:

$$\gamma_{uv}(\mathbf{h}) = \sum_{k=1}^{K} \sum_{j=1}^{2} a_{uj}^k a_{vj}^k g_k(\mathbf{h}).$$

We can replace the products in the second summation by b_{uv}^k to obtain:

$$\gamma_{uv}(\mathbf{h}) = \sum_{k=1}^{K} b_{uv}^k g_k(\mathbf{h}).$$

The b_{uv}^k are the nugget and sill variances of the independent components if they are bounded, and for unbounded models they are the nugget variances and gradients.

Cokriging

Once to coregionalization has been modelled it can be used to predict the spatial relations between two or more variables by cokriging. There are generally two reasons for using cokriging:

1. Where one variable is under-sampled compared with another with which it is correlated. The sparsely sampled property can be estimated with greater precision by co-kriging because the spatial information from the more intensely measured one is used in the estimation. The increase in precision depends on the degree of under-sampling and the strength of the coregionalization.

2. When values of all of the variables are known at all sample points, cokriging can improve the coherence between the estimated values by taking account of the relation between them.

If there are V variables, $l = 1,2,..., V$, and the one to be predicted is u, which in our case has been less densely sampled than the others. In ordinary cokriging the estimate is the linear sum:

$$\hat{Z}_u(B) = \sum_{l=1}^{V}\sum_{i=1}^{n_l} \lambda_{il} z_l(\mathbf{x}_i),$$

where the subscript l refers to the variables, of which there are V, and the subscript i refers to the sites, of which there are n_l where the variable l has been measured. The λ_{il} are the weights, satisfying:

$$\sum_{i=1}^{n_l}\lambda_{il} = 1, \quad l=u; \quad \text{and} \quad \sum_{i=1}^{n_l}\lambda_{il} = 0, \quad l \neq u.$$

These are the non-bias conditions, and subject to them the estimation variance of $\hat{Z}_u(B)$ for a block, B, is minimized by solving equations :

$$\sum_{l=1}^{V}\sum_{i=1}^{n_l} \lambda_{il}\gamma_{vl}(\mathbf{x}_i,\mathbf{x}_j) + \psi_v = \bar{\gamma}_{uv}(\mathbf{x}_j,B) \qquad \text{for all } v=1,2 \text{ to } V \text{ and all } j=1,2 \text{ to } n_v.$$

The quantity $\gamma_{lv}(x_i, x_j)$ is the cross semivariance between variables l and v at sites i and j, separated by the vector $x_i\text{-}x_j$; $\bar{\gamma}_{uv}(\mathbf{x}_j,B)$ is the average cross semivariance between a site j and the block B, and ψ_v is the Lagrange multiplier for the vth variable. The cokriging variance is obtained from:

$$\sigma_u^2(B) = \sum_{l=1}^{V}\sum_{i=1}^{n_l} \lambda_{jl}\bar{\gamma}_{ul}(\mathbf{x}_j,B) + \psi_u - \bar{\gamma}_{uu}(B,B)$$

where $\bar{\gamma}_{uu}(B,B)$ is the integral of $\gamma_{uu}(\mathbf{h})$ over B, i.e. the within-block variance of u.

Analysis and results of cokriging

Cross variogram

The experimental autovariograms for the raw values of elevation and temperature were computed first. They showed some similarity in their shapes and also ranges of spatial dependence (Figure 1). The autovariograms were then computed on the residuals from the linear trend for temperature and on the residuals from the quadratic trend for elevation. In addition the elevation was transformed to common logarithms and the variogram was also computed from the transformed data. Considering that the level of skewness is substantial

reducing it appears to have had little effect on the variogram. In fact it is less clearly bounded and less related to the variogram of temperature than that for the raw data. The variograms computed from the residuals were more erratic and more difficult to model than those of the raw data. Since the trend appears to be regional in the case of temperature, at the longer lags, I decided to do the analysis on the raw data and the residuals. For kriging it is the first few lags that are important and these are less likely to be affected by the trend than the longer lags.

Although it is important to check the data in this way, the changes did not appear to improve the variogram substantially. This will become evident when the cokriging results are discussed. However, cokriging was carried out on the raw data and the detrended data. During the remaining time on the project I might do some further tests, but I do not expect any major changes.

The experimental auto- and cross-variograms for the raw data are given in Figure1. They have a similar form and the individual autovariograms were fitted best by an exponential model with a distance parameter of about 0.86 units. The same form of model must fit all of the variograms and the range or distance parameter must be the same. The nugget variance, the sills of bounded models and the slope of unbounded models can be different. The coregionalization was modelled by an exponential function with a distance parameter of 0.86 units of latitude and the lower triangle of the sills is given below. The coregionalization of the residuals for elevation and temperature were also modelled and the values used for kriging. The variograms for the residuals were fitted best by a spherical function with a range of 1.01 units of latitude.

Table 3: Models of coregionalization fitted to the raw data and the residuals from the trend for temperature and elevation.

Fitted sills in lower triangle for the raw data

Fitted sills in lower triangle for the residuals

Nugget Variances	0.0		Elevation	0.0		Nugget variances
	0.0	0.6	Cross Temperature	0.0	1.4	

Sill Variances	350826.2		Elevation	258385.0		Sill variances
	-1169.6	6.3	Cross Temperature	-821.4	2.6	
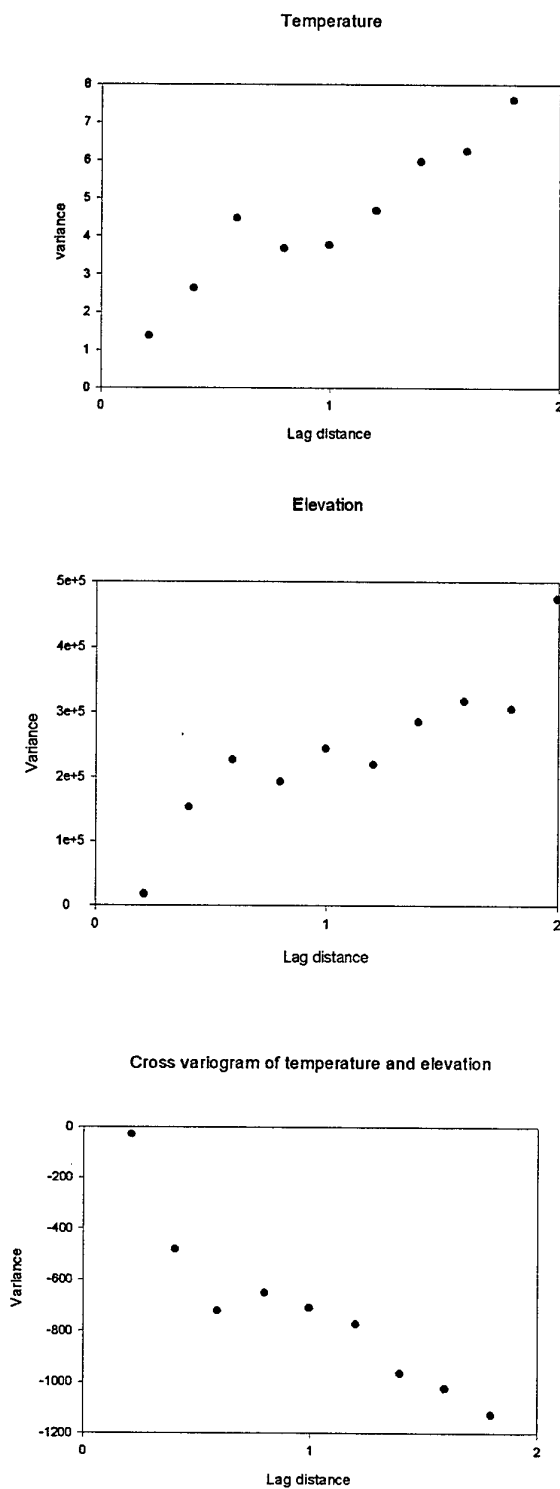
Figure 1: Experimental autovariograms of a) temperature and b) elevation, and c) the experimental cross variogram .

Figure 2 shows the experimental cross variograms, the fitted models together with the hull of perfect correlation (the two outer lines). The cross variogram of the residuals coincide with the hull showing a strong correlation. That for the raw data is close to the hull.

a)
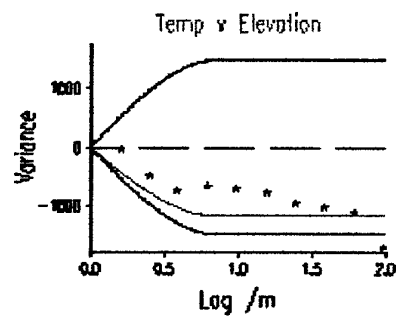
b)
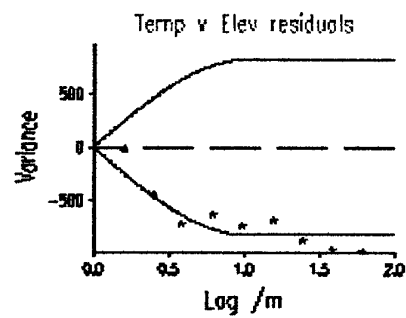
Figure 2: a) Cross variogram of the raw data and b) cross variogram of the residuals, with the hulls of perfect correlation.

Cokriging

The first analysis was to test the modelling and to assess the effects on the estimates of using either the raw data or the residuals. Twenty five of the 100 sites were removed from the raw data and the residuals. Using the models of coregionalization given above the values at the 25 validation points were estimated by punctual cokriging for the raw and residual data, respectively. In addition the raw data were used for autokriging the validation points. The original values, the estimates and the standard errors are given in Table 2.
For every validation point the cokriged estimate has a smaller standard error than the autokriged estimate. The differences are small, but they show consistently that cokriging confers a small benefit in terms of estimating temperature more reliably. In addition the estimates are consistently closer to the original values for cokriging of the raw data. For the residuals the standard errors from cokriging are smaller for 15 of the 25 validation points. This was somewhat surprising in relation to the fact that the variograms of the residuals did not appear to be an improvement over that of the raw data. For the residuals the trend was added back so that the values could be compared with the raw data. The estimates are not as consistently good as they are for cokriging with the raw data.

Table 4: Comparison between the raw temperature data, the autokriged estimates and the cokriged estimates, and the cokriged estimates for the residuals and with the trend added back.

X	Y	Original Value	Autokriging Estimate	SE	Cokriging Estimate	SE	Cokriging residuals Estimate	Est+trend	SE
-127.05	37.90	54.0	53.33	2.48	53.32	2.43	0.5392	53.48	2.40
-127.10	37.70	54.0	54.35	1.73	54.25	1.67	0.8142	53.71	1.91
-126.50	33.50	60.0	60.03	1.63	60.07	1.56	-1.3596	58.38	1.82
-128.10	35.20	57.0	57.19	2.19	57.36	2.12	-0.0677	57.96	2.16
-127.75	37.90	53.0	53.86	1.55	53.64	1.49	0.5506	53.74	1.79
-128.00	36.20	54.0	55.17	4.09	55.13	4.08	-0.4151	56.08	3.84
-126.60	37.50	54.0	53.17	2.63	53.24	2.60	0.3207	54.11	2.57
-128.90	37.10	48.0	54.50	4.52	54.47	4.51	-0.0800	55.76	4.03
-129.40	37.00	55.0	55.01	5.43	55.01	5.42	0.1675	56.91	4.31
-126.75	34.30	58.0	58.36	5.29	58.33	5.28	-0.5767	58.26	4.30
-127.65	37.45	56.0	53.82	2.99	53.75	2.97	0.2831	54.34	2.84
-125.65	39.60	50.0	49.56	4.68	49.63	4.66	0.2680	49.52	4.02
-129.01	35.10	59.0	57.95	1.96	57.87	1.93	-0.5659	58.47	2.09
-124.80	40.45	49.0	49.22	4.73	49.36	4.72	0.6924	48.36	3.86
-128.30	41.80	33.0	42.68	4.71	42.71	4.68	-2.4696	40.90	3.72
-128.60	35.90	57.0	56.81	1.71	56.80	1.63	-0.0015	57.47	1.83
-126.50	36.75	54.0	53.60	3.01	53.22	2.97	-1.7979	53.47	2.74
-127.10	37.45	54.0	54.94	1.93	54.89	1.89	1.0006	54.88	2.10
-128.20	36.40	58.0	54.79	3.35	54.76	3.33	-0.4044	55.91	3.15
-127.95	37.40	53.0	53.25	0.98	53.30	0.93	0.1380	54.47	1.53
-129.40	36.03	58.0	56.87	1.50	56.92	1.43	0.5288	58.85	1.69
-124.65	38.00	52.0	51.97	1.66	51.68	1.60	-0.4415	53.86	1.81
-126.40	34.80	58.0	57.45	5.02	57.54	5.00	-0.6245	57.73	3.94
-125.80	39.25	51.0	49.95	4.83	50.00	4.82	0.1461	50.22	4.18
-130.40	42.30	45.0	47.26	6.34	47.38	6.33	-0.3178	45.31	4.23

The entire data set was cokriged as above, but this time using all of the elevation data. The estimates and the standard errors were mapped, Figures 3 to 5. Figures 3a and 4a show the maps of temperature from autokriged and cokriged estimates, respectively. There is remarkably little difference between them. Figure 5a shows the results of cokriging using the residuals and then adding the trend back. This is more different. This appears to show some distortion, however, it is difficult to be certain because we did not have the outline of Korea to superimpose on the estimates. This will be done at TEC. Figures 3b, 4b and 6b show the standard errors for temperature. They are slightly less for cokriging. These values show the pattern of sampling and also the coastline of the country.

Ordinary kriged estimates of temperature for Korea
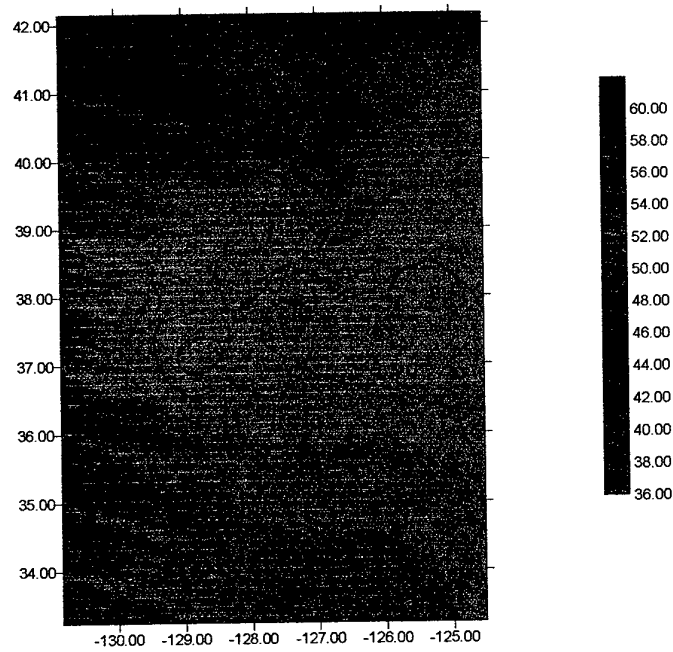
Standard errors from ordinary kriging of temperature for Korea
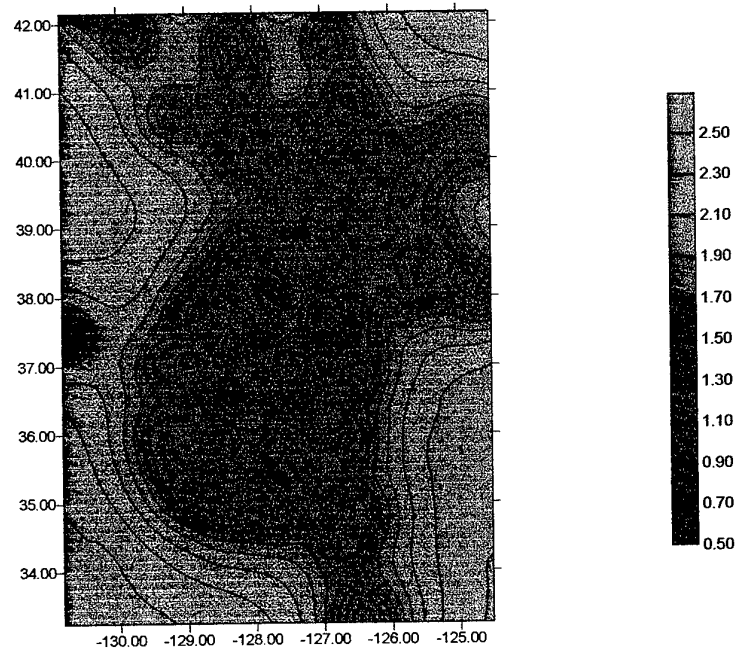
Figure 3: a) Map of estimates from autokriging of temperature for Korea,
b) map of the standard errors from autokriging of temperature

Cokriged estimates of temperature for Korea
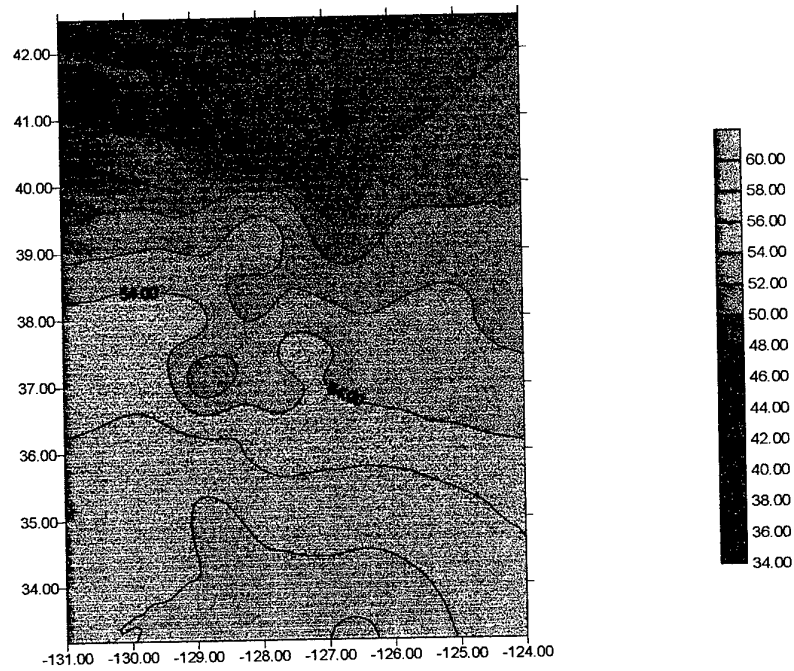
Standard errors from cokriging temperature for Korea
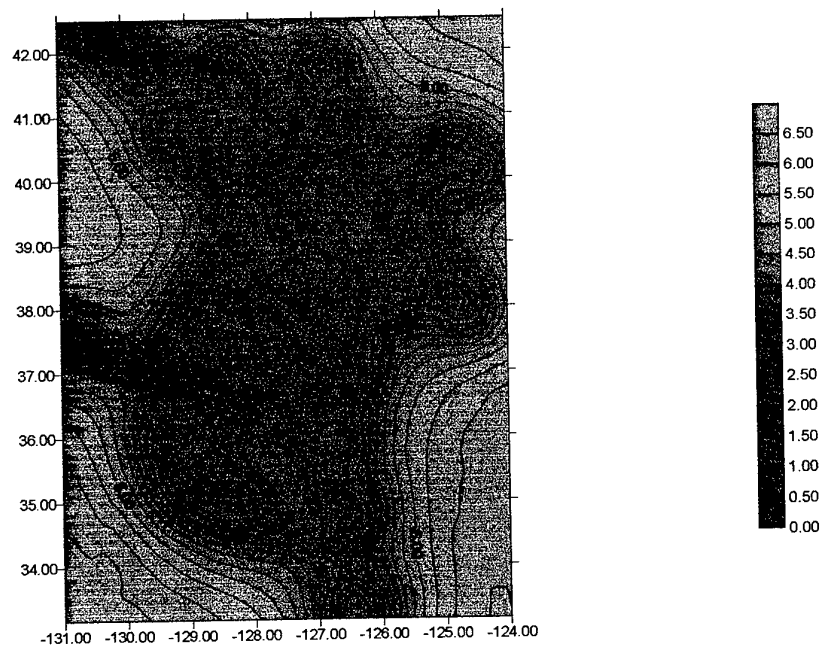
Figure 4: a) Map of cokriged estimates of temperature for Korea,
          b) map of the standard errors from cokriging of temperature.

Cokriged estimates of residuals of temperature with trend added back for Korea
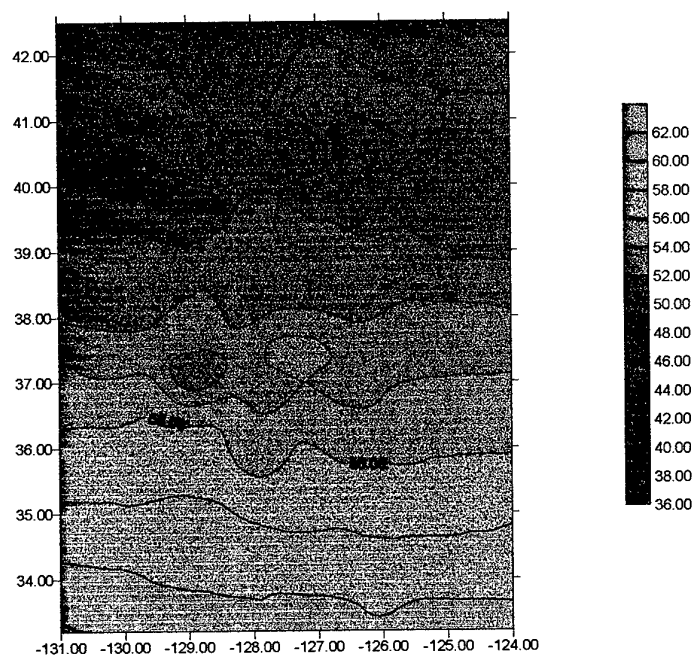
Standard errors of residuals from cokriging temperature for Korea
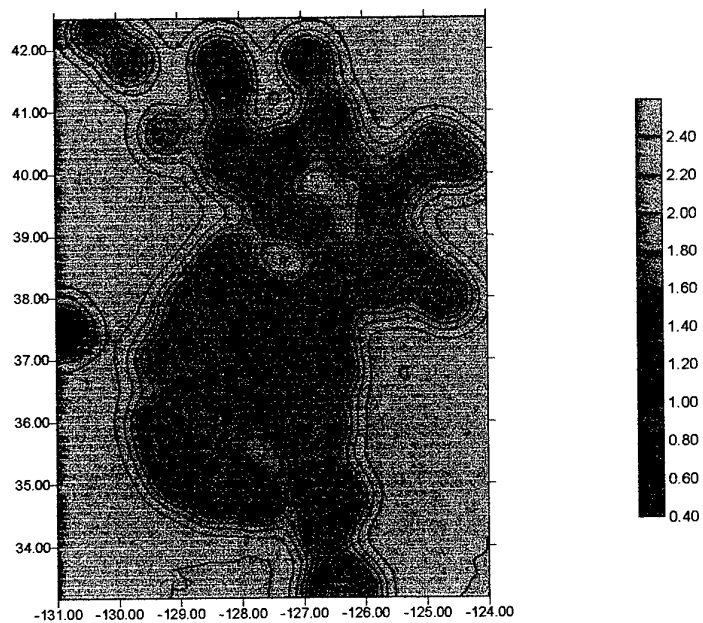
Figure 5: a) Map of the cokriged estimates of the residuals for temperature with trend added back for Korea, b) map of the standard errors from cokriging the residuals of temperature.

PART III: Comparing wavelets and kriging for exploring nested scales of variation

M. A. Oliver and E. Bosch

This work has continued to use part of the SPOT image around Anderson Camp. However, it is slightly different in extent from that used previously to accommodate the wavelet analysis. To apply the discrete wavelet transform we need the rows and columns of the area to be analysed to be some power of 2; the area chosen was $2^7 \times 2^7 = 128 \times 128$. As a result the variogram analysis and factorial kriging had to be redone so that the results relate to this new region and are comparable with the subsequent wavelet analyses. The theory of factorial kriging was given in the final report for Project 3 (Contract number N68171-97-C-9029). As an addendum to this report the paper presented at the geoENV98 conference is appended and this includes the theory of factorial kriging. The application and theory of wavelets is only summarised briefly here.

Summary of wavelet analysis

Wavelets have some similarities with the windowed Fourier functions. Both of them have their energy well localized in time. This means that these functions decay rapidly in time or space, i.e. they go to zero fast, throughout the whole real/complex line. However, they can also have compact support, they are non-zero in a finite interval. In addition, the respective Fourier transforms of these functions have their energy concentrated about a small set of frequencies. An advantage of the wavelet transform over the windowed Fourier transform is that low frequency and high frequency resolutions can be characterized simultaneously. This means that wavelet analysis is suitable for situations where there are different levels of resolution of variation superimposed on each other (Daubechies, 1992). Wavelets are also good for describing transient data, whereas the Fourier transform is not. Wavelet analysis is not affected by local non-stationarity and this is an advantage it has compared with geostatistics, which assumes that the data are at least quasi-stationary (i.e. locally stationary). Local non-stationarity can arise where there are marked boundaries that result in a marked change in the local means of the variable of interest (see Part V of this report).

Wavelets are oscillatory components that operate locally. The wavelet analysis starts with the choice of a mother wavelet, $w(t)$, which is fixed. The mother wavelet can be dilated or shrunk to examine components in the variation that occur at different spatial or temporal scales. This enables multi-resolution analysis where different levels of variation are superimposed on one another (Mallat, 1998). This is our first aim in this investigation. The second relates to redundancy, which is a major problem with image data because of the amount of information involved. Wavelets are also of great value for data compression because they are able to remove redundant information and to retain the important structure of the data.

Theory

Wavelet analysis allows a signal (information) to be represented in terms of a set of basis functions, i.e. basis vectors or kernels. The basis functions are a set of linearly

independent functions that can be used to produce all admissible functions of $f(t)$ (Strang and Nguyen, 1996). Choosing the basis functions determines the kind of information that can be extracted. Thus, a function $f(t)$ can be expressed as

$$f(t) = \sum_s \sum_u b_{su} w_{su}(t) \qquad (1)$$

where b_{su} is the wavelet coefficient and $w_{su}(t)$ is the wavelet at scale s, translated by u. A special feature of the wavelet basis is that its elements $w_{su}(t)$ are constructed by scaling and translating a single mother wavelet $w(t)$:

$$w_{su}(t) = w(t/2^s - u)/2^{s/2} \qquad (2)$$

Using Fourier techniques, Mallat (1998) shows how to construct a wavelet function $w(t)$. The wavelet function $w(t)$ is constructed from a scaling function $\phi(t)$ which can be specified by a discrete filter $l[n]$. This means that you can obtain the discrete filter $l[n]$ from the scaling function $\phi(t)$ or you can obtain the continuous function $\phi(t)$ from the discrete filter $l[n]$. The proofs are not trivial but he provides a thorough explanation. Associated with the wavelet function $w(t)$ is a discrete filter $h[n]$. The filter $l[n]$, associated with the scaling function $\phi(t)$, is a low pass frequency filter while the filter $h[n]$, associated with the wavelet $w(t)$, is a high pass frequency filter. The low pass filter smoothes the signal while the high pass filter retains the detail in the signal. This is no coincidence since these are the properties that are sought in the construction of such filters and functions. Furthermore, it is these filters, and not the continuous functions themselves, which are used to compute the Discrete Wavelet Transform. That is, the results obtained by convolving a signal with these filters are the same as those obtained by convolving the signal with the continuous functions. This is a remarkable feature since the filters consist of a smaller number of elements, thus reducing the amount of computation.

As was mentioned above, some wavelets have compact support. Mallat (1998) shows that the scaling function $\phi(t)$ has compact support if and only if the discrete filter $l[n]$ has compact support. Furthermore, their support is equal. Also, if the support of $\phi(t)$ and $l[n]$ is $[N_1,N_2]$, then the support of the wavelet function $w(t)$ is $[(N_1-N_2+1)/2,(N_2-N_1+1)/2]$.

Wavelets can be orthogonal which implies that

$$\int_{-\infty}^{\infty} w_{su}(t) w_{SU}(t) dt = 0 \qquad (3)$$

This means that the above integral will be zero when $s \neq S$ or $u \neq U$. That is, (3) will be zero at different scales s or translates u of $w(t)$. Also, when $s = S$ and $u = U$, then (3) is equal to 1. This leads to a simple formula for each coefficient b_{SU} in the expansion of $f(t)$. The expansion in equation (1) is multiplied by w_{JK} and integrated by:

$$\int_{-\infty}^{\infty} f(t) w_{SU}(t) dt = b_{SU} \int_{-\infty}^{\infty} (w_{SU}(t))^2 dt. \qquad (4)$$

All other terms disappear because of the orthogonality. Mallat (1998) shows how the components b_{su} are computed with the discrete filters $l[n]$ and $h[n]$.

A wavelet needs to satisfy the following condition

$$\int_{-\infty}^{+\infty} w(t)dt = 0 \qquad (5)$$

for perfect reconstruction. That is, equation (5) needs to be satisfied to be able to reconstruct exactly $f(t)$ from the Forward Wavelet Transform.

Multiresolution

The dilation of the mother wavelet $w(t)$ allows us to analyse the signal at different levels of resolution. Again, instead of using the scaling function and the wavelet function to compute the discrete wavelet transform of a discrete signal $f(n)$, we use the two filters described above, low pass l[n] and high pass h[n] . We assume that the number of samples of the signal $f(n)$ is a power of two. To obtain the first level of the multiresolution decomposition of the signal $f(n)$ we do as follows:

We apply the high frequency filter h[n] to the signal $f(n)$. This portion of the transform contains the fine detail structure of the signal. That is, h[n] filters out the smooth segments of the signal and retains the sharp transitions or discontinuities of the signal. The dilations and translations of the continuous wavelet transform, are reflected in the discrete filters l[n] and h[n] as decimation and translation, respectively. Thus, each filter produces half the number of sample points as those of $f(n)$. Since we are dealing with a finite number of sampling points, we can express the application of the filter h[n] to the signal f_0 $\equiv f(n)$ in terms of matrix and vector notation $fh_1 \equiv H_1 f_0$, where H_1 is a matrix whose rows comprise the elements of the filter h[n] and f_0 is the vector containing the elements of $f(n)$. When this has been done, we then apply the low frequency filter l[n] to the signal $f(n)$, whose purpose is to smooth the signal. When the filter is applied to the signal, the sample size is reduced to half the number of sampling points in $f(n)$. Similarly, we can express the application of the filter l[n] to the signal $f(n)$ in terms of matrix and vector notation $fl_1 \equiv L_1 f_0$, where L_1 is a matrix whose rows comprise the elements of the filter l[n] and f_0 is the vector containing the elements of $f(n)$. Note that with this notation, H refers to high frequency and L refers to low frequency. These two sets of high fh_1 and low fl_1 frequency components comprise the first level of the multiresolution decomposition of the signal $f(n)$. Since these filters (wavelets) are orthogonal, we can obtain $f(n)$ from fh_1 and from fl_1 by the following:

$$f_0 \equiv f = H_1'(fh_1) + L_1'(fl_1) = H_1'(H_1 f) + L_1'(L_1 f), \qquad (6)$$

where H_1' and L_1' are the transpose matrices of H_1 and L_1 respectively. This means that

$$H_1'(H_1 f) + L_1'(L_1 f) = (H_1'H_1)f + (L_1'L_1)f = (H_1'H_1 + L_1'L_1)f$$
$$= I_0 f = f, \qquad (7)$$

where I_0 is the identity matrix of order corresponding to the size of the original signal $f(n)$.

To obtain the second level of the multiresolution decomposition of the signal $f(n)$ we do as follows:

The same two filters $h[n]$ and $l[n]$ are now applied to the reduced resolution signal fl_1. We leave the first high frequency resolution level components fh_1 untouched. Recall that the sample size of fl_1 is half that of f_0. In matrix notation, when applying the filter $h[n]$ to fl_1, we have the high frequency component of fl_1 in $fh_2 \equiv H_2 fl_1$ and the low frequency component of fl_1 in $fl_2 \equiv L_2 fl_1$. Again, since the filters are orthogonal, we can obtain fl_1 from fh_2 and from fl_2 by the following:

$$fl_1 = H_2'(fh_2) + L_2'(fl_2) = H_2'(H_2 fl_1) + L_2'(L_2 fl_1), \qquad (8)$$

which means that

$$I_1 = H_2'H_2 + L_2'L_2. \qquad (9)$$

To compute the subsequent multiresolution levels, we proceed in this fashion by applying the low and high frequency filters to the previous set of low frequency components. Since $f(n)$ has a finite sample size, we can only perform this decomposition a finite number of times. Suppose the signal $f(n)$ has $2^4 = 16$ sampling points. Then this decomposition has 4 steps. The resolution levels can be labelled as follows:

$$[(fl_4), (fh_4), (fh_3), (fh_2), (fh_1)], \qquad (10)$$

where (fh_1) has 8 sample points, (fh_2) has 4, (fh_3) has 2 and both (fh_4) and (fl_4) have 1 sampling point each. Each $H_{j+1} fl_j$ contains high frequency information of $f(n)$ but at a reduced resolution (grosser scale). This analysis allows us to examine features locally and at different scales. Note that we can reconstruct perfectly $f(n)$ from $[(fl_4), (fh_4), (fh_3), (fh_2), (fh_1)]$ since $h[n]$ and $l[n]$ are orthogonal filters.

At a given resolution, the scaling functions $\phi(t/2^s - u)$ form a basis for the set of admissible signals. The level is set by s, and the steps at the level are 2^s. The detail at the level s is represented by the wavelets $w(t/2^s - u)$. Multiresolution divides the frequencies into octave bands, from w to $2w$, rather then different frequencies.

From this analysis, to invert from a grosser resolution to a better resolution Mallat (1998) represents this as follows:

$$\begin{array}{l} \text{signal at level } s + 1 \text{ (local differences)} \quad \searrow \\ + \qquad\qquad\qquad\qquad\qquad\qquad\qquad \text{signal at level } s \\ \text{details at level } s + 1 \text{ (local averages)} \quad \nearrow \end{array}$$

Note that as s increases, the details in the signal are further degraded or washed out. Using this notation and the transform coefficients of the example in (10), to obtain fl_3 from fl_4 and fh_4 we do the following:

$$(H_4'fh_4) + (L_4'fl_4) = (H_4'H_4 fl_3) + (L_4'L_4 fl_3) = fl_3.$$

Thus the signal, such as the NIR information from an image, can analysed at different resolutions by the wavelet transform. The coefficients provide us with a measure of the energy the basis vector has at time t and/or scale s. The discrete wavelet transform decomposes the signal into a set of high and low frequency components which correspond to the coefficients of the dilated and translated basis functions $w(t)$ and $\phi(t)$ respectively. The high frequency component wavelet-coefficient $wf(s,u)$, provides a measure of the variation of f in a neighbourhood u whose size is proportional to s. This measure of variation in smooth signals is negligible while the variation tends to be significant in signals with jump discontinuities. Furthermore, increasing the dilation parameter s while filtering the signal produces a larger region of integration, which in turn smoothes the signal further. That is, less detail and lower frequencies are obtained as the dilation parameter increases. On the other hand, decreasing the dilation parameter s in the convolution process, generates smaller windows of integration allowing more detail and higher frequencies to come through.

There are many different kinds of wavelets (adaptive, continuous, discrete, orthogonal, biorthogonal, real and complex), the most simple being the Haar. Nevertheless, those of Daubechies (Daubechies, 1988) have been used quite often since they first came out.

Analysis of the A.P. Hill data

SPOT Image

The part of the scene covering Fort A. P. Hill, Figure 6, is slightly smaller than that used before (see report N68171-97-C-9029), but it covers the same part of the image. Analyses were carried out on the complete data set and on sub-samples of 1 pixel in 2 for each column and row (or 1 pixel from a block of 4), 1 pixel in 4 for each row and column (1 pixel from a block of 16), and 1 pixel in 8 for each row and column (1 pixel from a block of 64 pixels). The sub-sets were used to assess the accuracy of data reconstruction by the two methods. Table 5 gives the summary statistics for the full data set.

Table 5: Summary statistics for NIR for the 128 pixels by 128 pixels region of Fort A. P. Hill

Statistic	NIR	Hermite polynomials of NIR
Count	16384.0	16384.0
Minimum	37.00	-4.496
Maximum	183.00	4.009
Mean	117.83	0.0287
Variance	268.99	0.9995
Standard deviation	16.401	0.9997
Skewness	-0.7408	-0.0943
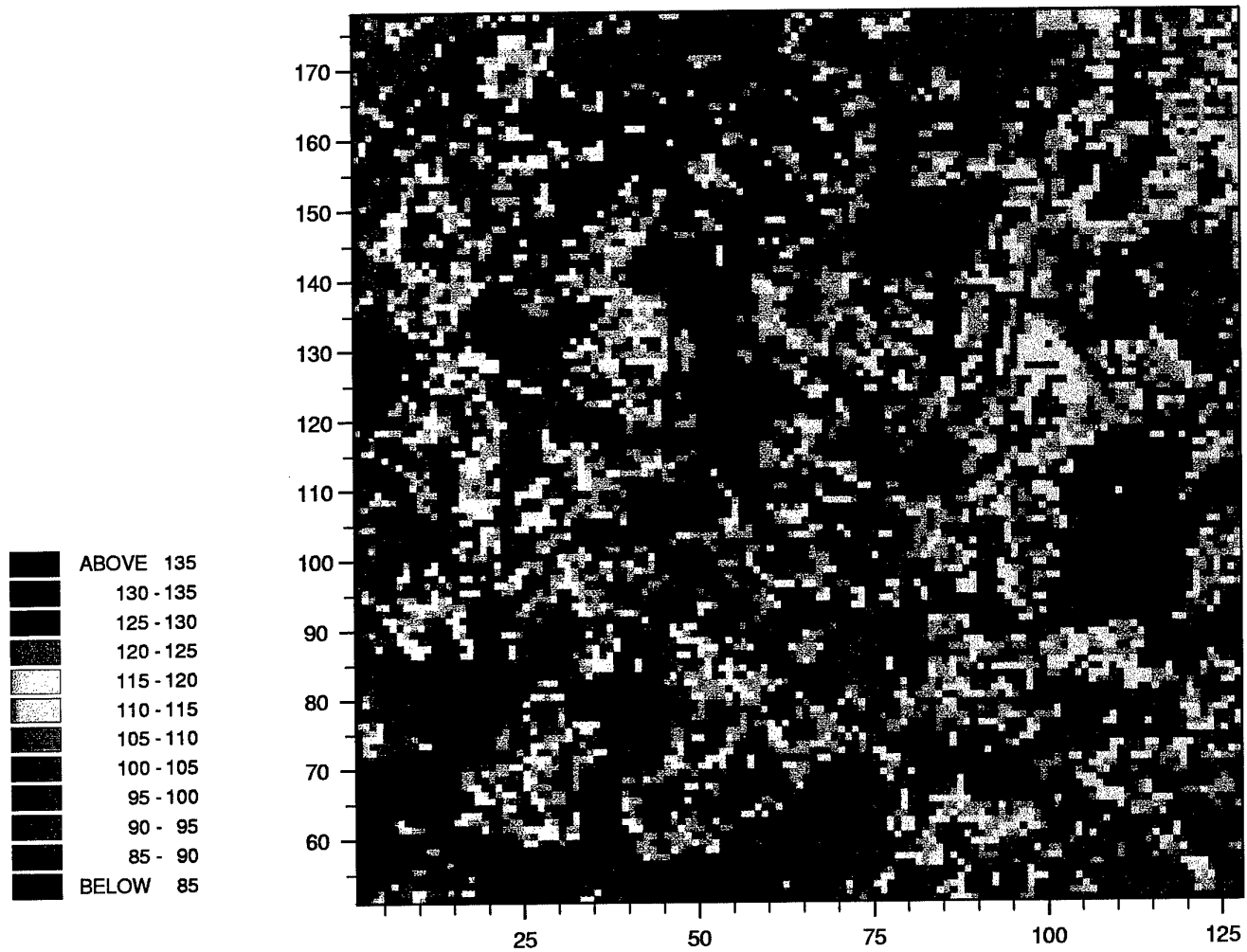
Figure 6: Pixel map of the near infra read (NIR) of part of the SPOT image (128 by 128 pixels) for Fort A. P. Hill.

Wavelet analysis

The method of wavelet analysis that Edward Bosch used was that of Daubechies wavelets (Daubechies, 1988). The size of the image was $2^7 \times 2^7$, i.e. 128 rows and 128 columns of pixel information for the NIR waveband. This region chosen from the part of the SPOT image that we analysed and described in the previous report (1998), and the size was such to avoid any need to pad the data to create appropriate resolution levels for the wavelet analysis.

The wavelet transform was done with a pair of filters and not the wavelets themselves. The two-dimensional wavelet transform is separable which means that we can apply the filters in the horizontal direction and then in the vertical direction to obtain the desired results. As we described above, the convolutions can be represented in terms of two matrices **L** and **H**. The matrix **L** is made up of shifts of the low frequency filter l[n], and **H** is made up of shifts of the high frequency filter h[n]. These shifts force every other point in the output of each convolution to be discarded (decimated).

In this study we used *Daubechies 6*-component wavelet filters. This wavelet satisfies three orthogonality conditions and three vanishing moments. The orthogonality condition implies that the filter is orthogonal to its shifts by two. Increasing the number of vanishing moments of the wavelet and its filter, forces the wavelet to be smoother (continuous and differentiable), but at the same time it increases the support of the wavelet and the number of sampling points in the corresponding filters.

As we mentioned above, the wavelet-coefficient $wf(s,u)$ provides a measure of variation of the signal $f(t)$ at s and u. The smoother the signal, with three vanishing moments, the high pass filter zeros out the low frequency content in the signal leaving behind little information. Since the high pass filter h[n] is designed to discard a certain amount of information, which depends on the number of vanishing moments, the low pass filter l[n] thus must retain most of the 'energy' or information.

Given that the image used is 128 rows by 128 columns in size ($2^7 \times 2^7$), using Mallat's scheme, the original resolution level is 0. Applying the discrete wavelet transform (DWT) to the data once produces high and low frequency components at resolution level 1. This results in four quarter sets of data of size 64 by 64 pixels. The first quarter of the data represents in essence a sample of 1 in 2 of the rows and columns of the data matrix. This quarter contains the scaling coefficients which correspond to the low pass filter. The other three quarters contain the wavelet coefficients which are high frequency: quarter two contains the vertical coefficients, quarter 3 the horizontal ones and quarter 4 the diagonal coefficients.

For this analysis the low and high frequency components were used separately to assess their overall contribution to the original image and to analyse the effect this had on the variogram of the original image. That is, we computed the inverse wavelet transform at several levels with only the corresponding low frequency components. Also, we computed the inverse wavelet transform at several levels without the low frequency content.

Geostatistical analyses

The variogram was computed and modelled as usual using the smaller data set with a total of 16 384 pixels, Figure 7. This variogram was then used with the pixel information to filter the information by factorial kriging into the long-range and short-range components. Ordinary kriging was used to estimate the values of NIR at positions where pixels had been removed from the data. In other words the estimates coincided with the locations of the original values so that a direct comparison could be made between the estimates and these.

Results

The variogram for the new data is still a nested structure, but the correlation ranges are smaller than for the larger part of the scene that we investigated before. The model fitted was a nested spherical function with two structures. Since the variogram was somewhat wavy at the longer lags, to improve the fit I modelled it to a lag of 40 only. The short-range structure was 6.6 pixels or 130 m and the long-range structure was 21 pixels or 420 m. The experimental variogram (points) and the fitted model (line) are given in Figure 7 a. The parameters of the models fitted to 100 and to 40 lags are given in Table 6. Since the data were skewed I transformed them using Hermite polynomials and computed the variogram from the transformed data, Figure 7 b and Table 6. There was little difference from the raw variogram, therefore, I did the analyses on the raw data.

a)
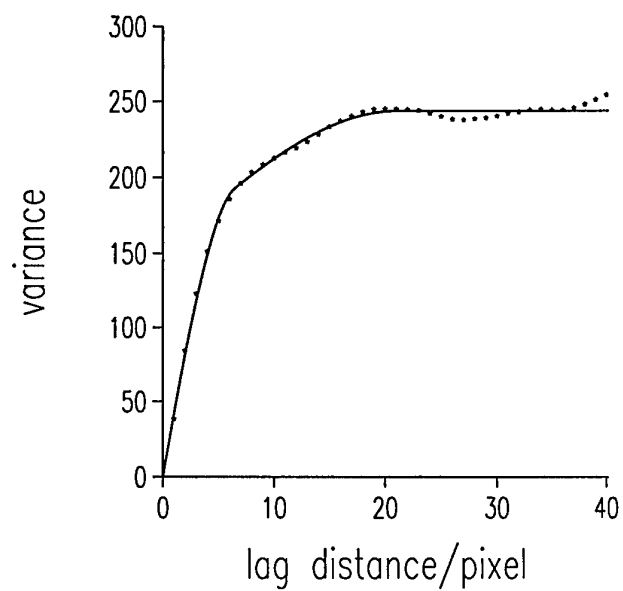
b)
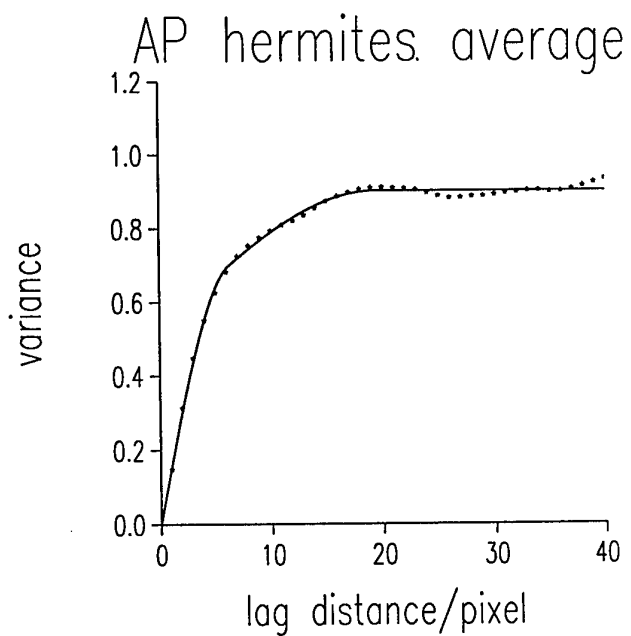
Figure 7: a) Variogram of the near infra read (NIR) of part of the SPOT image (128 by 128 pixels) for Fort A. P. Hill, b) variogram of the transformed pixel data using Hermite polynomials

Multiresolution analysis (filtering)

The variogram suggests that there are two clear scales of spatial variation present: one of about 120 m and the other of about 420. This is also evident in the pixel map of the ordinary kriged estimates, Figure 8. There is local detailed variation superimposed on a broader pattern of variation. The major large structures in the variation that are evident appear to be related to major relief forms: the drainage basins and the intervening spurs, and the major types of ground cover. Short-range variation is also evident related to the water bodies, buildings and the more local changes in ground cover and drainage. These were described in the previous final report.

Table 6: Model parameters for the variograms computed for the 128 by 128 pixel area of the SPOT image

Variable	Model type	Nugget variance	Sill(1) variance	Range(1) pixels (m)	Sill(2) variance	Range(2) pixels (m)
NIR (100 lags)	Nested Exponential	0	227.0	13.2 (264)	4.40	85.1 (1701.6)
NIR (40 lags)	Nested Spherical	0	152.2	6.46 (130)	91.71	21.11 (420)
Hermite polynomials	Nested Spherical	0	0.5240	6.21 (125)	0.3755	19.45 (390)
Long-range component	Circular	0	113.9	17.2 (544)		
Short-range component	Spherical	0	87.9	4.30 (86)		
Low frequ -ency 1 in 2	Nested Spherical	0	146.7	8.40 (168)	74.82	22.2 (444)
High frequ -ency 1 in 2	Pure nugget					
High frequ -ency 1 in 4	Circular	0	41.7	2.944 (58.88)		
High frequ -ency 1 in 8	Circular	0	68.30	6.690 (133.8)		
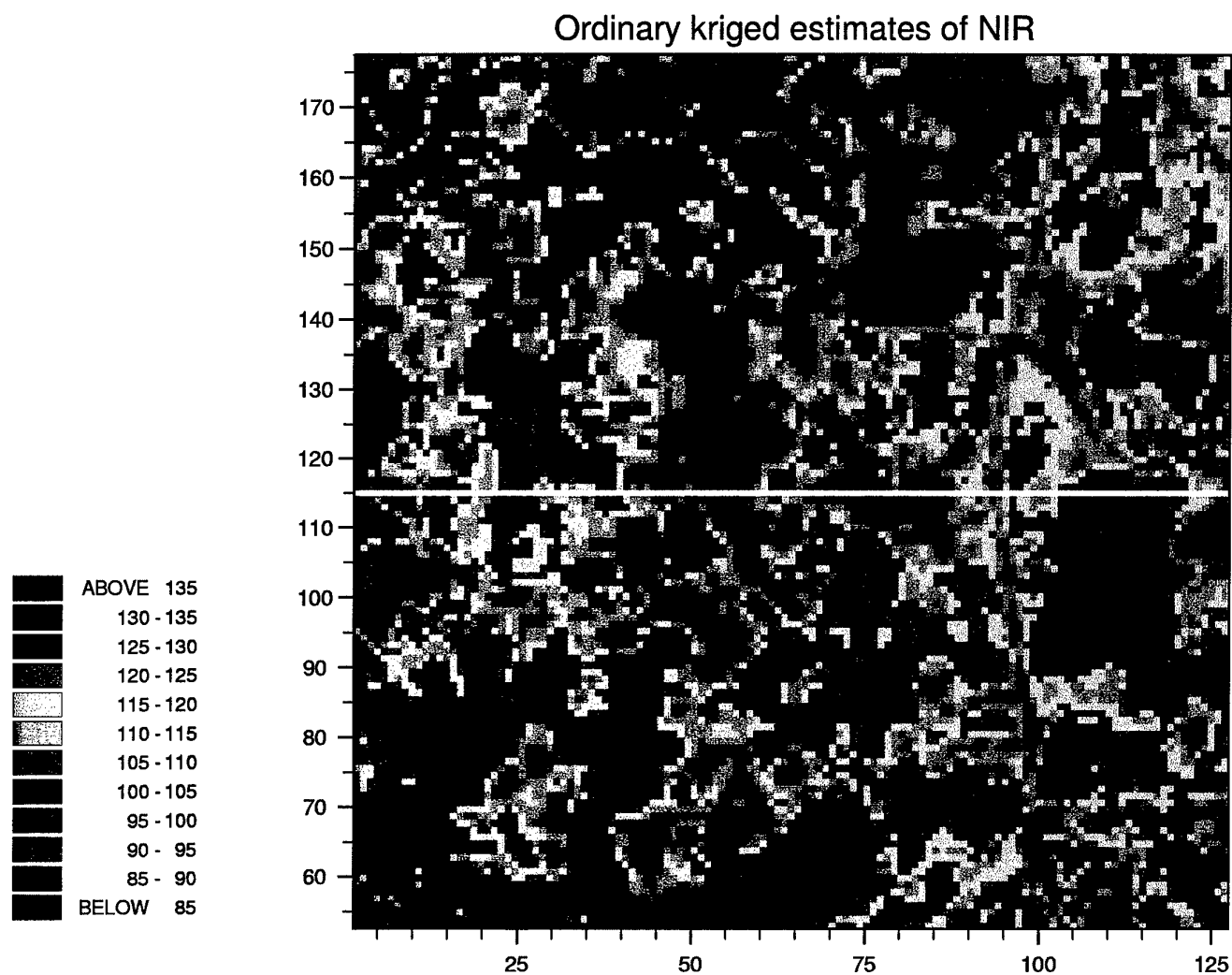
Figure 8: Pixel map of the kriged NIR of part of the SPOT image (128 by 128 pixels) for Fort A. P. Hill

Factorial kriging and wavelet analysis enable the different spatial scales to be separated in theory. For factorial kriging this is controlled by the variogram which describes the variation present in the data. For the wavelet analysis this is controlled by the resolution level, which in turn is controlled by the octave bands and as a consequence is more arbitrary. One aspect of future research is to consider how the variogram could be used to guide the factoring process that controls the wavelet multiresolution analysis.

Figure 9 is a pixel map of the kriged estimates of the long-range component of the variation filtered using the variogram. The large scale variation is related to the main relief features. The band of dark colours in the North and central part of the map are damper and wetter areas, and the lighter ones the spurs, upper slopes and built areas. This map could be used effectively to guide future sampling. If the end-user is interested in retrieving this level of information then a suitable sampling interval can be chosen using the range of the variogram. A sampling interval of 200 m would be adequate to ensure that this resolution of variation is identified.

The pixel map of the short-range variation (Figure 10) shows the detail that is also evident in Figure 8, but less clearly so. The lakes are recovered well by this resolution. The dark patches in the bottom left hand corner (1 to 20 on the x-axis and 55 to 60 on the y-axis), in the central area (64 to 90 on the x-axis and 115 to 125 on the y-axis), and at the top of the map (45 to 70 on the x-axis and 158 to 180 on the y-axis). The road running N-S is also evident extending N along longitude 100 (on this map). The other short-range structures probably relate to changes in local drainage conditions and vegetation. For many surveys recovering this intensity of variation at a scale of about 120 m would require too much sampling. A sampling interval of 50 m to 60 m would be needed to resolve this short-range variation. If a sampling scheme of about 200 m were recommended in relation to the long-range variation this information on short-range variation would be lost. These maps enable us to demonstrate to the end-user the extent of information that is likely to be lost by adopting the coarser sampling. Sampling between 60 m and 200 m would be of little benefit because most of the short-range variation would not be identified and sampling at less than 200 m would be inefficient to identify the long-range variation. Variograms were computed from the estimates of the long-range (Figure 11 a) and the short-range (Figure 11 b) components. They recover the spatial scale of the variation quite well, but both variograms were difficult to model satisfactorily.

For the first wavelet analysis the level of resolution was 1. The coefficients were derived as described earlier. The low frequency and the high frequency coefficients were reconstructed by the inverse wavelet transform, which restored each of the 64 by 64 sets coefficients to the size of the original data set. These are shown as pixel maps and should be compared with the appropriate kriged and the filtered maps, Figures 8 to 10. In addition variograms were computed for each of these four reconstructions: one low frequency (Figure 12 a) and three high frequency ones (the one is shown in Figure 12 b is the average as they were similar).

The low frequency reconstruction, Figure 13, is very similar to the ordinary kriged output for the image, Figure 8. It is important to remember that the ordinary kriged
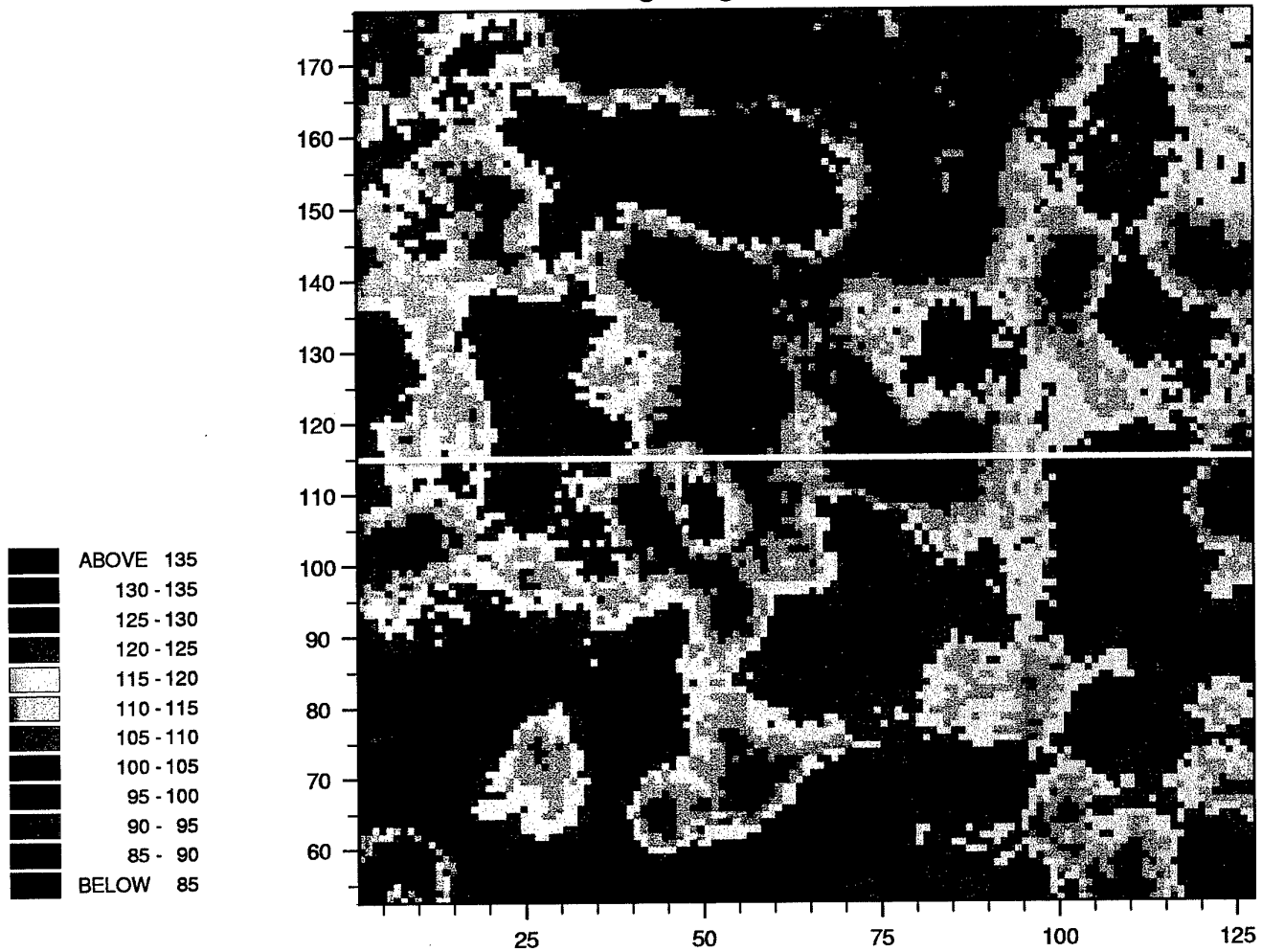
Figure 9: Pixel map of the long-range component of the variation in NIR of part of the SPOT image (128 by 128 pixels) for Fort A. P. Hill

Short-range estimates of NIR
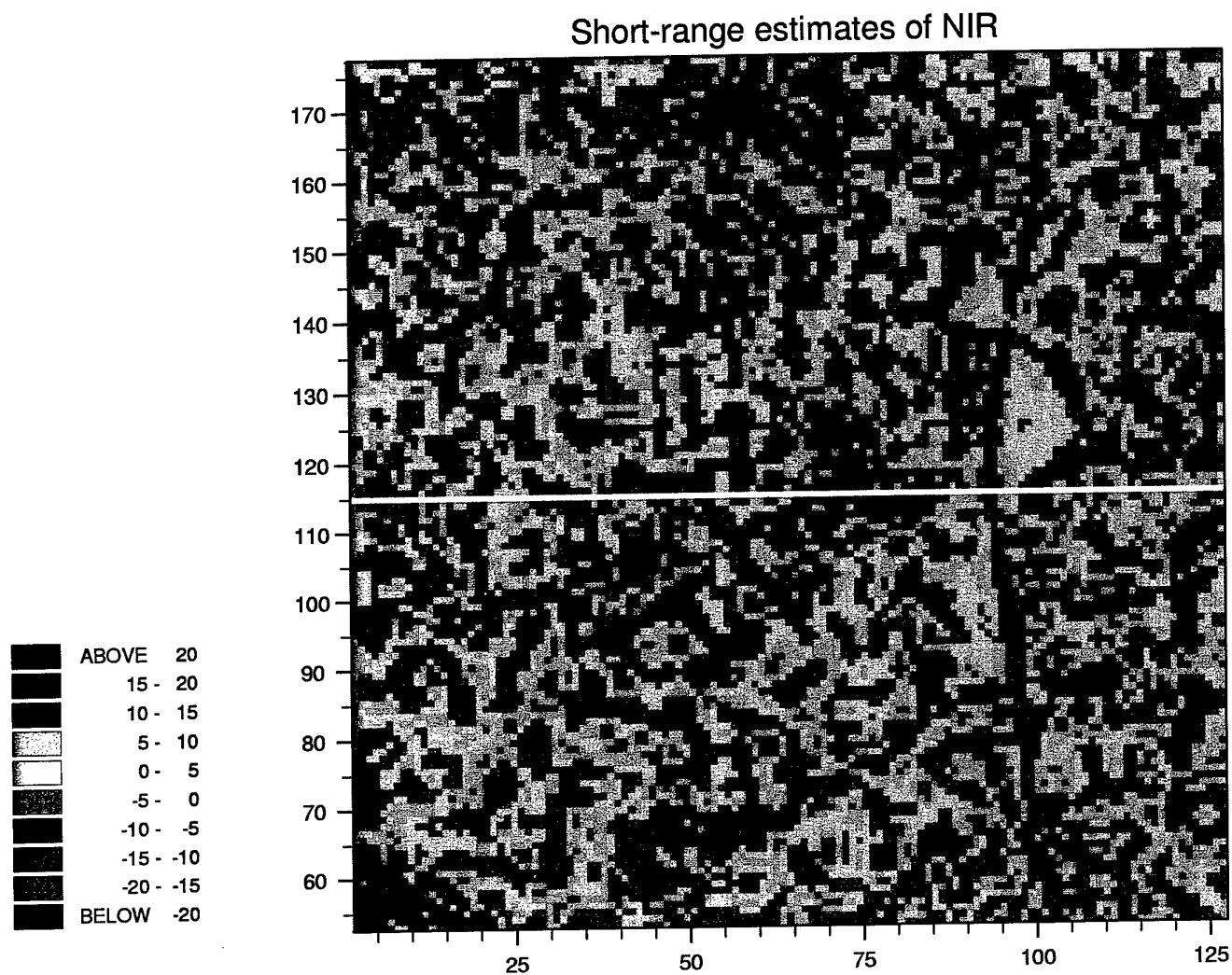
Figure 10: Pixel map of the short-range component of the variation in NIR of part of the SPOT image (128 by 128 pixels) for Fort A. P. Hill

a)

Long-range component

b)

Short range component
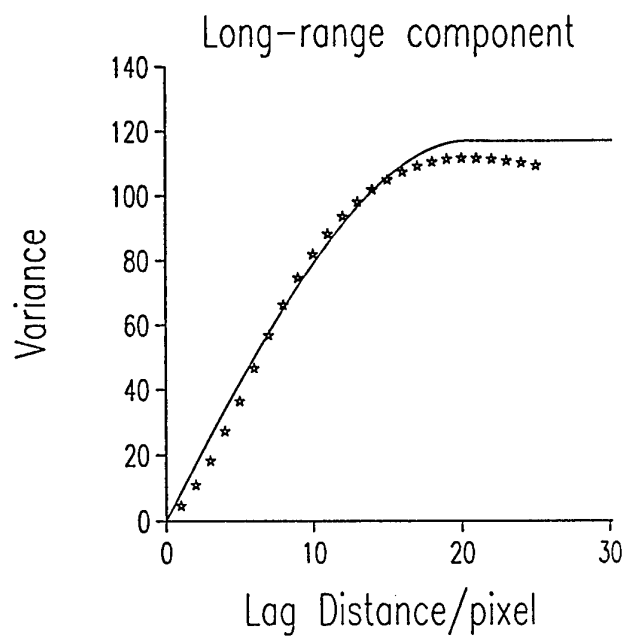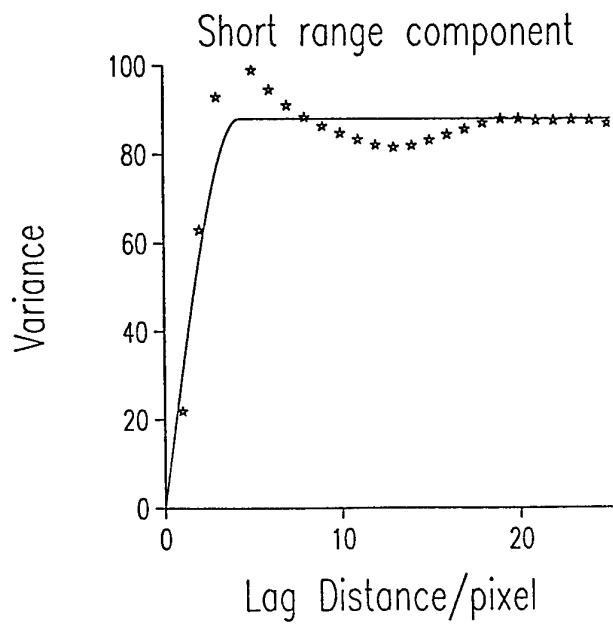
Figure 11: a) Variogram of the long-range component, and b) variogram of the short-range component of the variation in NIR of part of the SPOT image (128 by 128 pixels) for Fort A. P. Hill

a)

b)

Figure 12: a) Variogram of the low-frequency component, and b) variogram of the average of the high-frequency components for NIR of part of the SPOT image (128 by 128 pixels) for Fort A. P. Hill from a wavelet analysis at a resolution of 1 in 2

map was made from estimates using all of the data, whereas the low frequency wavelet reconstruction used the 1 in 2 sample, i.e. 25% of the original data. Both the long- and short-range components of the variation are evident, although there has been some loss of detail in the short-range variation. Fo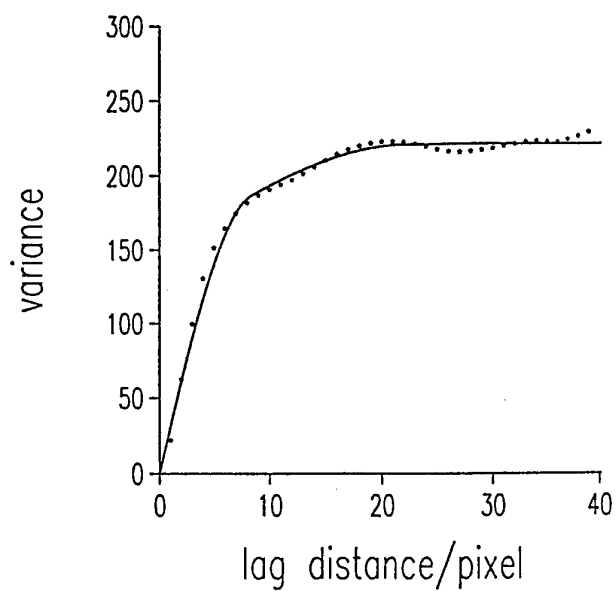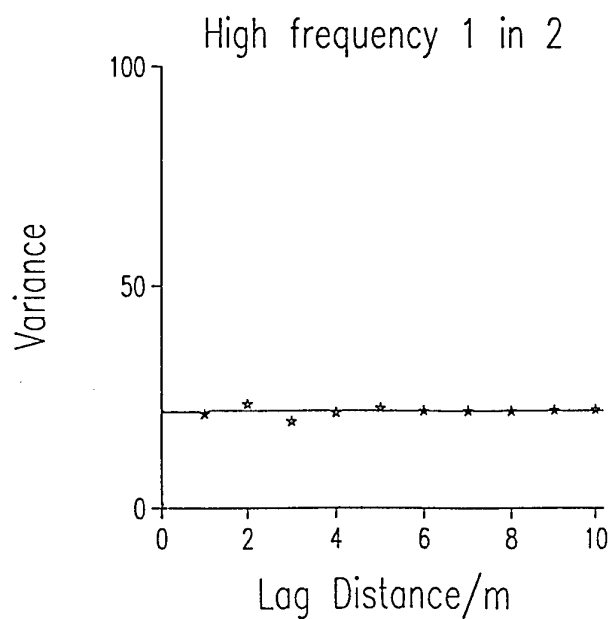r example the road is less clear in Figure 13 than in Figure 8. The variogram computed from the low frequency reconstruction, Figure 12 a, was very similar to the variogram of the raw data, Figure 7 a. Hence the spatial structure at both scales has been retained at this level of resolution. The most surprising finding was that related to the high frequency reconstruction. The map of the high frequency component (Figure 14) does not appear to reflect the kind of variation present in the map of the short-range component from factorial kriging. However, when we examined them in detail there is some weak evidence of the lakes, which are so clear in Figure 10. The variograms computed from these data are pure nugget, as shown in Figure 12 b. This means that the high frequency components are noise at this level of resolution; they contain no spatial structure. The latter is all retained in the low frequency reconstruction.

To determine whether we could retrieve the long- and short-range components using wavelets we explored the next resolution, 2, in effect a sampling of 1 in 4 (or 1 pixel in 16). Figure 15 shows the low frequency reconstruction. There is still long- and short-range variation evident, although the short range variation is becoming less distinct; for example the road and the lakes are still visible but their margins are less clearly defined. Figure 16 shows the pixel map for the average of the high frequency reconstruction and it is clear that there is more of the short-range component of the variation evident. The variogram of the high frequency reconstruction now shows some structure, Figure 17 a. Table 6 gives the model parameters of this variogram.

The low frequency reconstruction of the 1 in 8 resolution 3 now shows the long-range component of the variation identified by factorial kriging, Figure 18. This resolution is fairly close to the short-range component of the variogram, i.e. 6.5 pixels, and this level of variation appears to have been filtered out now. So it seems that once the resolution of the short-range structure has been reached the effect was to remove the short-range variation. The map, Figure 19, of the high frequency reconstruction now shows some of the features evident in the kriged map of the short-range component of the variation. In particular the lakes are evident. The variogram computed from the average of the three high frequency reconstructions, Figure 17 b, shows clear evidence of structure and the range of spatial correlation described, 6.69 pixels, is close to the short-range component of the variogram of the original data.

Summary

It is clear that factorial kriging works well with multiresolution data. The main reason for this is that the filtering is controlled by the variogram which is a function of the data being analysed. It is a valuable method for directing future sampling for ground surveys because it can show what degree of variation is likely to be recovered. The multiresolution analysis using wavelets produces a different outcome. At the first resolution the high frequency components remove the noise, i.e spatially uncorrelated variation, but none of the short-range variation is resolved. At the subsequent resolutions close to the short-range component in the variogram the high frequency wavelets recovered the short-range variation, especially at level 2, evident in Figure 10.

10. To recover the long-range component of variation it seems that choosing a resolution near to that of the short-range component identified by the variogram is an effective way of avoiding several iterations of the wavelet analysis. Once the scales of variation have been identified by the variogram the choice of wavelet coefficients retained can be optimized. This presents an interesting consideration for further work.

Wavelet reconstruction for 1 in 2 selection

ABOVE 135	
130 - 135	
125 - 130	
120 - 125	
115 - 120	
110 - 115	
105 - 110	
100 - 105	
95 - 100	
90 - 95	
85 - 90	
BELOW 85	
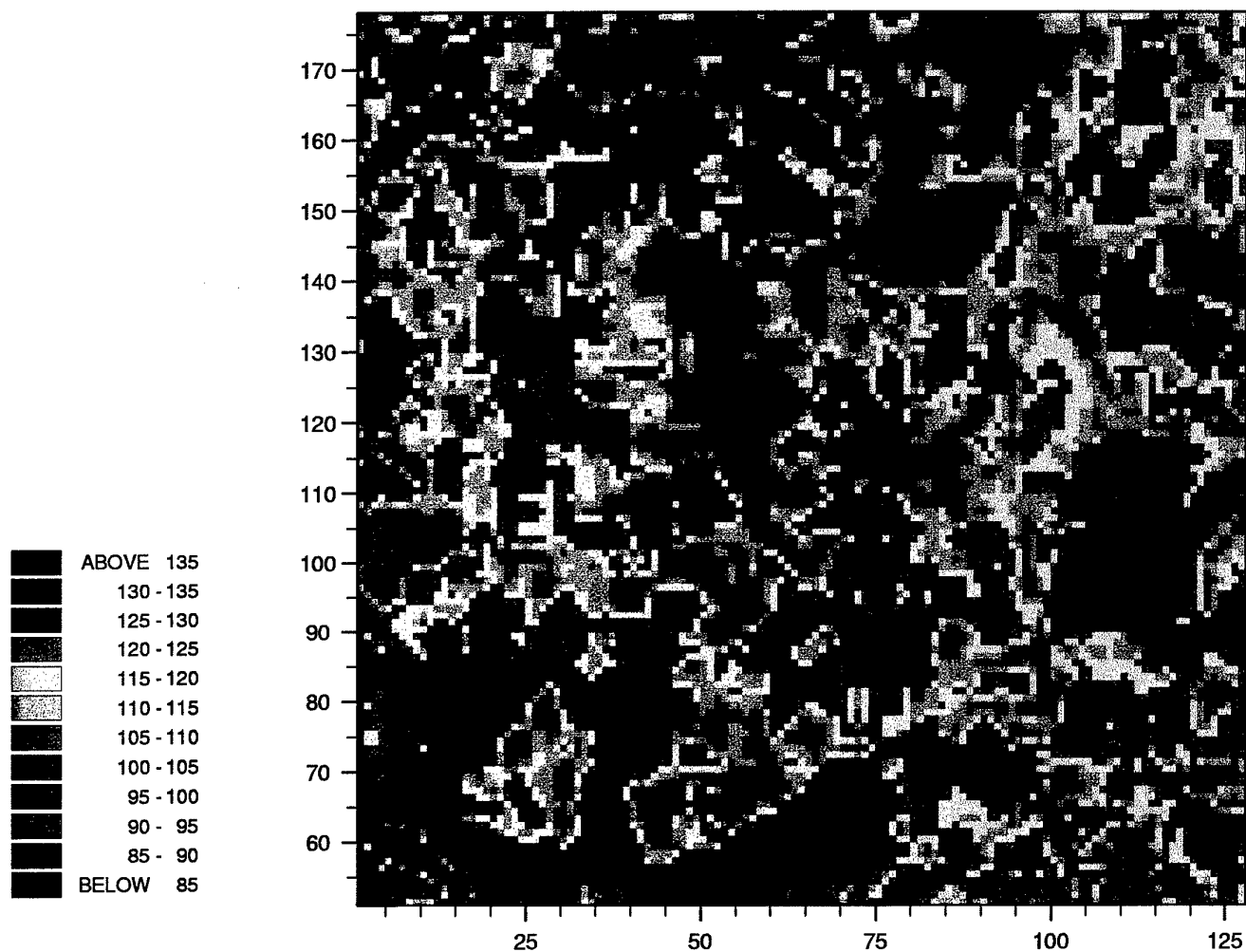
Figure 13: Pixel map of the low frequency reconstruction from the wavelet analysis of NIR of part of the SPOT image (128 by 128 pixels) for Fort A. P. Hill at a resolution of 1 in 2

High frequency reconstruction 1 in 2
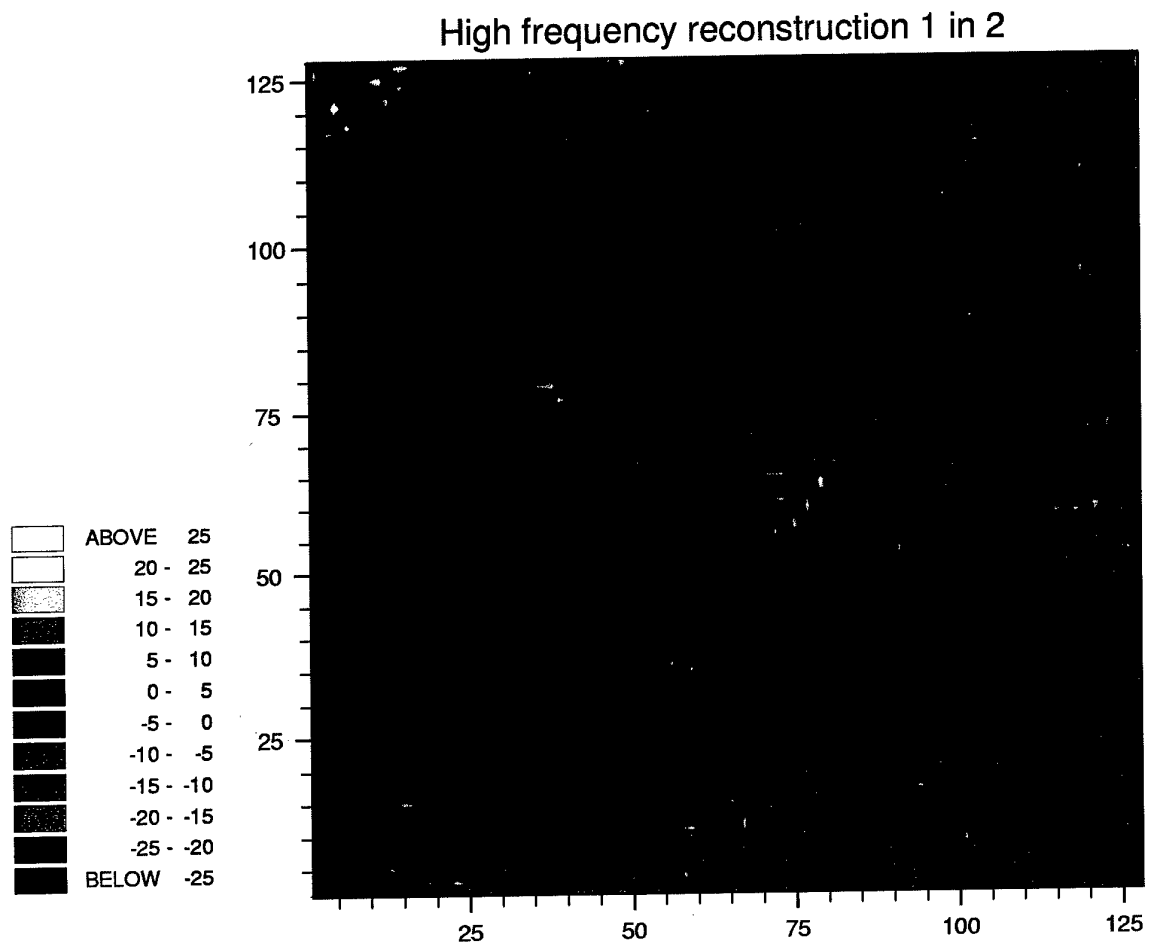
Figure 14: Pixel map of the average reconstruction of the high frequency wavelets from the wavelet analysis of NIR of part of the SPOT image (128 by 128 pixels) for Fort A. P. Hill at a resolution of 1 in 2
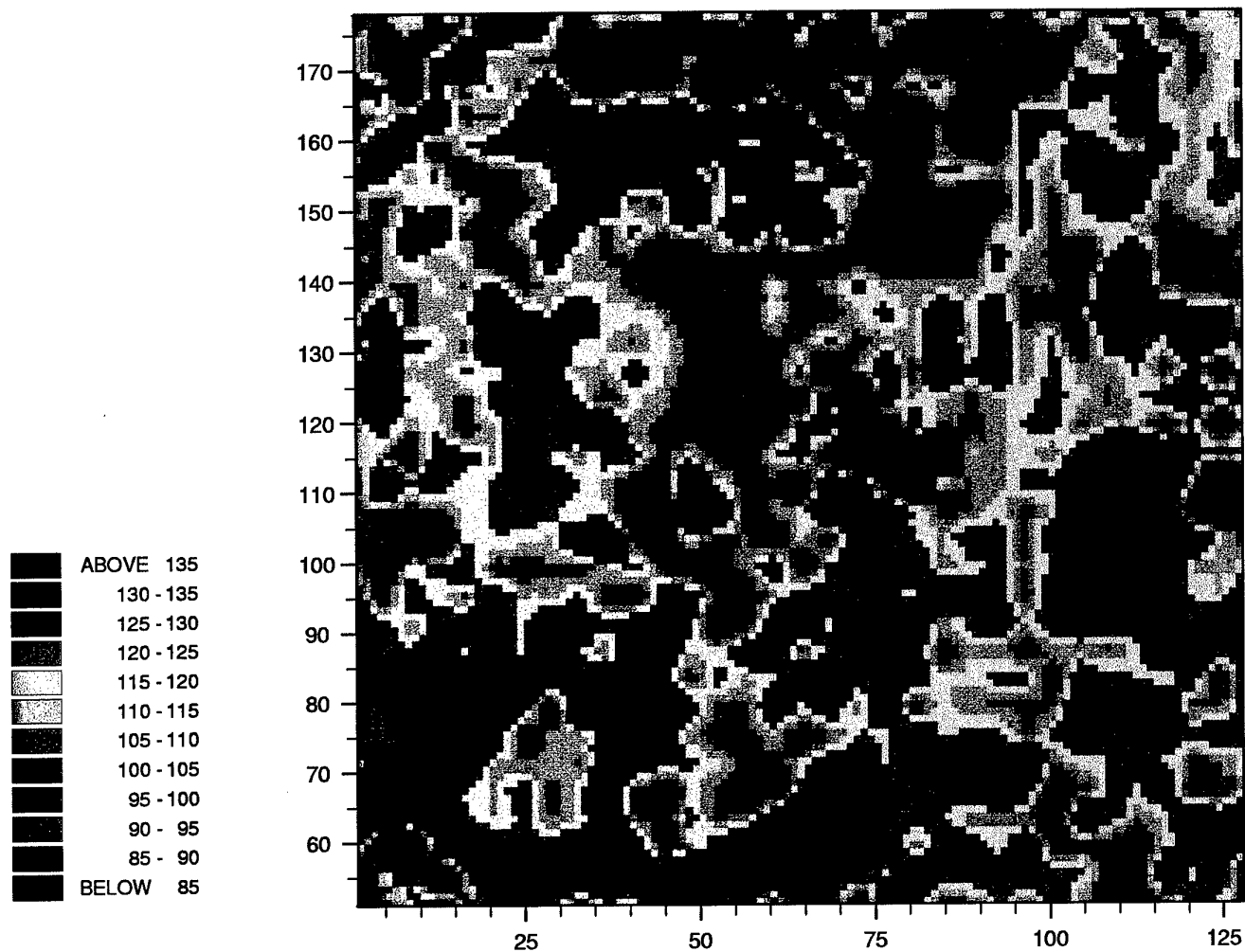
Figure 15: Pixel map of the low frequency reconstruction from the wavelet analysis of NIR of part of the SPOT image (128 by 128 pixels) for Fort A. P. Hill at a resolution of 1 in 4

High frequency reconstruction 1 in 4


```
ABOVE   25
   20 -  25
   15 -  20
   10 -  15
    5 -  10
    0 -   5
   -5 -   0
  -10 -  -5
  -15 - -10
  -20 - -15
  -25 - -20
BELOW  -25
```

Figure 16: Pixel map of the average high frequency reconstruction from the wavelet analysis of NIR of part of the SPOT image (128 by 128 pixels) for Fort A. P. Hill at a resolution of 1 in 4

a)

b)
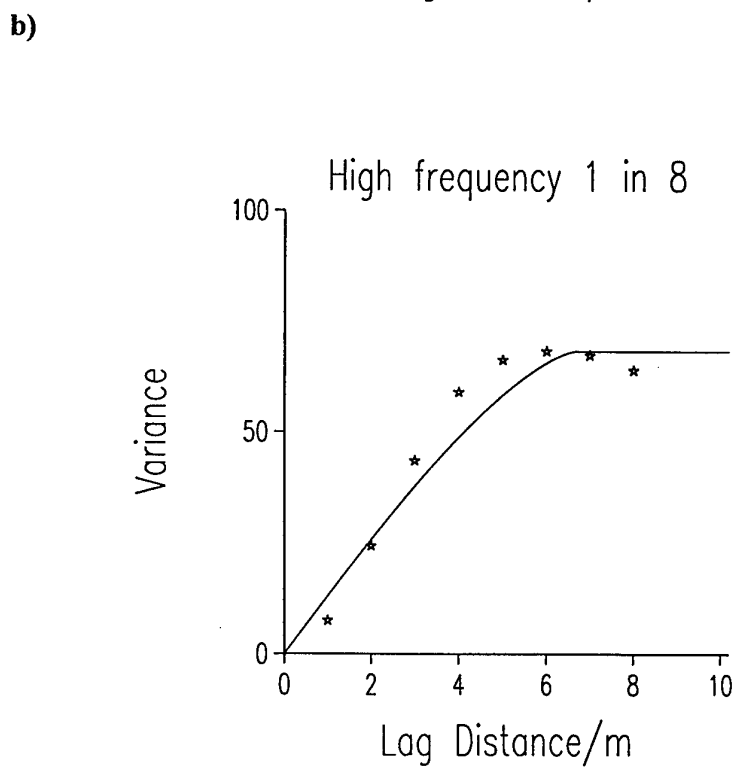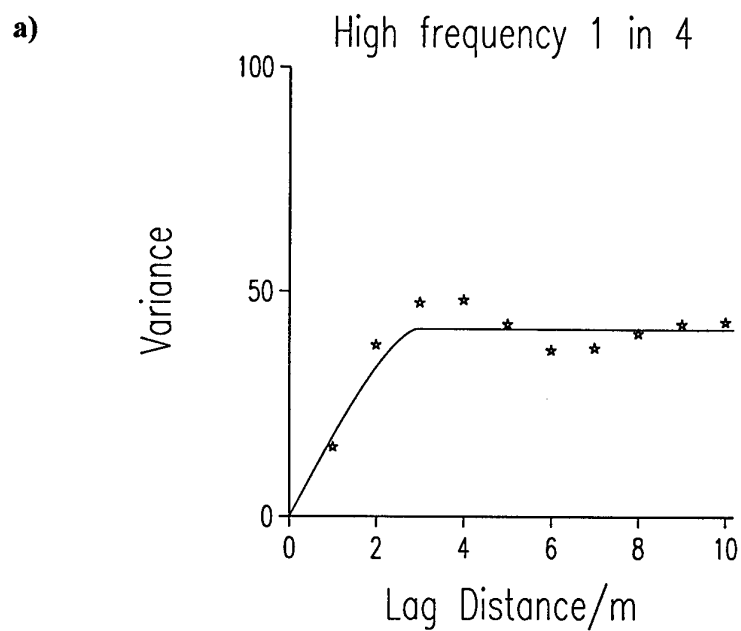
Figure 17: a) Variogram of the high-frequency component for the 1 in 4 resolution, and b) variogram of the high-frequency component for the 1 in 8 from the wavelet analysis of NIR at Fort A. P. Hill
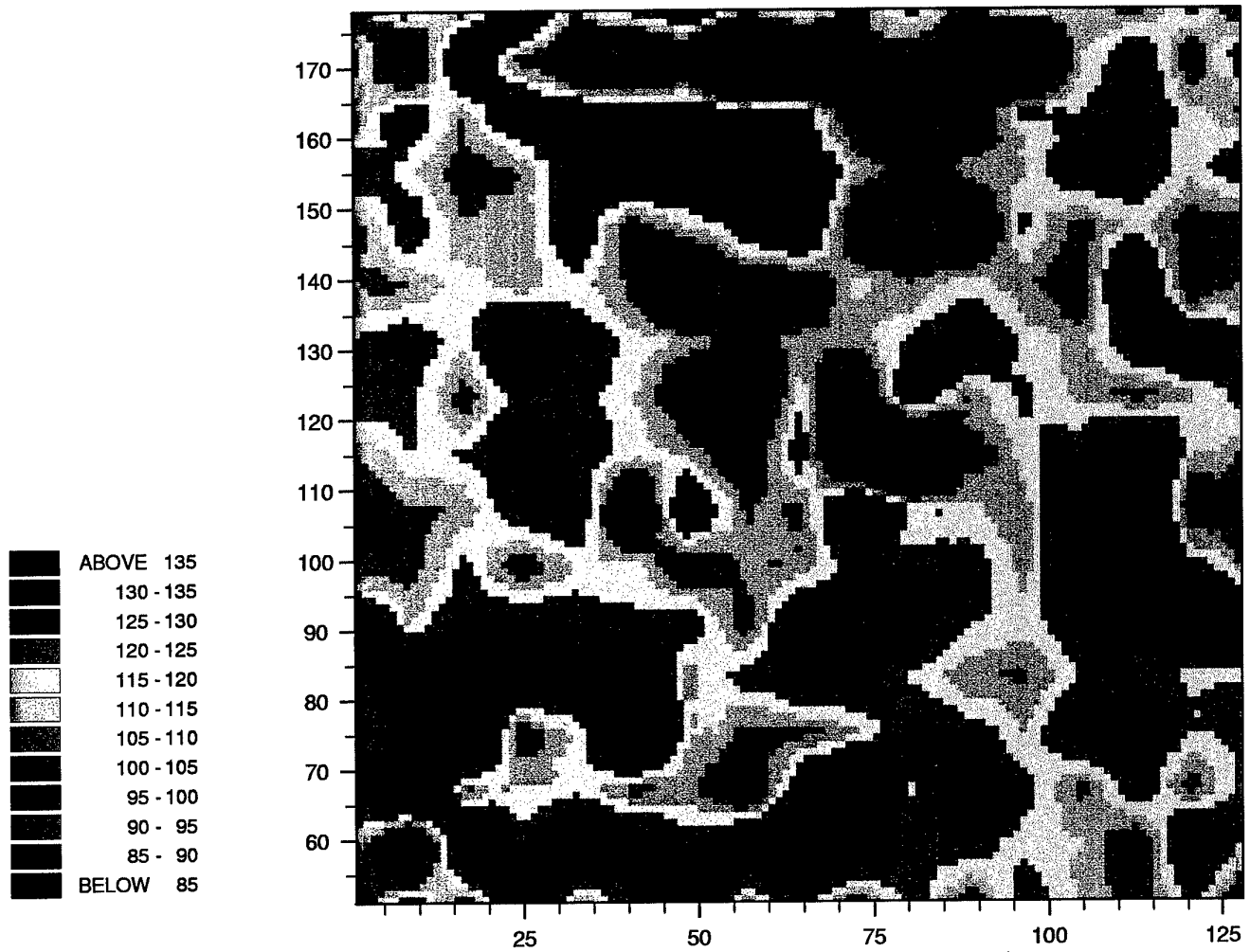
Figure 18: Pixel map of the low frequency reconstruction from the wavelet analysis of NIR of part of the SPOT image (128 by 128 pixels) for Fort A. P. Hill at a resolution of 1 in 8

Figure 19: Pixel map of the average high frequency reconstruction from the wavelet analysis of NIR of part of the SPOT image (128 by 128 pixels) for Fort A. P. Hill at a resolution of 1 in 8

Data reconstruction

The 128 by 128 pixels were sampled by taking one pixel in every two for each row and column (or a sample of 1 in 4) which matches resolution level 1 in the wavelet analysis, one pixel in every four for every row and column (or a sample of 1 in 16), a wavelet resolution of 2, and one pixel in every eight for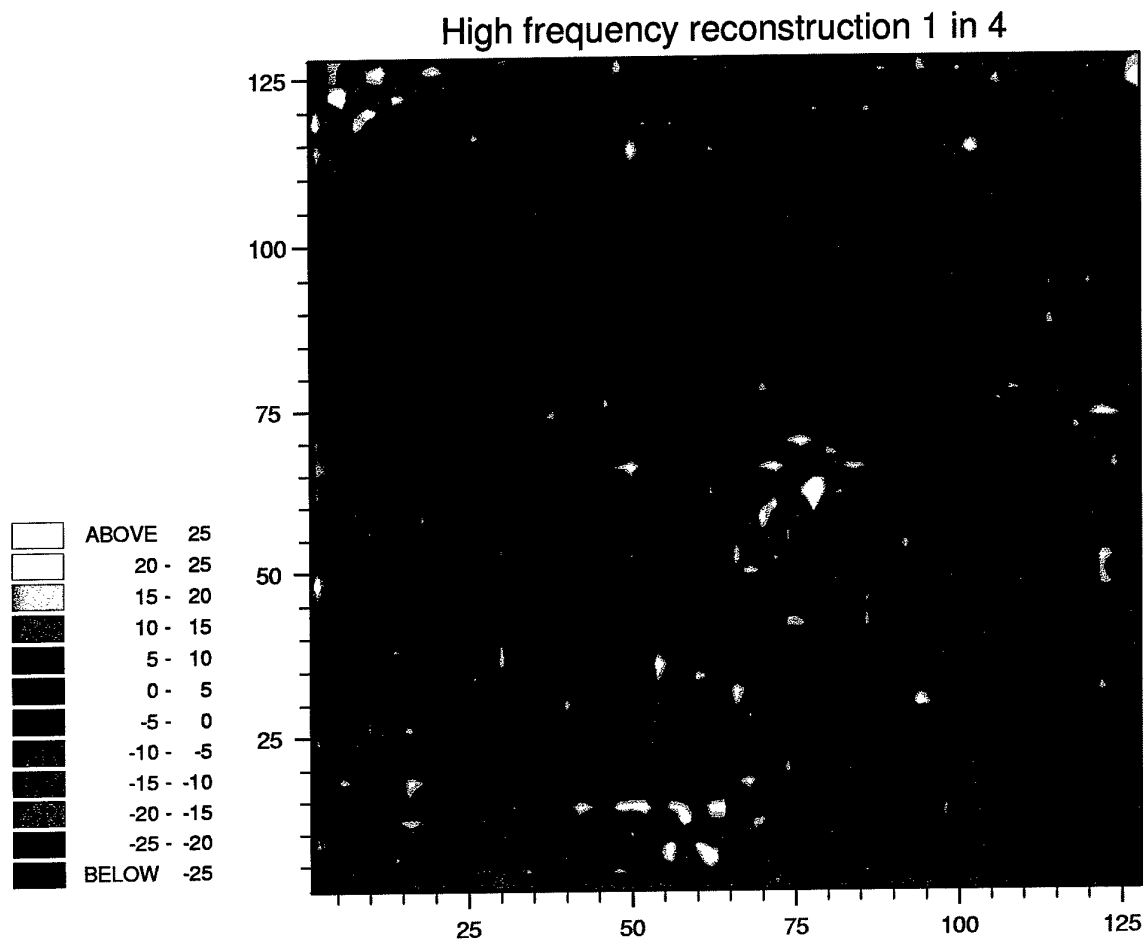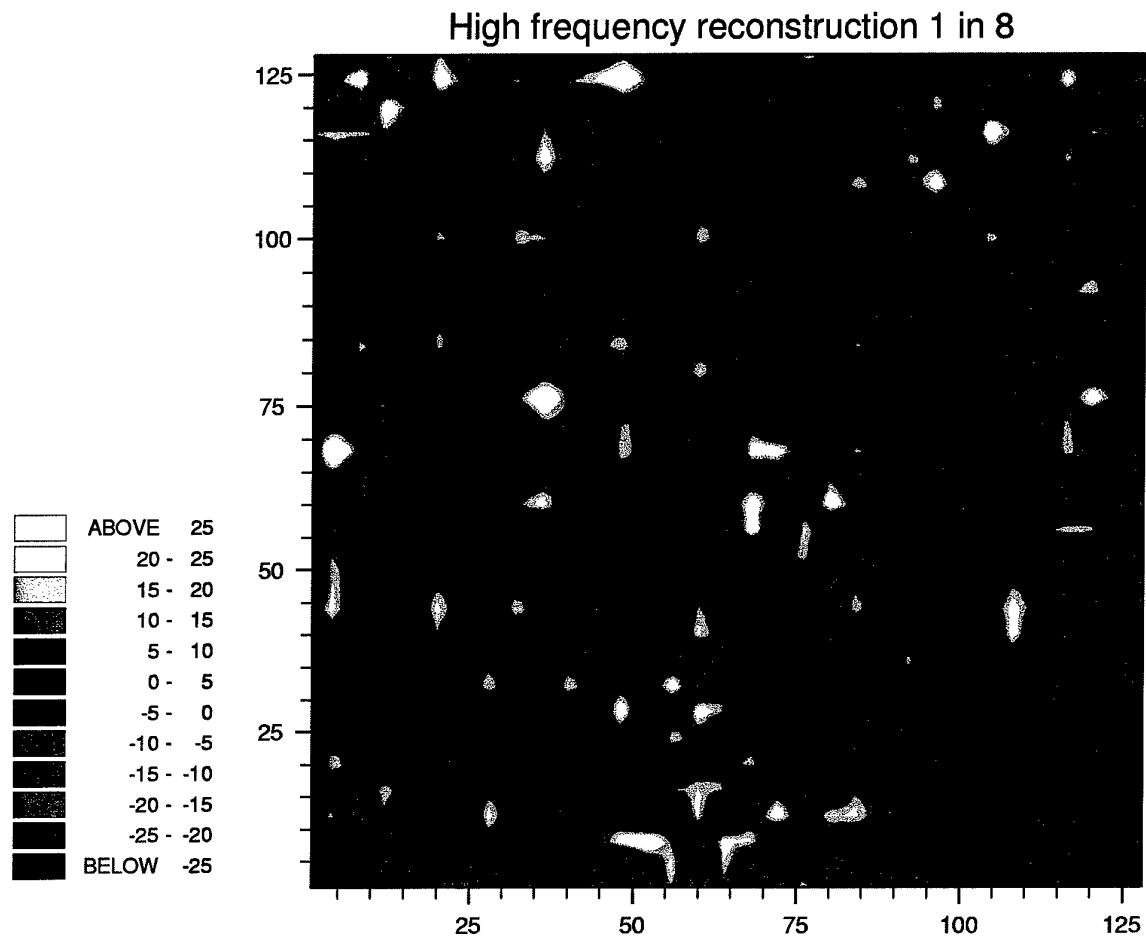 each row and column (or a sample of 1 in 64), a wavelet resolution of 3. The low frequency wavelet coefficients were inverted to reconstruct the image as before. Kriged estimates were made to coincide with the original data points for each data set using the variogram model from the full set of data. These maps are all shown as pixel maps.

To evaluate the accuracy of the estimates by the wavelet reconstruction and kriging every value was compared with the original values of NIR. First the differences were calculated between the estimates and original values for both analyses and for the three sub-samples, and these are shown as pixel maps (Figures 21 and 22, 26 and 27, 31 and 32). The statistical distribution of these differences or errors has also been determined and these are shown as histograms (Figures 23, 28 and 33). In addition the mean squared differences or mean squared error (mse) was calculated (Table 4).

Results

The results were not entirely what we expected and we have been making sure that the kriging program and analyses have been correct. From the theory of geostatistics we should expect that the kriged estimates would have the smallest mse, but they do not for any of the analyses. It was this that led us to explore the differences in more detail to try to gain insight into the results from the two methods. In spite of the fact that the forward and inverse wavelet transform are linear operators, reconstructing the data with only some of the wavelet transform components is not done in a linear setting. Mallat (1998) says, "It is often easy to find a basis that produces a smaller non-linear error than a Karhunen-Loeve basis, ...". Although in this study we are not using the Karhunen-Loeve transform (principal component analysis), some methods will provide smaller errors than others depending on the model used.

Sample of 1 in 2

The pixel maps for the low frequency wavelet reconstruction and kriging from the 1 in 2 data, Figures 13 and 20, respectively appear to be very similar to each other. The slight 'spottiness' evident on the kriged map is because punctual kriging was used and this is a true estimator returning the value at the data points. Table 7 gives the mean squared errors for both methods. That for the wavelets is less. The maps of errors or comparisons, Figures 21 (wavelet) and 22 (kriging), show a similar pattern in general. However, the differences between them help to explain why the mse is greater for the kriged estimates than for the wavelet reconstruction. There are large differences associated with the lakes where there are clearly marked local changes associated with boundaries in the variation. This is evidence of local non-stationarity which violates the assumptions of kriging. Wavelets are known to be suitable for dealing with local non-stationarity, and these results support this. Kriging has the largest absolute differences and there are more of them than for the low frequency wavelet

Kriged estimates for 1 in 2 selection
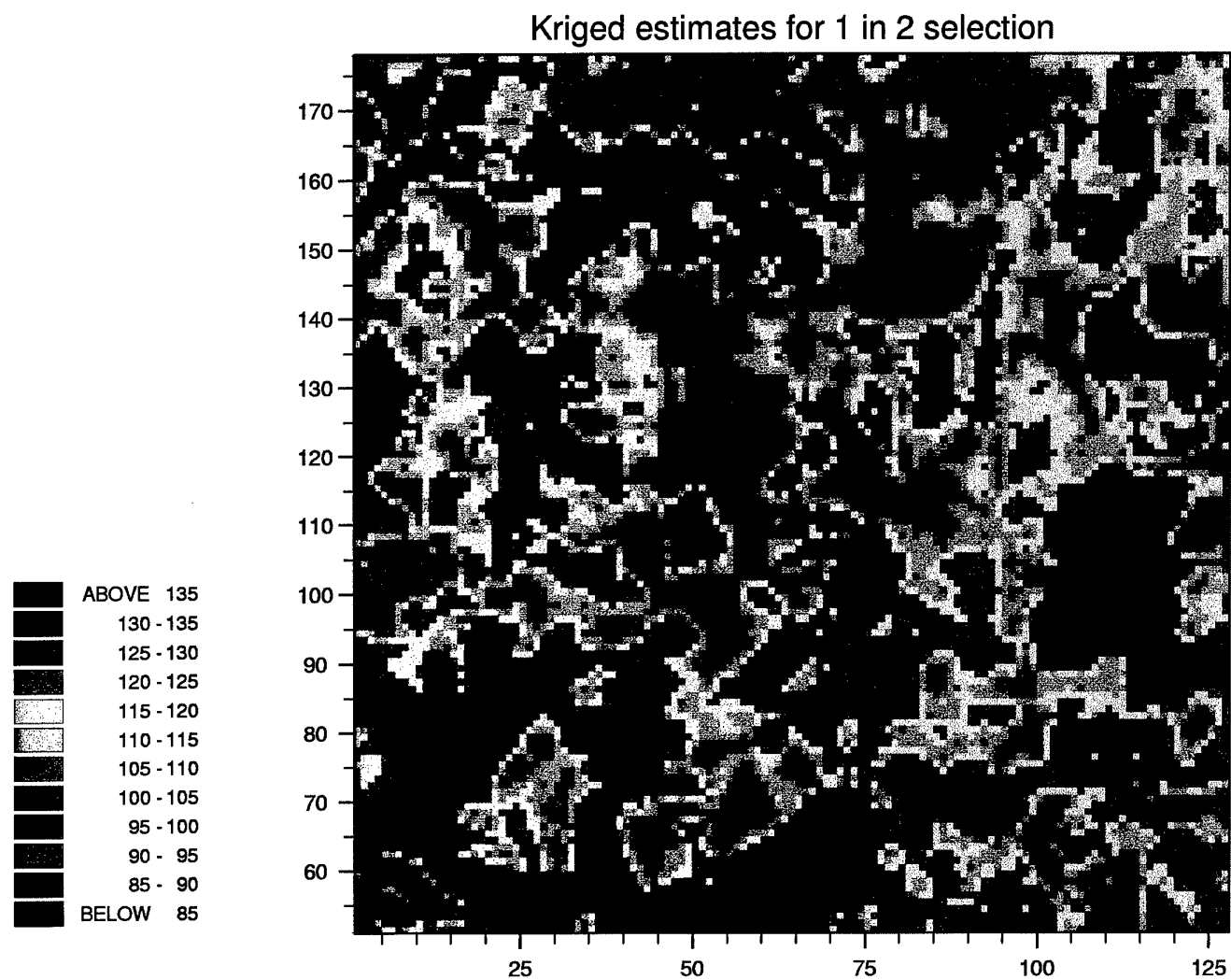
Figure 20: Pixel map of the kriged estimates for the 1 in 2 sample of NIR of part of the SPOT image (128 by 128 pixels) for Fort A. P. Hill
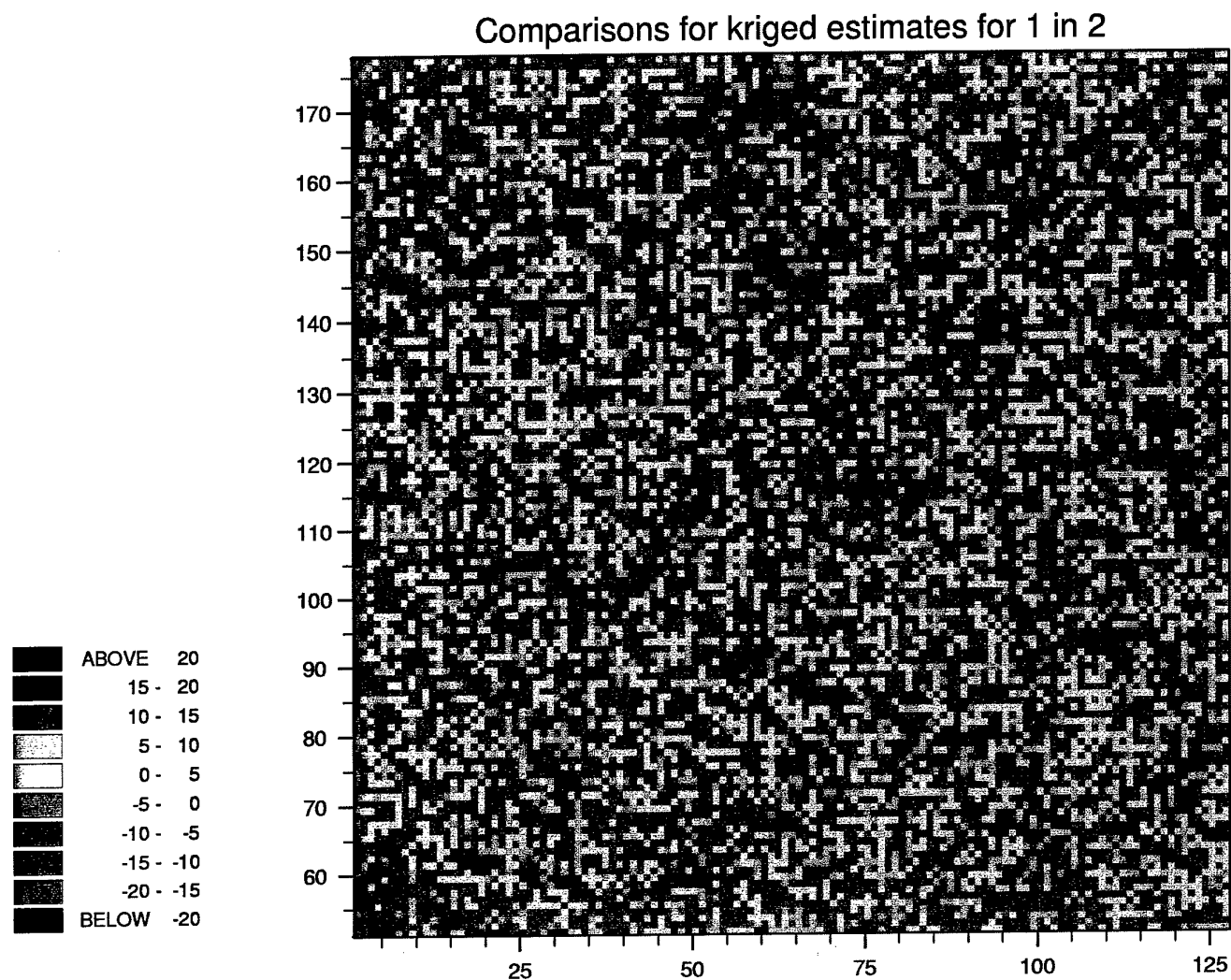
Figure 21: Pixel map of the comparisons between the kriged estimates for the 1 in 2 data with the original NIR values of part of the SPOT image (128 by 128 pixels) for Fort A. P. Hill

Figure 22: Pixel map of the comparisons between the low frequency wavelet reconstructed values for the 1 in 2 data with the original NIR values of part of the SPOT image (128 by 128 pixels) for Fort A. P. Hill

a)
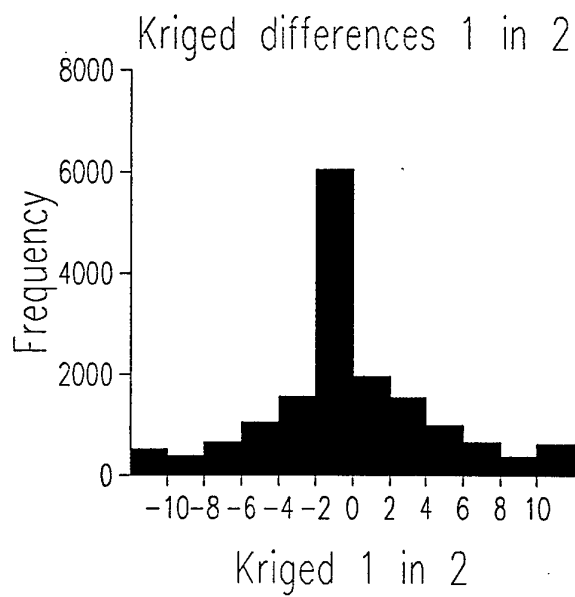
b)
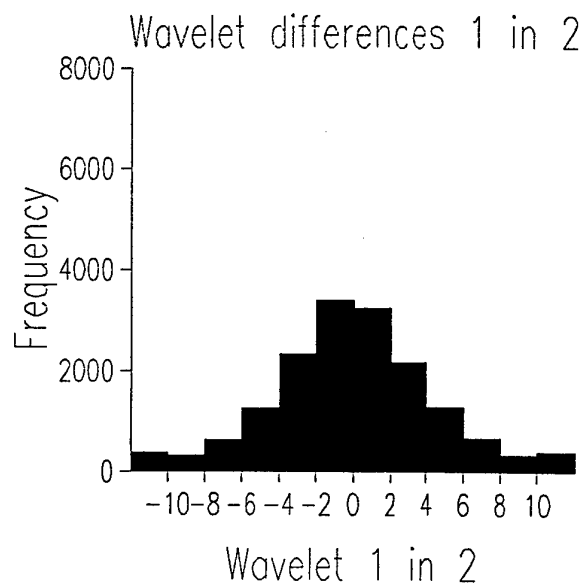
Figure 23: Histograms of a) the kriged errors and b) the wavelet errors for the 1 in 2 sampling for NIR of part of the SPOT image (128 by 128 pixels) for Fort A. P. Hill

reconstruction. However, compared to the number of pixels in the data these larger differences are few compared with the many much smaller differences for the majority of the estimates.

To explore the reasons for the results in more detail the histograms of the differences were examined. Figure 23 a and b are the histograms of the differences for the wavelet and kriging analyses, respectively. It is clear that punctual kriging, which is a true estimator at the data points has a larger number of small errors than the wavelet analysis. However, this is not consistent as the number of data points retained is reduced.

Sample of 1 in 4

Figure 24 shows the result of kriging this sub-sample. It is evident that much of the short-range variation has been lost even though the variogram of the full data set was used. This map is similar to that for the long-range component. The map of the low frequency reconstruction, Figure 25, shows more of the short-range variation and appears to be much more accurate visually than the kriged map. The maps of the differences, Figures 26 and 27, appear to be similar overall, but closer examination shows that the patches where the differences are large for kriging are more extensive than those for the wavelet analysis. The values of the MSEs for kriging and the wavelet analysis in Table 7 also suggest that kriging performs worse than wavelets. The histograms, Figure 28 a (kriging) and b (wavelets), suggest that more of the kriged values have smaller differences from the original values than those for the wavelet reconstruction. However, the number of large errors is also greater for the kriged values.

Sample of 1 in 8

Figure 29 shows the result of kriging this sub-sample. It is evident that much more of the detail in the variation has been lost. The pattern that is returned is coarse and no longer reflects even the long-range component of the variation as accurately. Figure 30 for the low frequency reconstruction from the wavelet analysis also shows how the detail has been lost. The maps of the differences, Figures 31 and 32 are again similar, but as before where the differences are greatest for the kriged differences (Figure 30) so their extent is also more extensive. It seems from the MSEs Table 7 that as the data become more sparse and separated by greater distances that kriging loses power in comparison with the wavelet analysis. The histograms, Figure 33 a (kriging) and b (wavelets), suggest that the wavelet analysis has performed better with this sub-set of the data. In the central part of the distribution there is little difference between the differences for wavelet analysis and kriging, but there seem to be many more large errors for kriging than the wavelets.
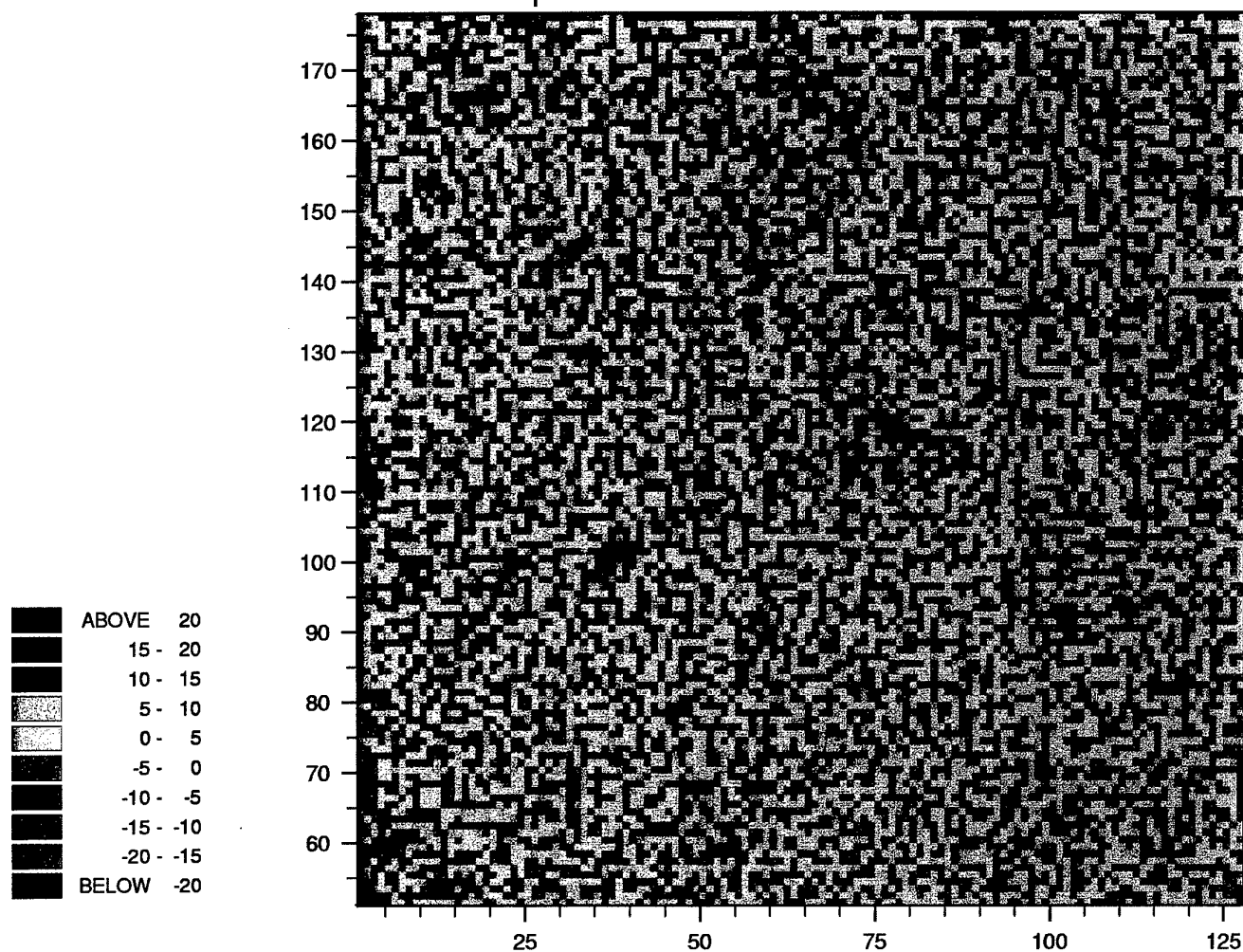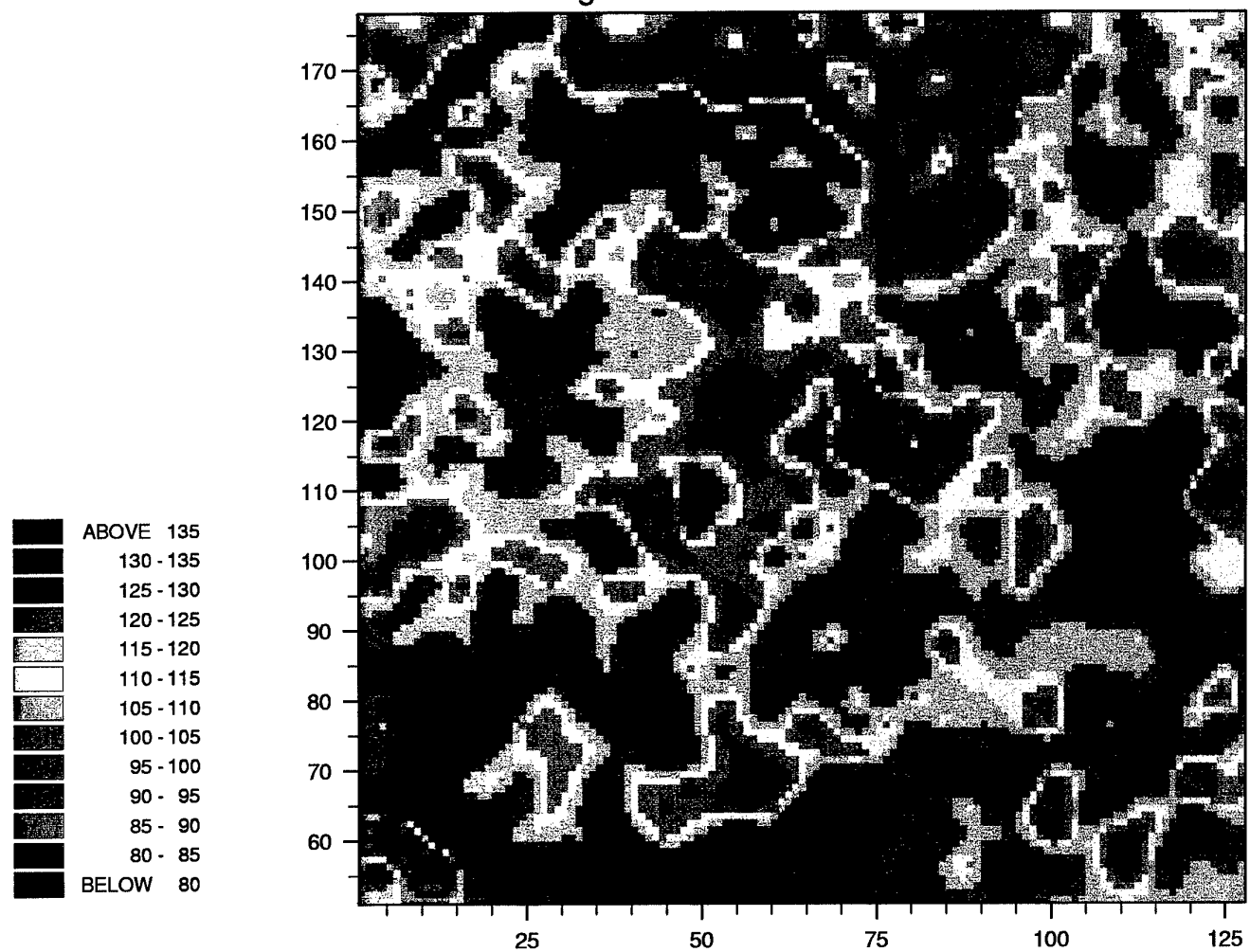
Figure 24: Pixel map of the kriged estimates for the 1 in 4 sample of NIR of part of the SPOT image (128 by 128 pixels) for Fort A. P. Hill

Wavelet reconstruction for 1 in 4 selection

ABOVE 135
130 - 135
125 - 130
120 - 125
115 - 120
110 - 115
105 - 110
100 - 105
95 - 100
90 - 95
85 - 90
BELOW 85
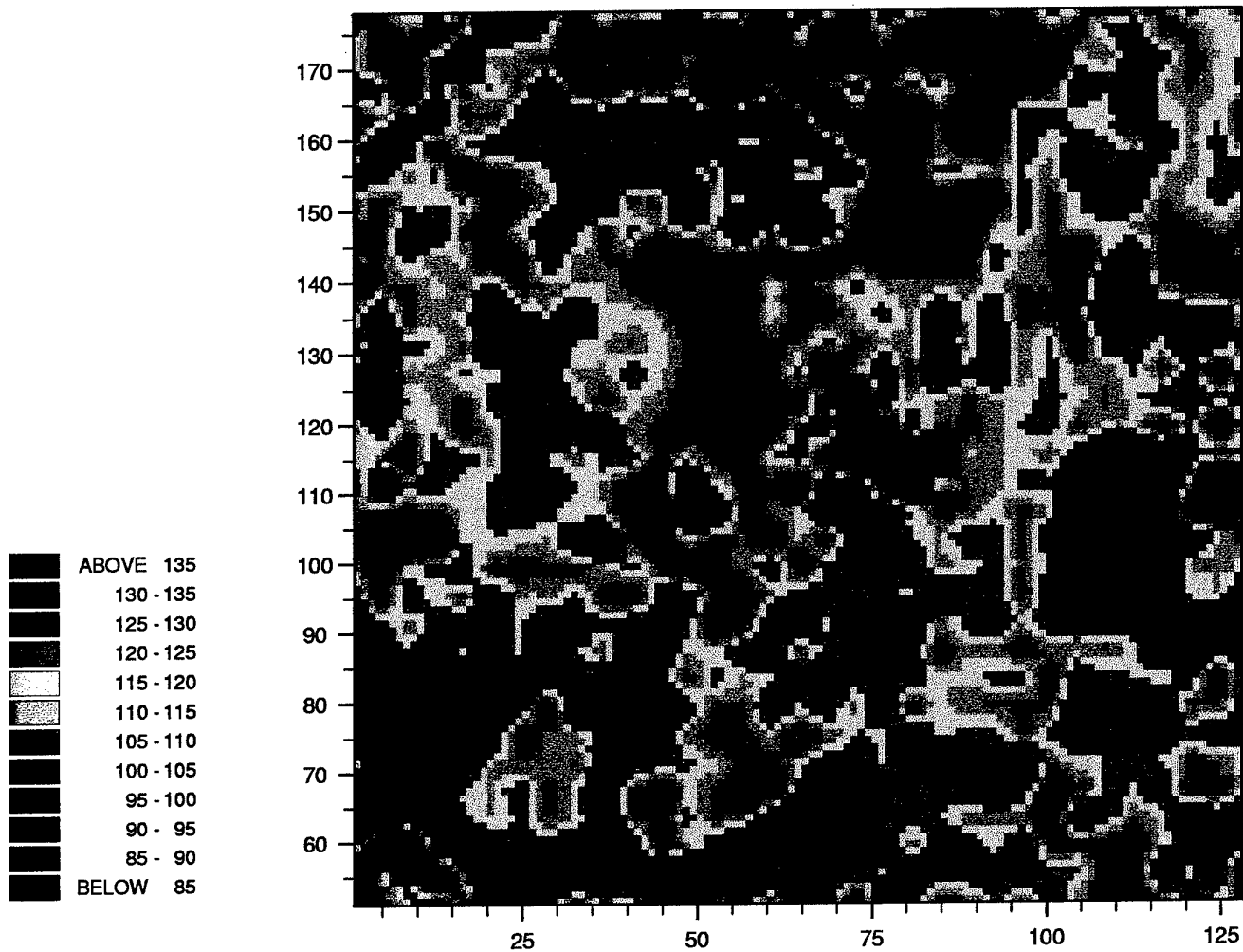
Figure 25: Pixel map of the low frequency reconstruction from the wavelet analysis of NIR of part of the SPOT image (128 by 128 pixels) for Fort A. P. Hill at a resolution of 1 in 4

Figure 26: Pixel map of the comparisons between the kriged estimates for the 1 in 4 data with the original NIR values of part of the SPOT image (128 by 128 pixels) for Fort A. P. Hill
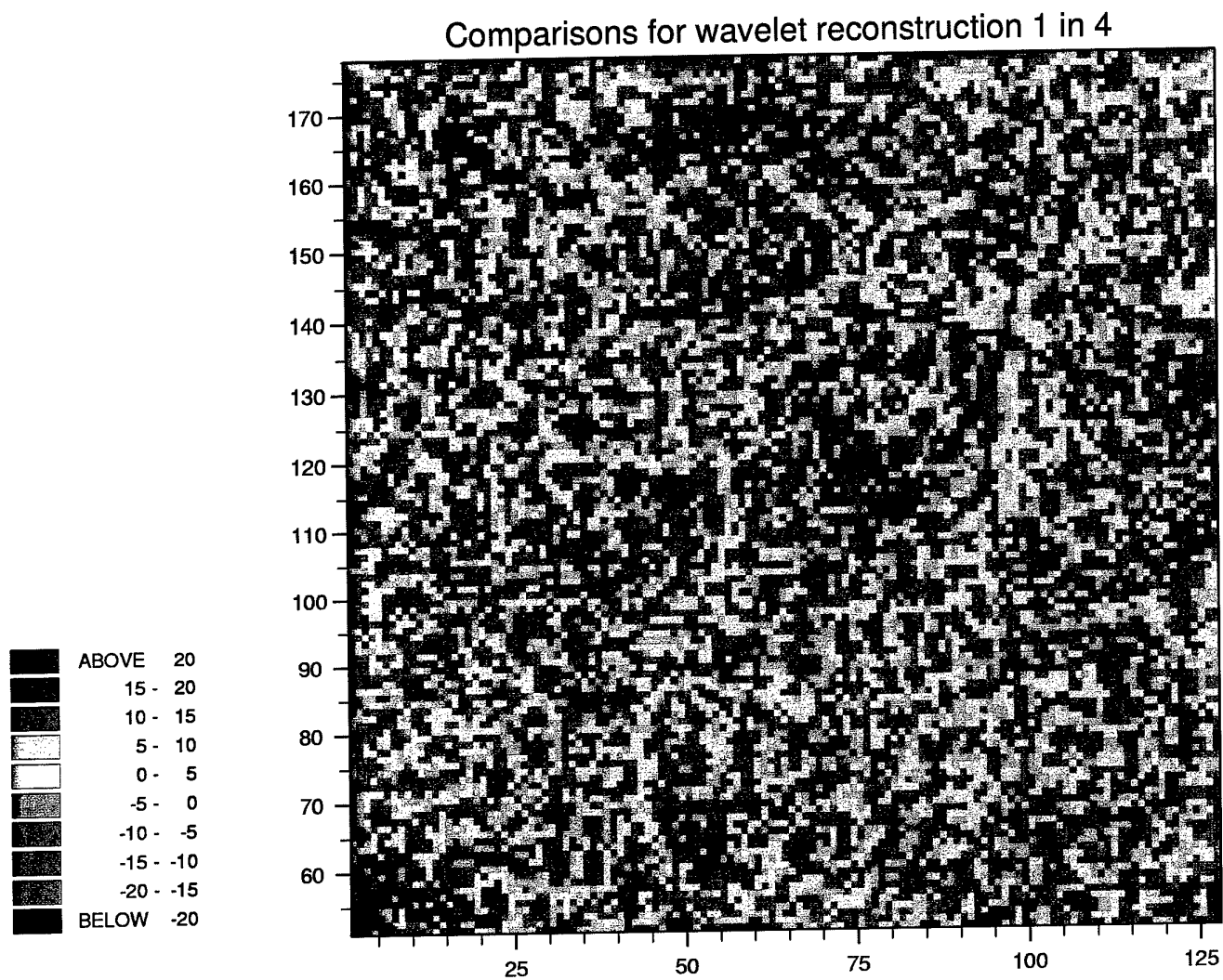
Figure 27: Pixel map of the comparisons between the low frequency wavelet reconstructed values for the 1 in 4 data with the original NIR values of part of the SPOT image (128 by 128 pixels) for Fort A. P. Hill

a)

b)
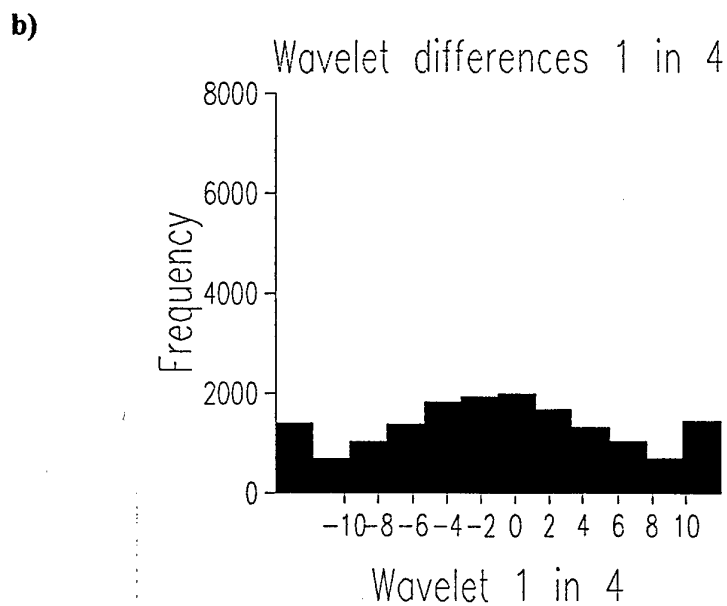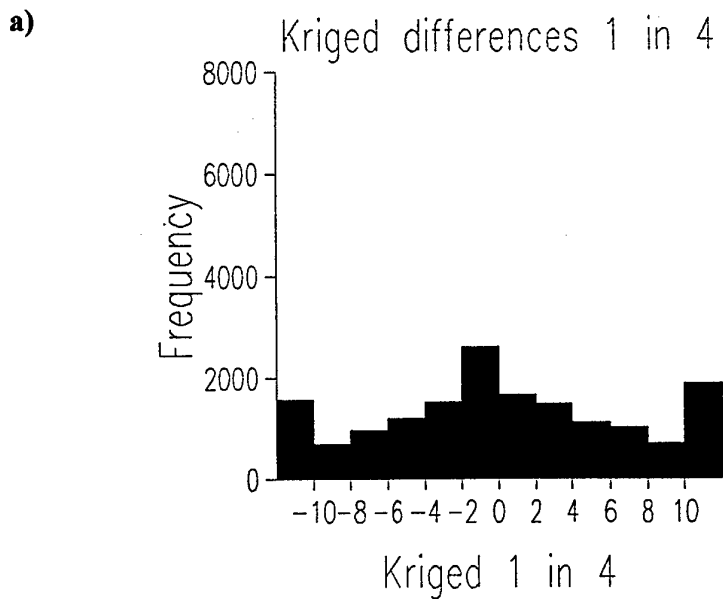
Figure 28: Histograms of a) the kriged errors and b) the wavelet errors for the 1 in 4 sampling for NIR of part of the SPOT image (128 by 128 pixels) for Fort A. P. Hill

Kriged estimates for 1 in 8 selection
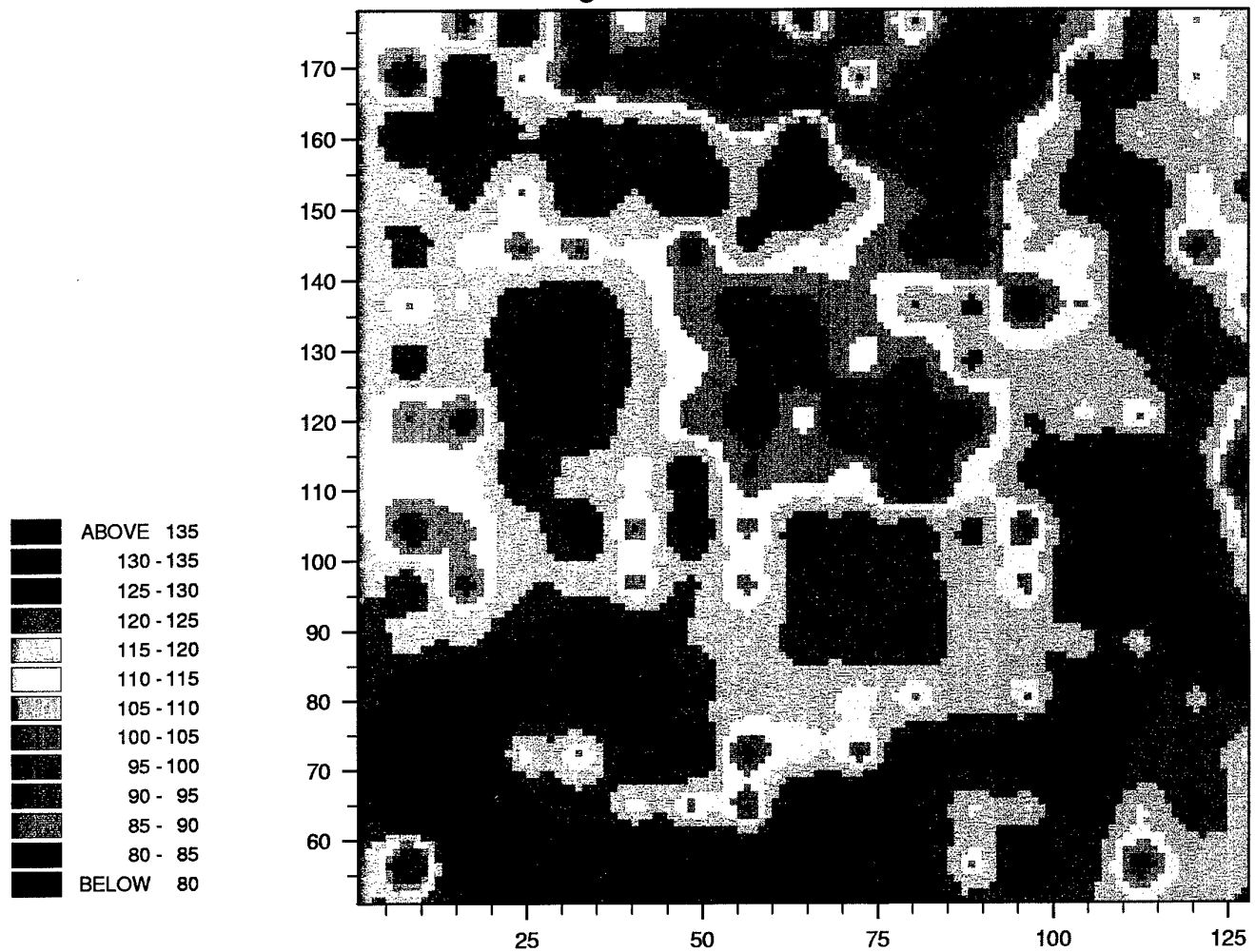
Figure 29: Pixel map of the kriged estimates for the 1 in 8 sample of NIR of part of the SPOT image (128 by 128 pixels) for Fort A. P. Hill

Figure 30: Pixel map of the low frequency reconstruction from the wavelet analysis of NIR of part of the SPOT image (128 by 128 pixels) for Fort A. P. Hill at a resolution of 1 in 8

Comparisons for kriged estimates 1 in 8
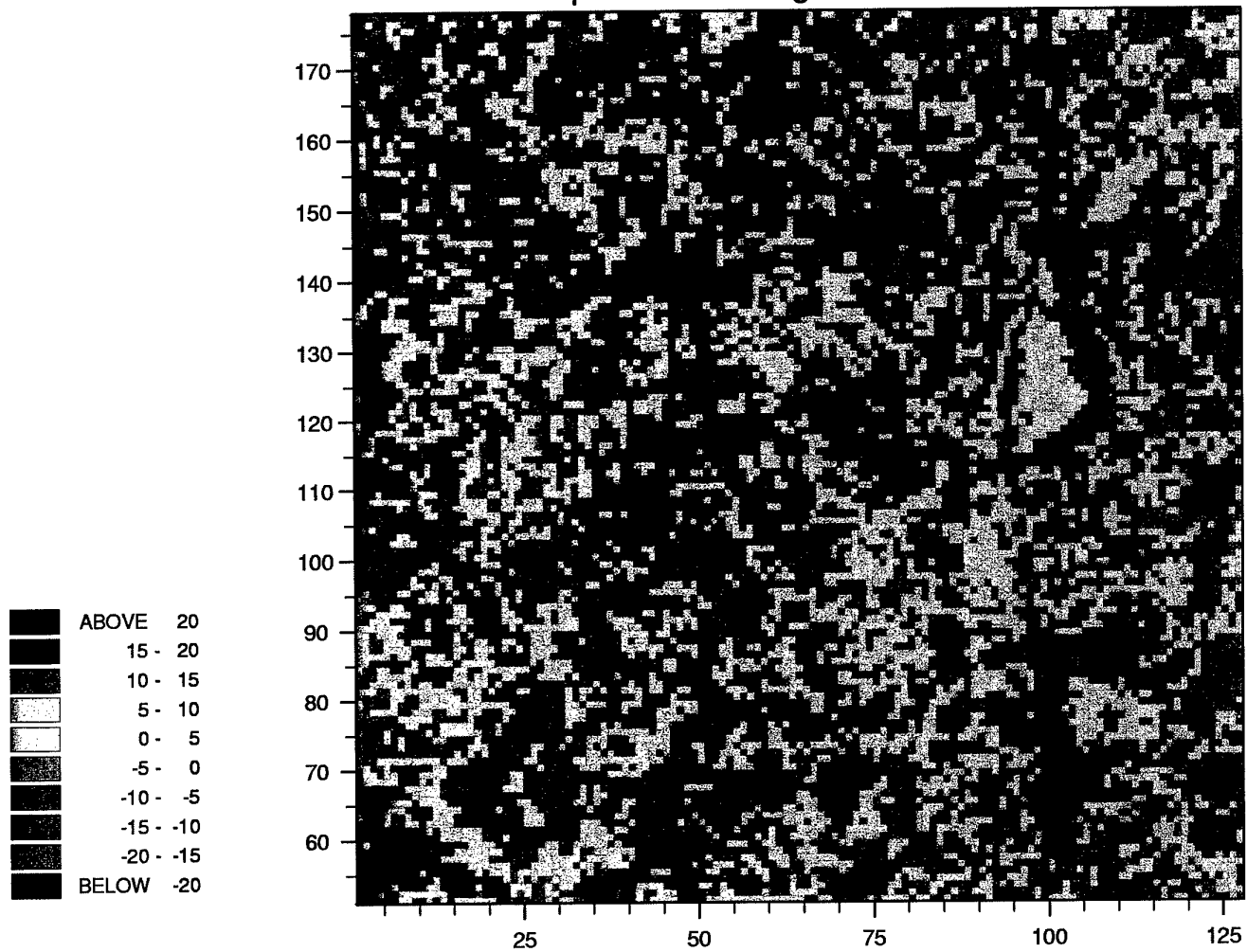
Figure 31: Pixel map of the comparisons between the kriged estimates for the 1 in 8 data with the original NIR values of part of the SPOT image (128 by 128 pixels) for Fort A. P. Hill
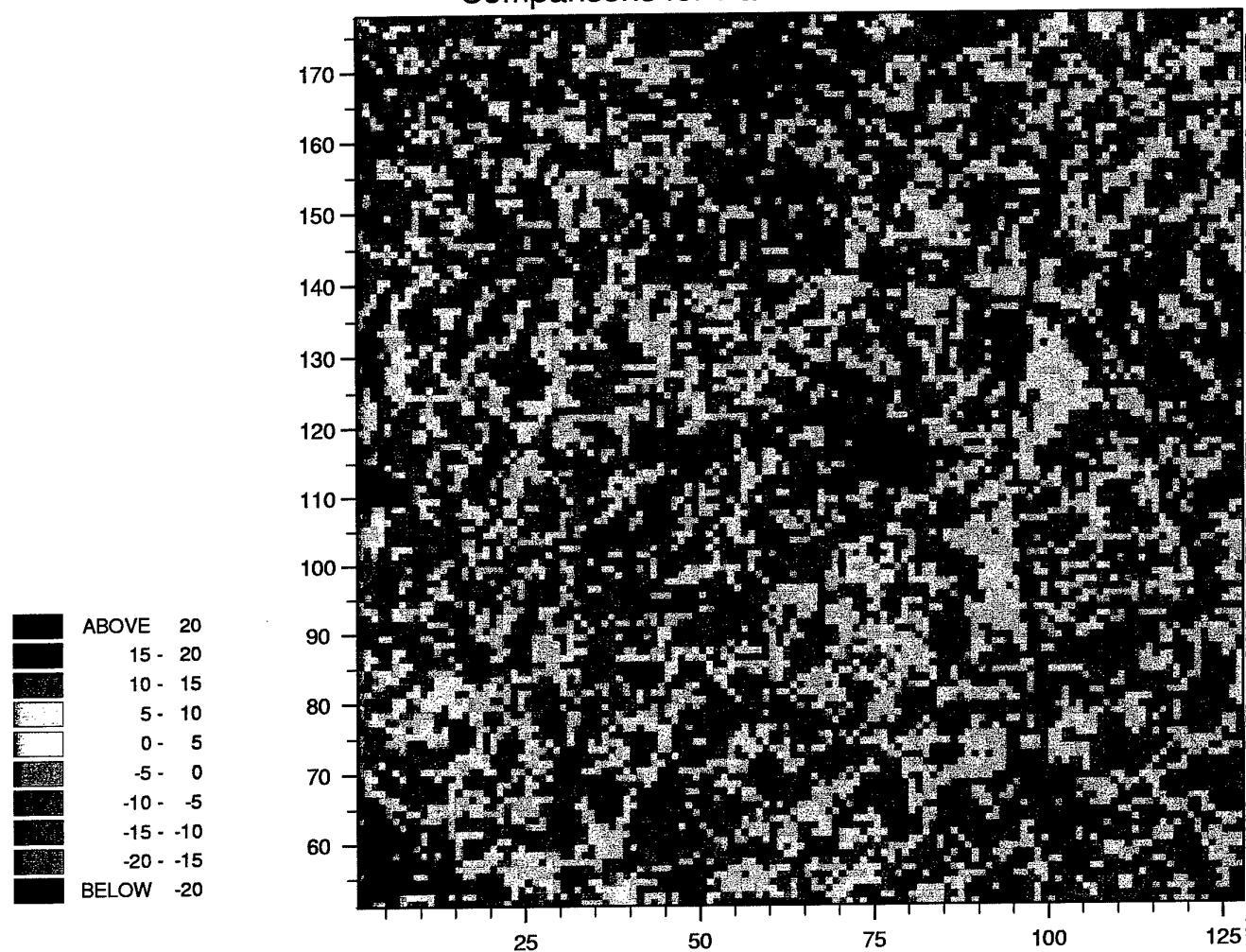
Figure 32: Pixel map of the comparisons between the low frequency wavelet reconstructed values for the 1 in 8 data with the original NIR values of part of the SPOT image (128 by 128 pixels) for Fort A. P. Hill

a)
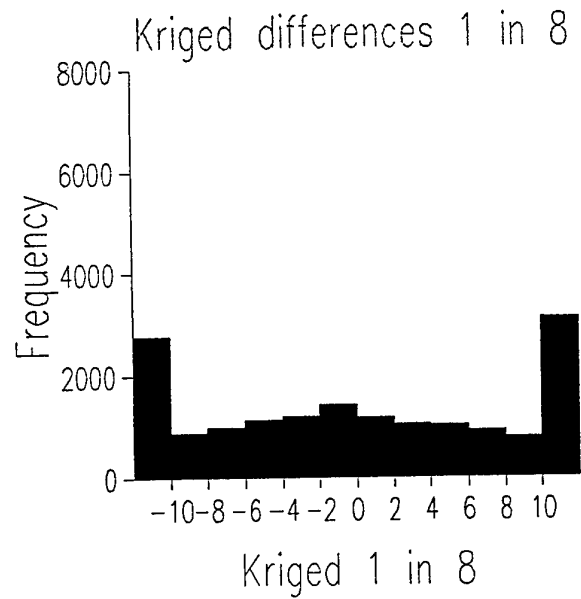
b)
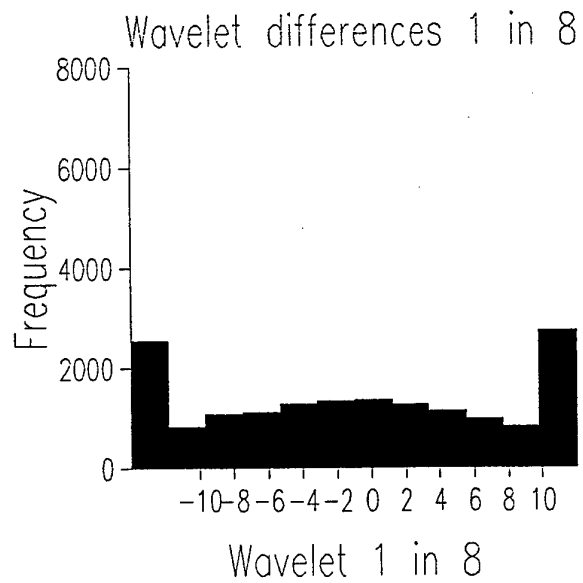
Figure 33: Histograms of a) the kriged errors and b) the wavelet errors for the 1 in 8 sampling for NIR of part of the SPOT image (128 by 128 pixels) for Fort A. P. Hill

58

Summary

The histograms of the differences are perhaps the most illuminating part of this analysis. It seems that we need to explore more, but that kriging performs well when fewer data have been removed than the wavelet analysis. It also suggests that the end-user can be provided with some insight to enable them to choose which is appropriate for their needs. It seems that for the 1 in 2 and 1in 4 data sub-sets more of the errors are small for kriging than for wavelets, but that the overall error is least for the wavelet analysis. The latter is clearly more successful at retaining the transition features present which kriging will not do well. Again what does the end user want?

Another thing that seems to emerge from this investigation is that the variogram could be used to choose an optimal subset of the data, based on the distance between the values. With the 1 in 2 sample both the long-range and short-range components of the variation were restored as we should expect from the correlation structures in the variogram: the distance between the pixels was less than the range of the short-range component. With the 1 in 4 sample only the long-range structure is successfully restored. If that is what is required then this can be chosen in a way that is driven by the data using the variogram.

It is interesting to note that the means of the kriged reconstructed values, Table 7, are close in each case to the mean of the original data, Table 5. The variances for the kriged values decrease as the sampling intensity decreases and is evidence of the smoothing of the variation that occurs with kriging. However, the variance of the kriged values for the 1 in 2 sample is closer to the original variance than any of the other analyses. The wavelet analysis retains the variance better as the sampling intensity decreases. Geostatistical simulation would probably perform even better in terms of retaining the variance in the data and this method should also be compared with wavelet analysis in the future.

Table 7: Summary values from comparisons between the restored values and the original values using kriging and wavelets

Data sub-sets	Mean difference (error)	Mean squared error (MSE)	Mean of reconstructed values	Variance of reconstructed values
1 in 2 (K) sub-sample	-0.0698	28.361	117.76	235.64
1 in 4 (K) sub-sample	-0.3017	87.122	117.53	196.97
1 in 8 (K) sub-sample	0.0627	159.78	117.89	114.20
1 in 2 (W) sub-sample	-0.0959	23.068	122.77	192.99
1 in 4 (W) sub-sample	0.0000	67.860	117.83	210.13
1 in 8 (W) sub-sample	0.0000	128.74	117.83	140.25

Part IV: The analysis of the vegetation surveys and comparisons with the SPOT data

Introduction

In this section the vegetation surveys and analyses will be described. It covers the analysis of the quantitative data from surveys 1 and 2, some parts of these data sets have been combined, and the qualitative data for surveys 2 and 4. The analysis of survey 3 was included in the final report for the previous contract (Contract N68171-97-C-9029).

Quantitative Surveys 1 and 2

Survey 1 was carried out in 1997 at A. P. Hill. The sample comprises several small transects that have random starting positions within the seven strata of the training areas. The plot size corresponded with the SPOT pixel size of 20 m by 20 m. The points along the transects were at 100 m intervals (see Figure 34). This survey mainly embraced either hard or soft woodland areas of vegetation. The second survey was a square grid with an interval of 300 m covering the whole of our study site at A. P. Hill (Figure 35). Since there were many sites without quantitative woodland information, because it included grassland, buildings and hard standing, the sites with quantitative information were analysed with the data from the first survey.
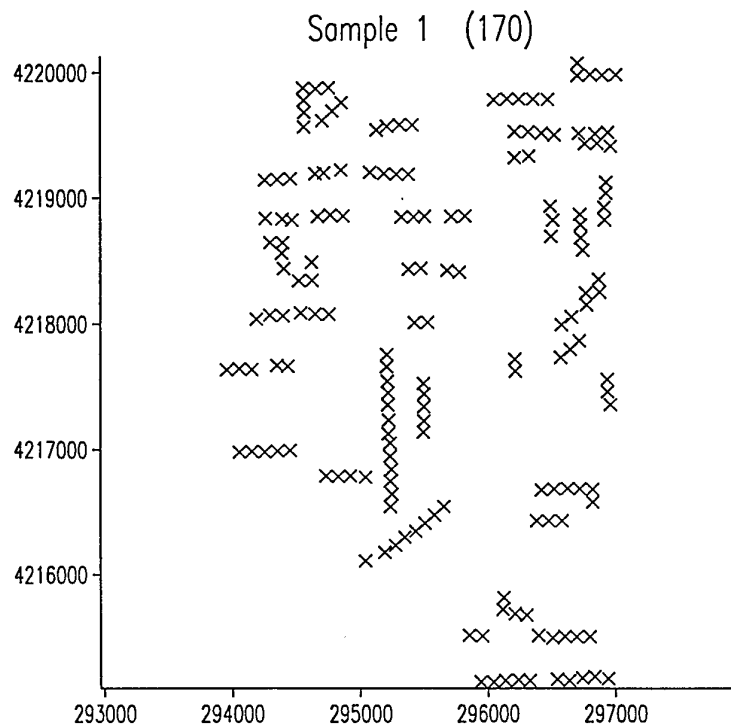
Figure 34: Map of sites for Survey 1.
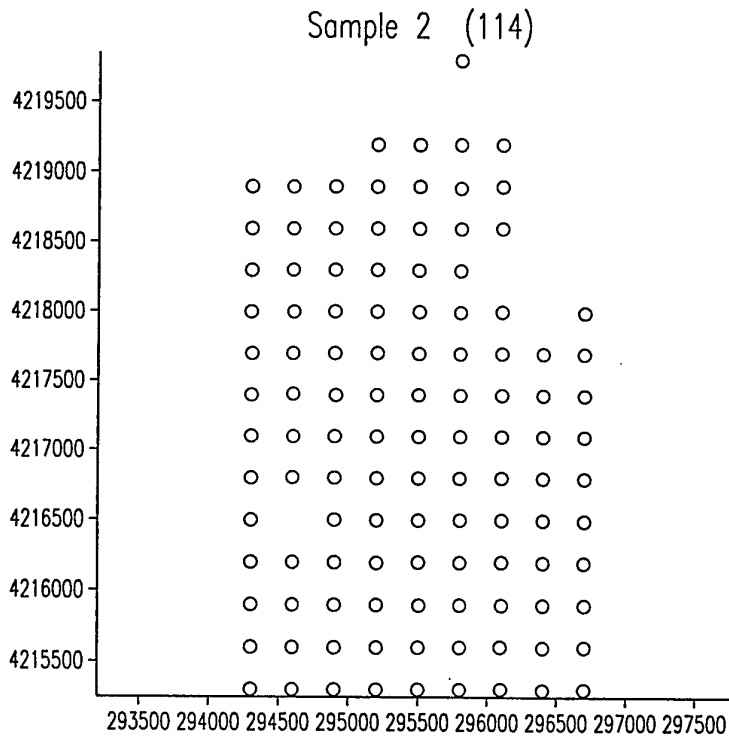
Figure 35: Map of sites for Survey 2.

Exploratory data analysis

The summary statistics of the 17 quantitative variables were analysed for surveys 1 and 2 separately. They are given in Tables 8 and 9. The skewness values are generally small showing that the statistical distribution does not depart seriously from normal, except for stem spacing (survey 1). This variable had one extreme value which was removed to obtain a near-normal distribution for the variogram analysis. Figures 36 and 37 show the histograms of the variables listed below for survey 1. The digital numbers for the three wavebands of the SPOT image that coincided with sites where the vegetation had been examined were also extracted and their summary statistics are given in Table 10 for both surveys. Their histograms are shown in Figure 38.

Variables analysed and their abbreviation:

This part of the list contains those variables related to forest density (Set A):

maxcc - maximum range of visual estimate of crown closure (%)
ovstmin - minimum range of overstory height (ft)

ovstmax - mamimum range of overstory height (ft)
undstmn - minimum range of understory height (ft)
undstmx - maximum range of understory height (ft)
ba_f - estimate of basal area per hectare (metric units)
stem - total stems in plot (count)
ba_tot - sum of all basal area for each tree per plot (square metres)
stemsp - average minimum distance between stems within each plot (metres)

This part of the list contains those variables related to tree species (Set B):

ba_so - percentage of total basal area that is softwood in each plot
ba_ha - percentage of total basal area that is hardwood in each plot
stem_so - percentage of total number of stems that are softwood in each plot
stem_ha - percentage of total number of stems that are hardwood in each plot
bad_so - percentage of dominant basal area that is softwood in each plot
bad_ha - percentage of dominant basal area that is hardwood in each plot
stemd_so - percentage of dominant number of stems that are softwood in each plot
stemd_ha - percentage of dominant number of stems that are hardwood in each plot

Table 8: Summary statistics for vegetation measures for Survey 1

Variable	N	Missing	Mean	Median	Min	Max	Variance	Standard deviation	Skewness	Kurtosis
maxcc	169	1	67.04	70.0	0.0	100.0	543.3	23.31	-1.22	0.43
minovst	169	1	73.72	80.0	15.0	110.0	395.1	19.88	-1.19	1.18
maxovst	169	1	78.54	80.0	20.0	110.0	405.1	20.13	-1.32	1.29
minunst	169	1	11.35	10.0	0.0	30.0	33.3	5.77	0.96	2.31
maxunst	169	1	20.66	20.0	0.0	35.0	62.2	7.89	-0.70	0.28
ba_f	168	1	34.36	34.3	2.4	76.2	199.4	14.12	0.05	0.31
stem	169	1	20.44	19.0	0.0	81.0	112.9	10.62	1.96	7.01
bat_tot	169	1	1.07	1.1	0.0	2.4	0.2	0.45	0.01	0.31
stemsp	168	2	2.33	2.2	0.9	7.3	0.6	0.78	2.00	9.10
ba_so	168	2	46.16	43.5	0.0	100.0	1487.1	38.56	0.13	-1.58
ba_ha	168	2	53.54	54.5	0.0	100.0	1487.1	38.56	0.13	-1.58
stem_so	138	2	41.01	33.3	0.0	100.0	1338.9	36.59	0.33	-1.41
stem_ha	168	2	58.99	66.7	0.0	100.0	1338.9	36.59	0.33	-1.41
bad_so	168	2	48.94	46.7	0.0	100.0	1610.3	40.13	0.06	-1.64
bad_ha	168	2	51.06	54.3	0.0	100.0	1610.3	40.13	0.06	-1.64
Stemd_ so	168	2	49.14	48.8	0.0	100.0	1570.7	39.63	0.02	-1.62
Stemd_ ha	168	2	50.86	51.2	0.0	100.0	1570.7	39.63	0.02	-1.62

Table 9: Summary statistics for vegetation measures for Survey 2

Variable	N	Missing	Mean	Median	Min	Max	Variance	Standard deviation	Skewness	Kurtosis
maxcc	60	54	68.17	80.0	5.0	100.0	674.5	25.97	-0.99	-0.02
minovst	0	114	*	*	*	*	*	*	*	*
maxovst	60	54	73.75	80.0	20.0	100.0	315.8	17.77	-1.32	1.52
minunst	17	97	8.59	10.0	1.0	20.0	34.9	5.91	0.28	-1.07
maxunst	54	60	15.11	15.0	3.0	25.0	23.9	4.89	-0.07	-0.31
ba_f	58	56	32.06	34.5	3.4	57.9	175.9	13.26	-0.35	-0.73
stem	58	56	19.91	18.5	5.0	44.0	96.1	9.80	0.63	-0.29
bat_tot	58	56	1.07	1.1	0.1	1.8	0.17	0.42	-0.35	-0.73
stemsp	58	56	2.50	2.4	1.2	5.0	0.57	0.76	1.05	1.19
ba_so	58	56	57.54	63.5	0.0	100.0	1360.3	36.88	-0.31	-1.46
ba_ha	58	56	42.46	36.5	0.0	100.0	1360.3	36.88	-0.31	-1.46
stem_so	58	56	50.33	52.1	0.0	100.0	1288.4	35.89	-0.05	-1.53
stem_ha	58	56	49.67	47.9	0.0	100.0	1288.4	35.89	-0.05	-1.53
bad_so	58	56	60.87	64.9	0.0	100.0	1472.5	38.37	-0.38	-1.43
bad_ha	58	56	39.14	35.1	0.0	100.0	1472.5	38.37	-0.38	-1.43
Stemd_so	58	56	60.15	71.8	0.0	100.0	1520.1	38.99	-0.34	-1.52
Stemd_ha	58	56	39.93	28.2	0.0	100.0	1520.1	38.99	-0.34	-1.52

Table 10: Summary statistics for the three wavebands from the SPOT data for Surveys 1 and 2

Variable	N	Missing	Mean	Median	Min	Max	Variance	Standard deviation	Skewness	Kurtosis
Red (1)	116	54	61.94	61.0	58.0	80.0	14.5	3.81	2.49	7.18
Green (2)	116	54	36.33	34.0	32.0	67.0	33.56	5.79	3.17	11.71
NIR (3)	116	54	119.3	121.0	62..0	148.0	249.5	15.79	-0.55	0.57
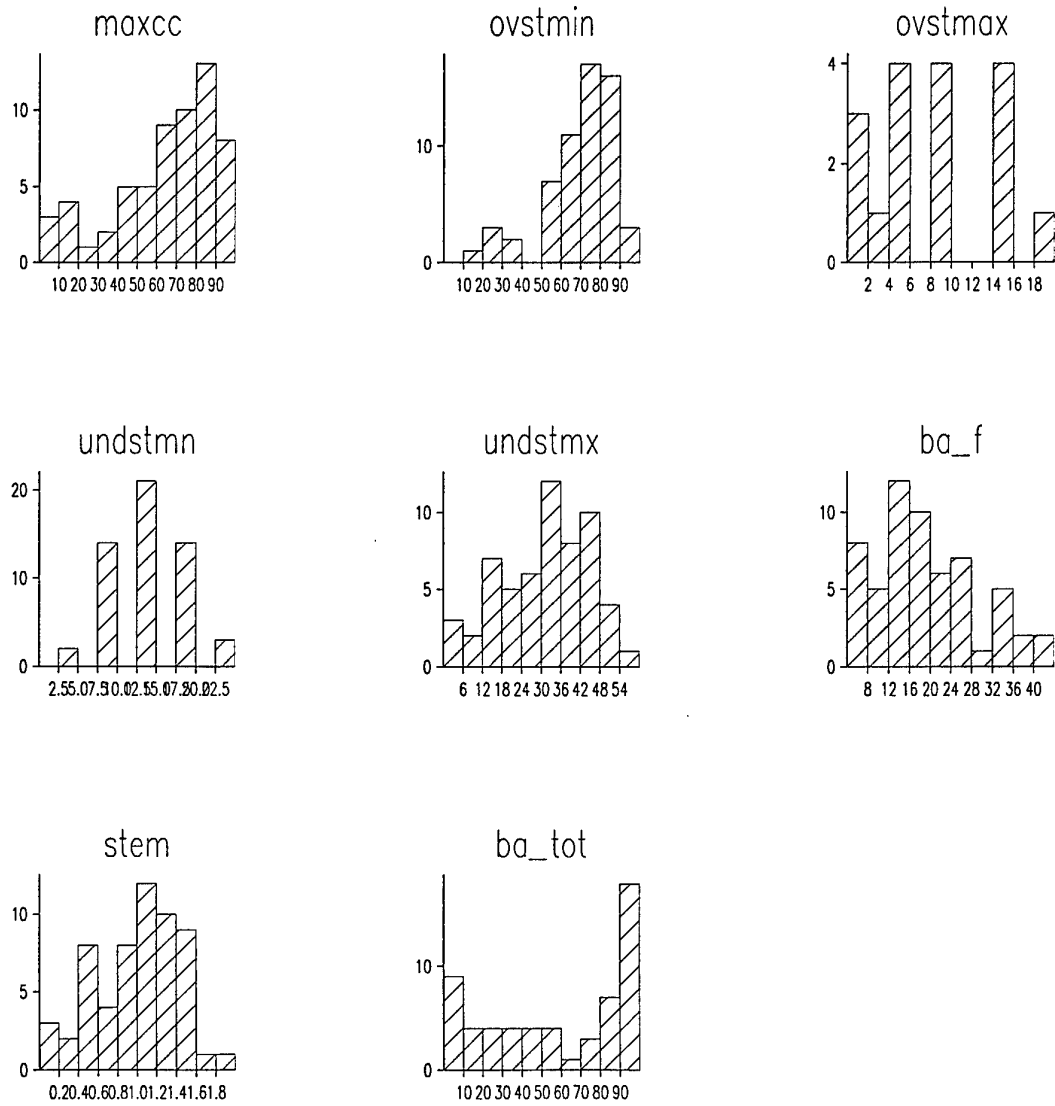
Figure 36: Histograms of variables in Set A of Survey 1.
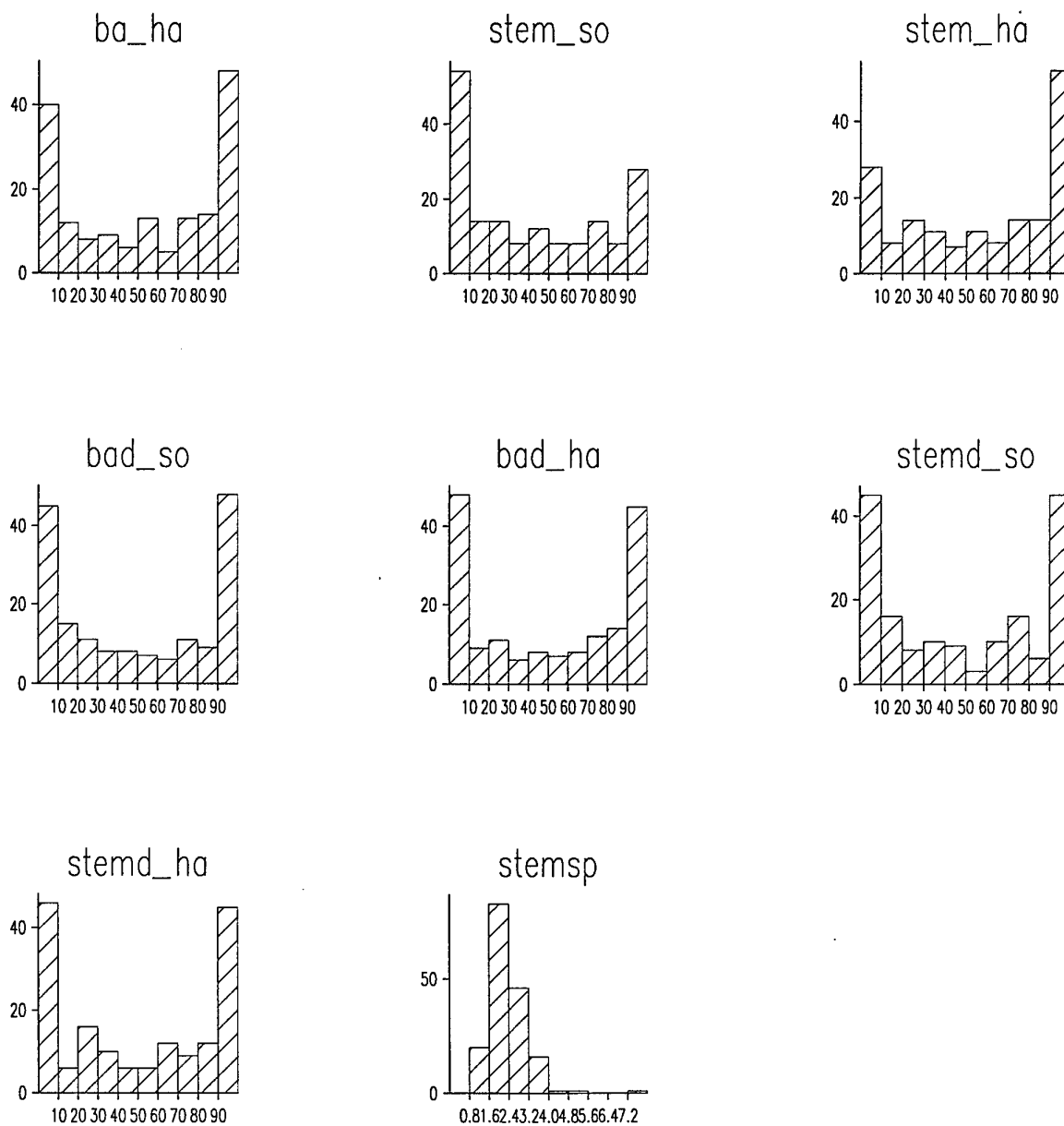
Figure 37: Histograms of variables in Set B of Survey 1.
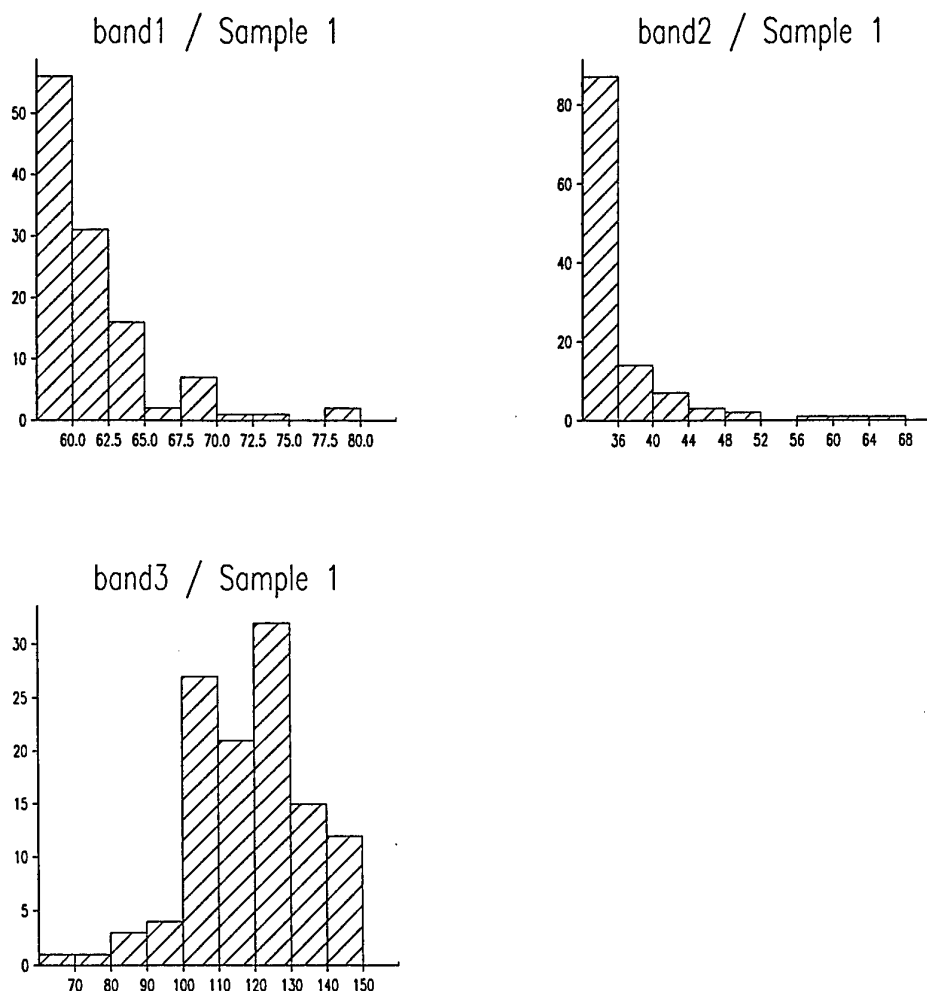
Figure 38: Histograms of wavebands 1 (Red), 2 (Green), 3 (NIR) and NDVI for sites coinciding with Surveys 1 and 2.

To assess which of these variables were likely to represent the variation the data most strongly a principal components analysis was done on the correlation matrix. The latter was used because it effectively standardizes the data. The first component accounted for 53.7% of the variation and the second 18%. The variables that 'loaded' most heavily on the first component were:

ba_so, ba_ha, stem_so, stem_so, stem_ha, bad_so, bad_ha, stemd_so and stem_ha.

The variables that 'loaded' most heavily on the second component were:

maxcc, ba_f, stem, ba_tot and stemsp.

A set of variables that is considered to express the variation and summarise it adequately is:

maxcc, ba_f, stem, stemsp, ovstmax, undstmx and ba_so.

These are based on the distribution of the variables in the plane of PC1 and PC2 (Figure 39).
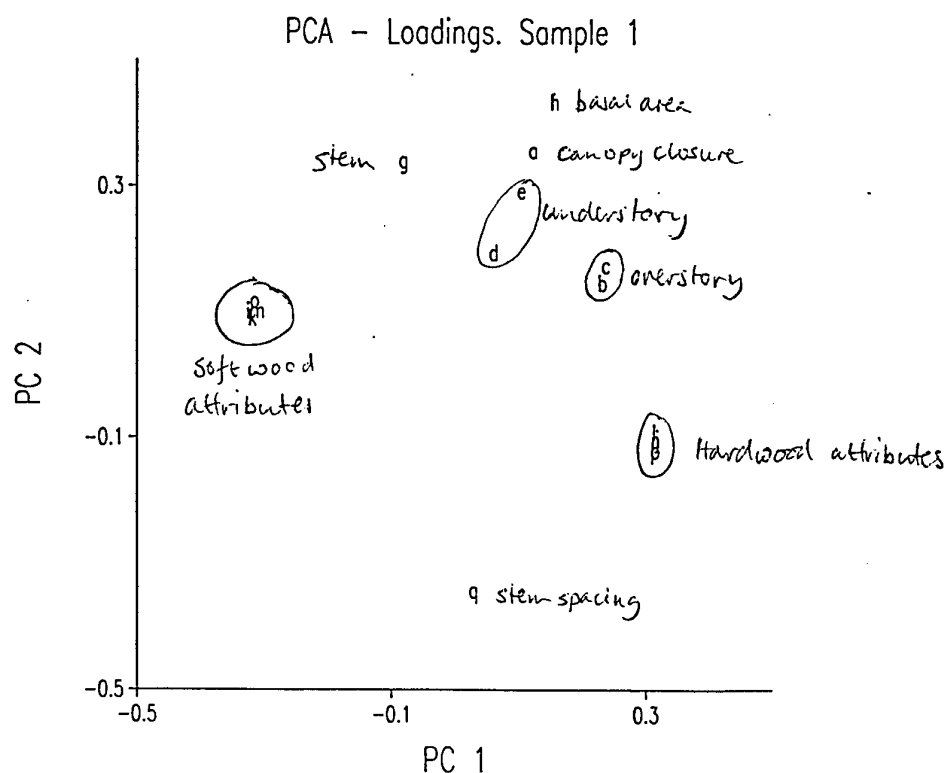
Figure 39: Plot of variables based on their loadings in the plane of PC1 and PC2.

Table 11 gives the correlations for the vegetation measures and the DNs of the wavebands. In general these are small for the vegetation measures and DNs. Those for NIR are the largest for maxcc, stem_so, ste_ha, stemd_so and stem_ha. There are some strong correlations for the vegetation measure which are to be expected, for example ba_so and ba_ha which add to 100%.

Table 11. Correlations for the vegetation measures and the three wavebands from the SPOT image.

```
*** Correlation matrix ***
     band1    1.000
     band2    0.960    1.000
     band3   -0.205   -0.308    1.000
        cc    0.023    0.017    0.227    1.000
    ovstmin   0.036    0.018    0.178    0.205    1.000
    ovstmax   0.030    0.021    0.198    0.237    0.956    1.000
    undstmn  -0.148   -0.113    0.076    0.145    0.196    0.217    1.000
    undstmx   0.073    0.080    0.099    0.260    0.427    0.487    0.515
       ba_f   0.179    0.177    0.087    0.518    0.557    0.594    0.141
       stem   0.081    0.098   -0.021    0.474   -0.346   -0.306    0.021
     ba_tot   0.178    0.177    0.087    0.518    0.557    0.594    0.141
      ba_so   0.005   -0.005   -0.182   -0.260   -0.596   -0.625   -0.014
      ba_ha  -0.005    0.005    0.182    0.260    0.596    0.625    0.014
    stem_so   0.004    0.010   -0.224   -0.230   -0.676   -0.687   -0.053
    stem_ha  -0.004   -0.010    0.224    0.230    0.676    0.687    0.053
     bad_so   0.002   -0.015   -0.158   -0.276   -0.541   -0.572    0.007
     bad_ha  -0.002    0.015    0.158    0.276    0.541    0.572   -0.007
    stemd_so  0.000   -0.006   -0.211   -0.274   -0.547   -0.568    0.009
    stemd_ha  0.000    0.006    0.211    0.274    0.547    0.568   -0.009
     stemsp  -0.007   -0.033   -0.030   -0.456    0.182    0.136   -0.015

             band1    band2    band3       cc  ovstmin  ovstmax  undstmn


    undstmx   1.000
       ba_f   0.396    1.000
       stem  -0.014    0.260    1.000
     ba_tot   0.396    1.000    0.260    1.000
      ba_so  -0.146   -0.385    0.267   -0.385    1.000
      ba_ha   0.146    0.385   -0.267    0.385   -1.000    1.000
    stem_so  -0.207   -0.385    0.309   -0.385    0.941   -0.941    1.000
    stem_ha   0.207    0.385   -0.309    0.385   -0.941    0.941   -1.000
     bad_so  -0.116   -0.376    0.243   -0.376    0.990   -0.990    0.894
     bad_ha   0.116    0.376   -0.243    0.376   -0.990    0.990   -0.894
    stemd_so -0.121   -0.349    0.269   -0.349    0.972   -0.972    0.939
    stemd_ha  0.121    0.349   -0.269    0.349   -0.972    0.972   -0.939
     stemsp  -0.174   -0.302   -0.660   -0.302   -0.122    0.122   -0.189

             undstmx     ba_f     stem   ba_tot    ba_so    ba_ha  stem_so


    stem_ha   1.000
     bad_so  -0.894    1.000
     bad_ha   0.894   -1.000    1.000
    stemd_so -0.939    0.966   -0.966    1.000
    stemd_ha  0.939   -0.966    0.966   -1.000    1.000
     stemsp   0.189   -0.076    0.076   -0.137    0.137    1.000

             stem_ha   bad_so   bad_ha stemd_so stemd_ha   stemsp
```

Variogram analysis

Experimental variograms were computed for all of the variables listed above for the combined data from surveys 1 and 2. Variograms were computed in four directions at the outset, but the number of sites is marginal for this. For set A variables the directions of maximum and minimum variation are not consistent, but for set B variables the variation in direction NNE to SSW (o) have the longest range of spatial dependence and the largest sill variances and those at right angles have the shortest ranges and the smaller sill variances (*) (Figures 40 and 41).

Figures 42 and 43 show the experimental omnidirectional variograms for the two sets of variables from surveys 1 and 2. Those that show reasonable spatial structure are: maxcc, ovstmin, ovstmax, undstmn, stem, ba_so, ba_ha, stem_so, stem_ha, bad_so, bad_ha, stemd_so and stemd_ha. For the twin variables, such as ba_so and ba_ha the variograms are identical for the reasons given earlier. The following variables were modelled: maxcc, overstory height (derived from ovstmin and ovstmax), understory height (derived from undstmn and undstmx), ba_f, stem, stem spacing, ba_so (equivalent to ba_ha also), stem_so, bad_so and stemd_so. In addition the multivariate variogram from this analysis was computed and modelled, also elevation, and the three wavebands and NDVI. They are shown in Figures 44 to 47.

Table 12 gives the model parameters of the variables modelled. The experimental variograms of many of the properties in Table 12 are somewhat erratic. This could be related to the irregular sampling scheme. However, there appears to be some evidence of periodicity in several variograms with wavelengths of between 500 m and 700 m. A previous report that contained transects of the pixels to match the vegetation ones also showed periodicity in the DNs. There appears to be some relation between the range of spatial dependence of elevation and several of the vegetation measures. The multivariate variogram has identified a short range component of variation of just over 300 m which matches with the short range component of NIR. The variograms of the vegetation classes are described later in this report. The models fitted to directional variograms of ba_so are revealing: the variation in direction 135° is 462 m and that in direction 45° is 1271 m. This suggests that the different ranges might reflect some anisotropy in the variation. This was identified in the image data, but because the sill heights were different this signalled zonal anisotropy which cannot be corrected simply. It suggests that there are distinct strata present and this is evident from the areas with different kinds of vegetation. There are also distinct landscape units which will be explored in the next report.
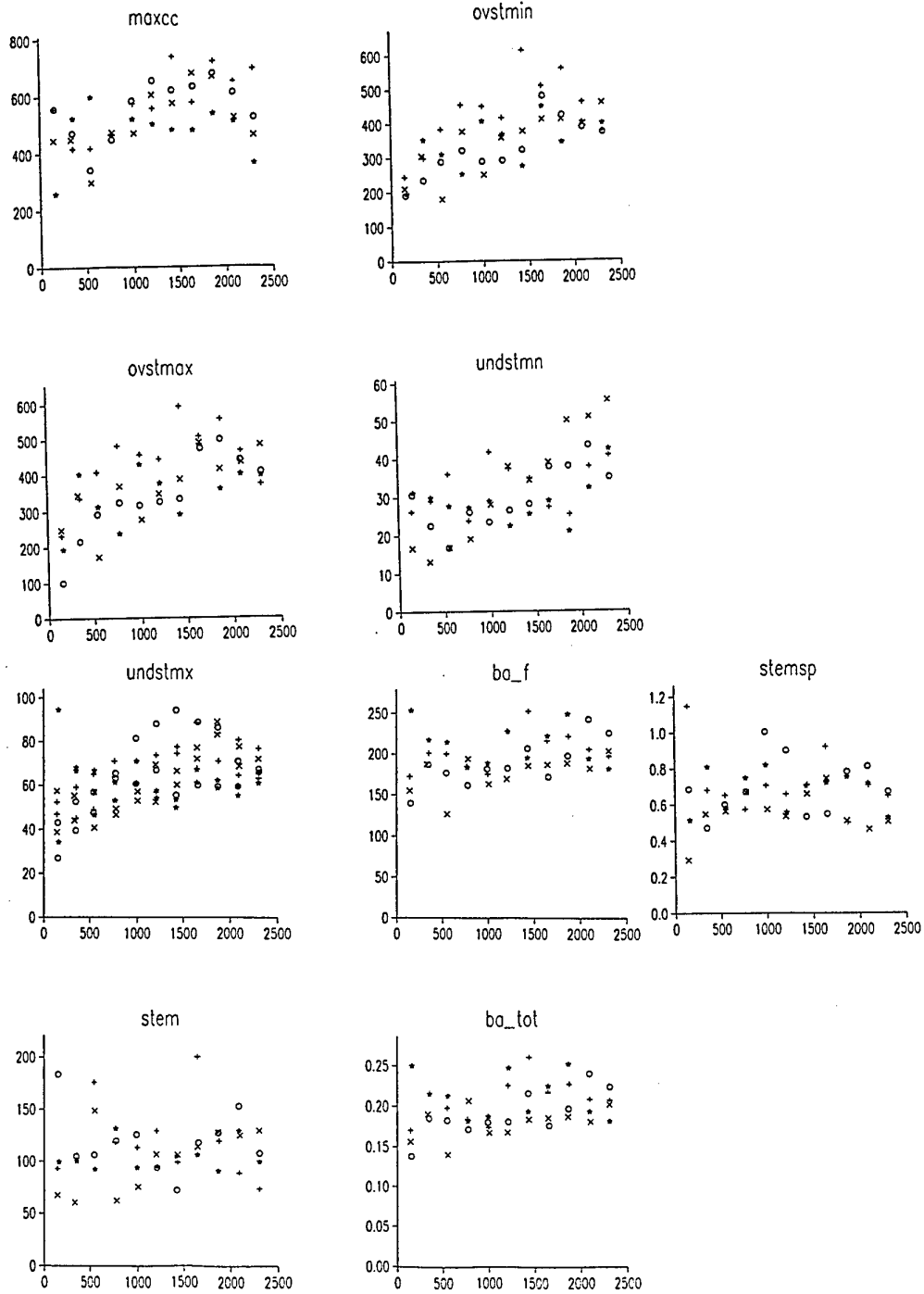
Figure 40: Directional experimental variograms for Set A variables for Surveys 1 and 2.
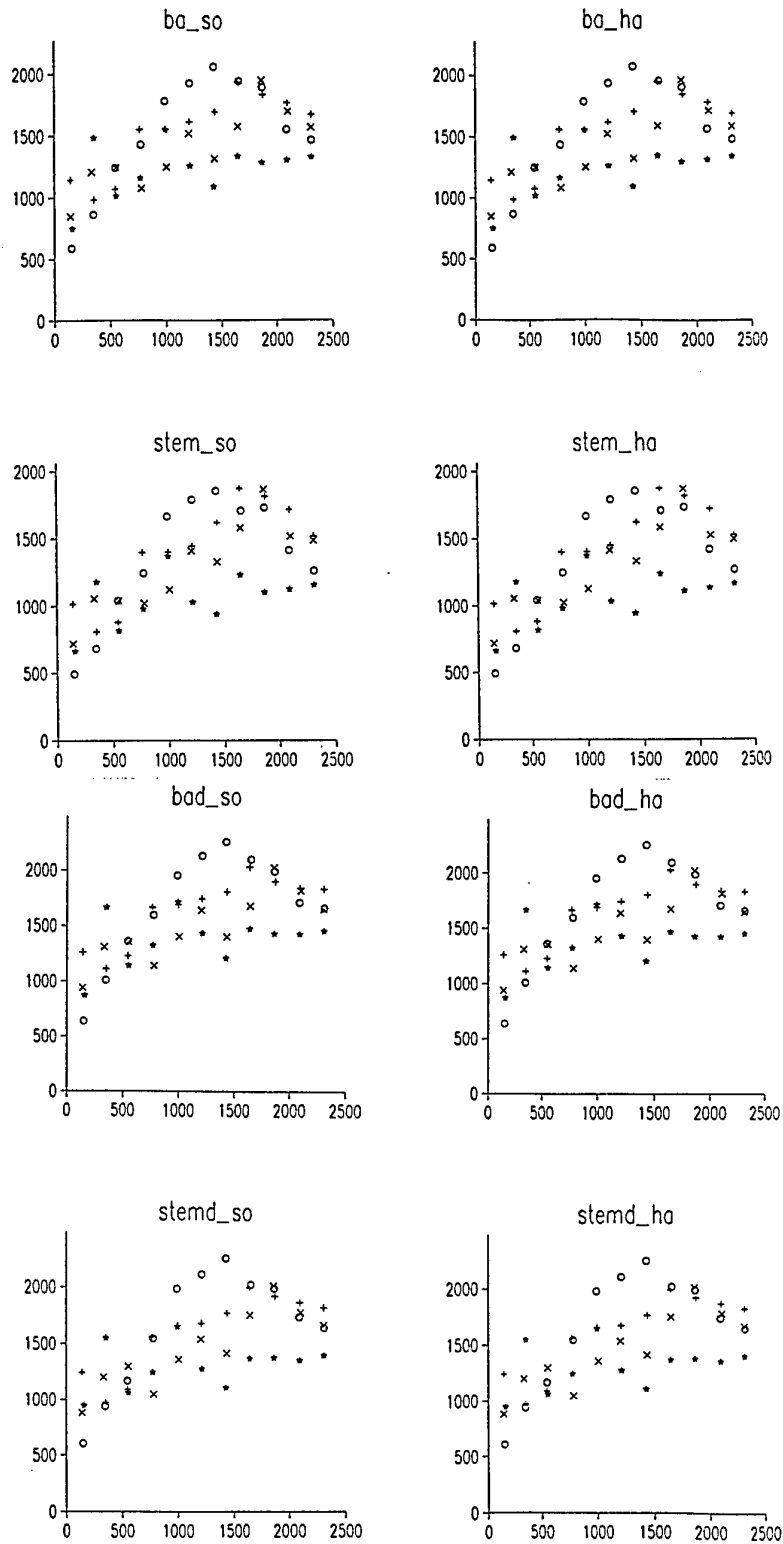
Figure 41: Directional experimental variograms for Set B variables for Surveys 1 and 2.
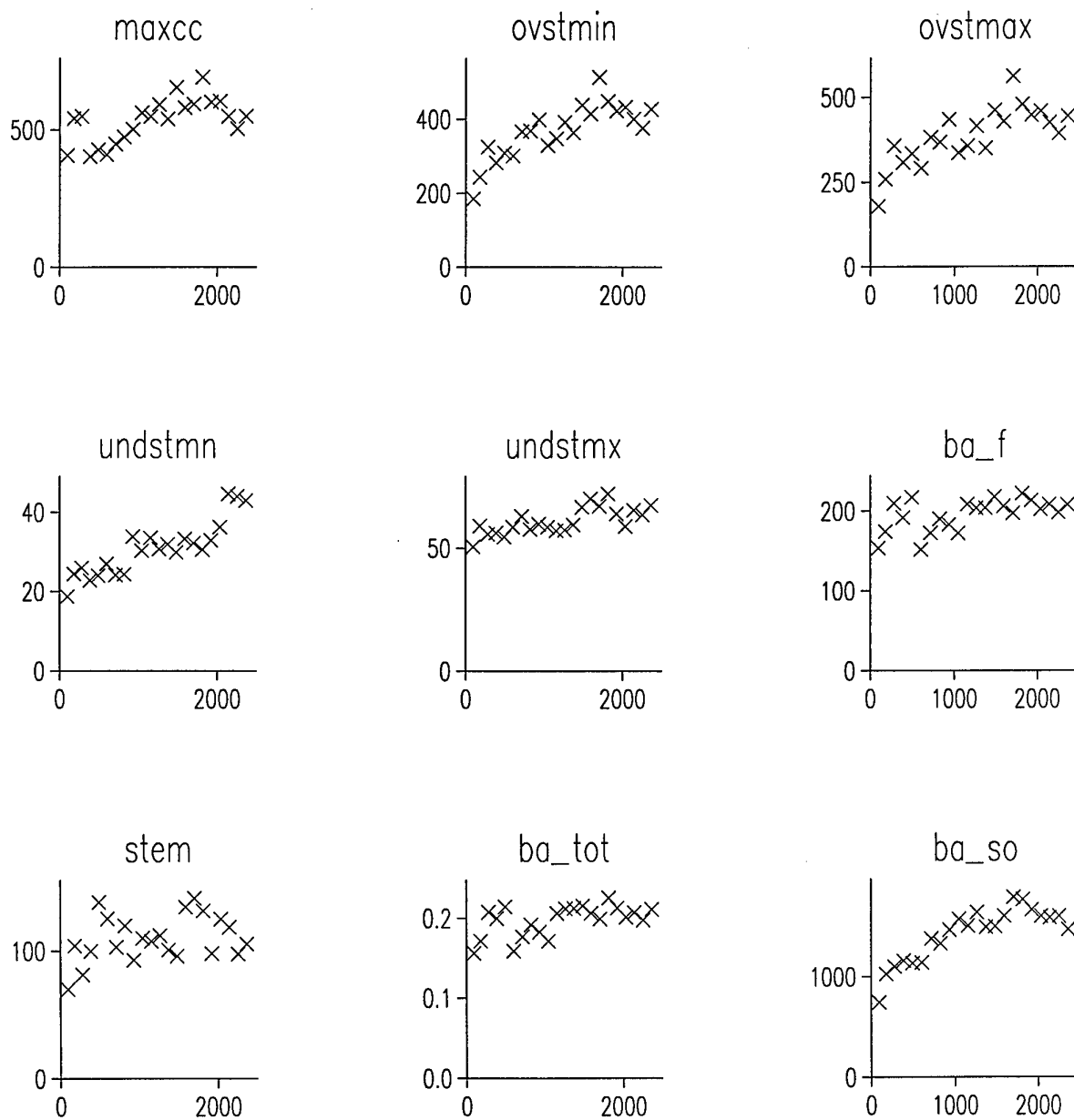
Figure 42: Omnidirectional experimental variograms of Set A variables from Surveys 1 and 2.
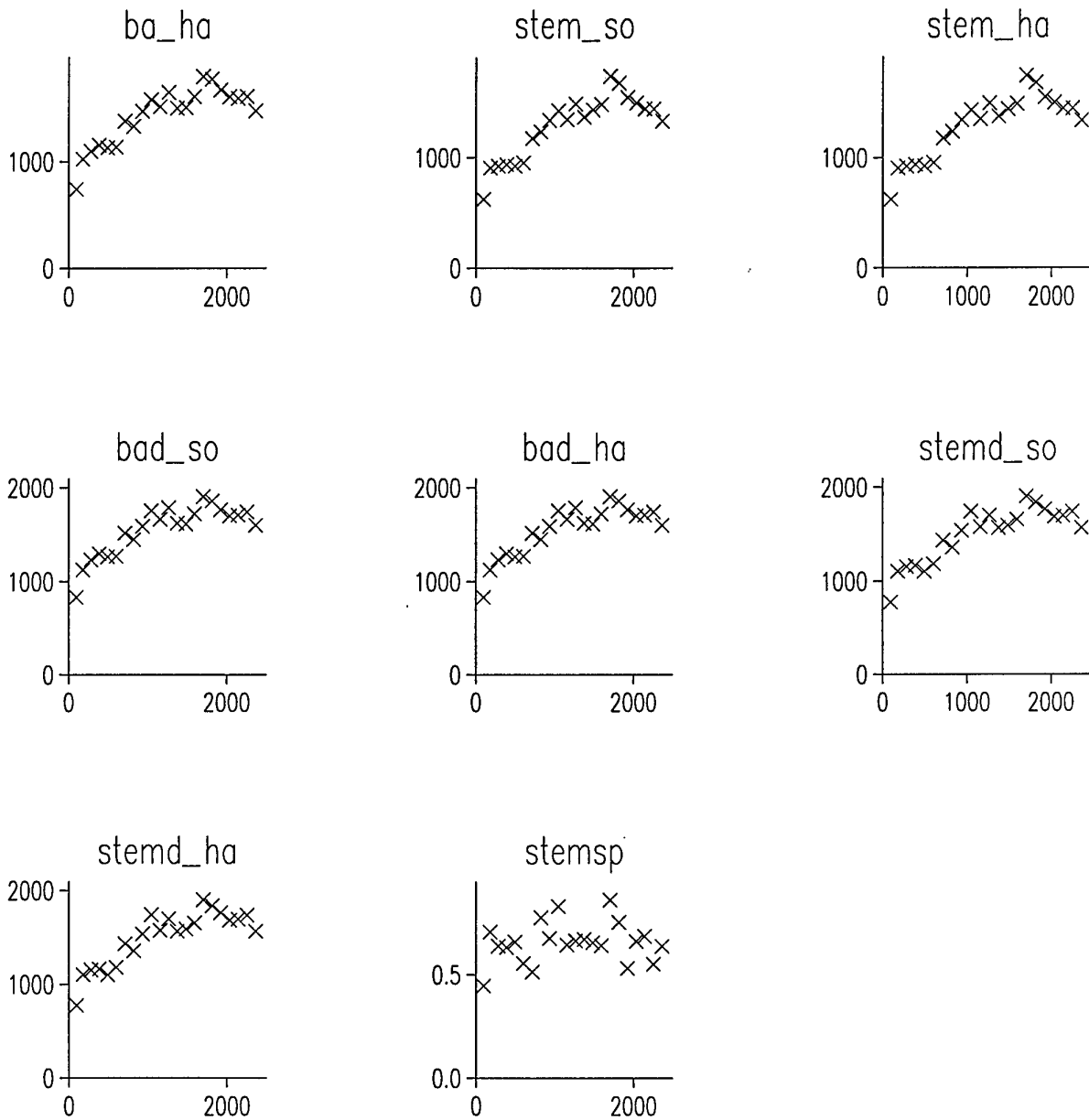
Figure 43: Omnidirectional experimental variograms of Set B variables from Surveys 1 and 2.

Table 12. Variogram model parameters for the quantitative information from Surveys 1 and 2, and for elevation and the image information.

Variables	Model type	Nugget variance	Sill c_1	Sill c_2	Range a_1 (m)	Range a_2 (m)
Canopy closure	Circular	379.1	211.4		1707.0	
Overstory height	Double spherical	0	275.9	124.9	243.0	2034.0
Understory height	Circular	19.2	12.6		1391.0	
Basal are (field)	Spherical	69.9	126.5		232.0	
Stem	Pentaspherical	21.4	65.7		380.0	
Stem spacing	Circular	0.305	0.193		407.0	
ba_so.ha	Double spherical	0	980.2	563.5	182.0	1553.0
ba_so/ha (45°)	Circular	662.3	1271.0		1271.0	
ba_so/ha (135°)	Circular	428.0	841.4		462.0	
stem_so/ha	Spherical	892.7	838.3		1428.0	
bad_so/ha	Spherical	909.1	819.9		1274.0	
stemd_so/ha	Circular	839.9	869.7		1432.0	
Multivariate variogram	Circular	6.05	3.08		309.9	
Elevation	Circular	93.05	312.5		1562.0	
Red (1)	Pentaspherical	2.21	17.89		906.0	
Green (2)	Double spherical	0	20.6	19.7	386.0	1047.0
NIR (3)	Circular	99.24	145.0		673.6	
NDVI	Double spherical	0.0015	0.00307	0.00202	666.8	1261.0
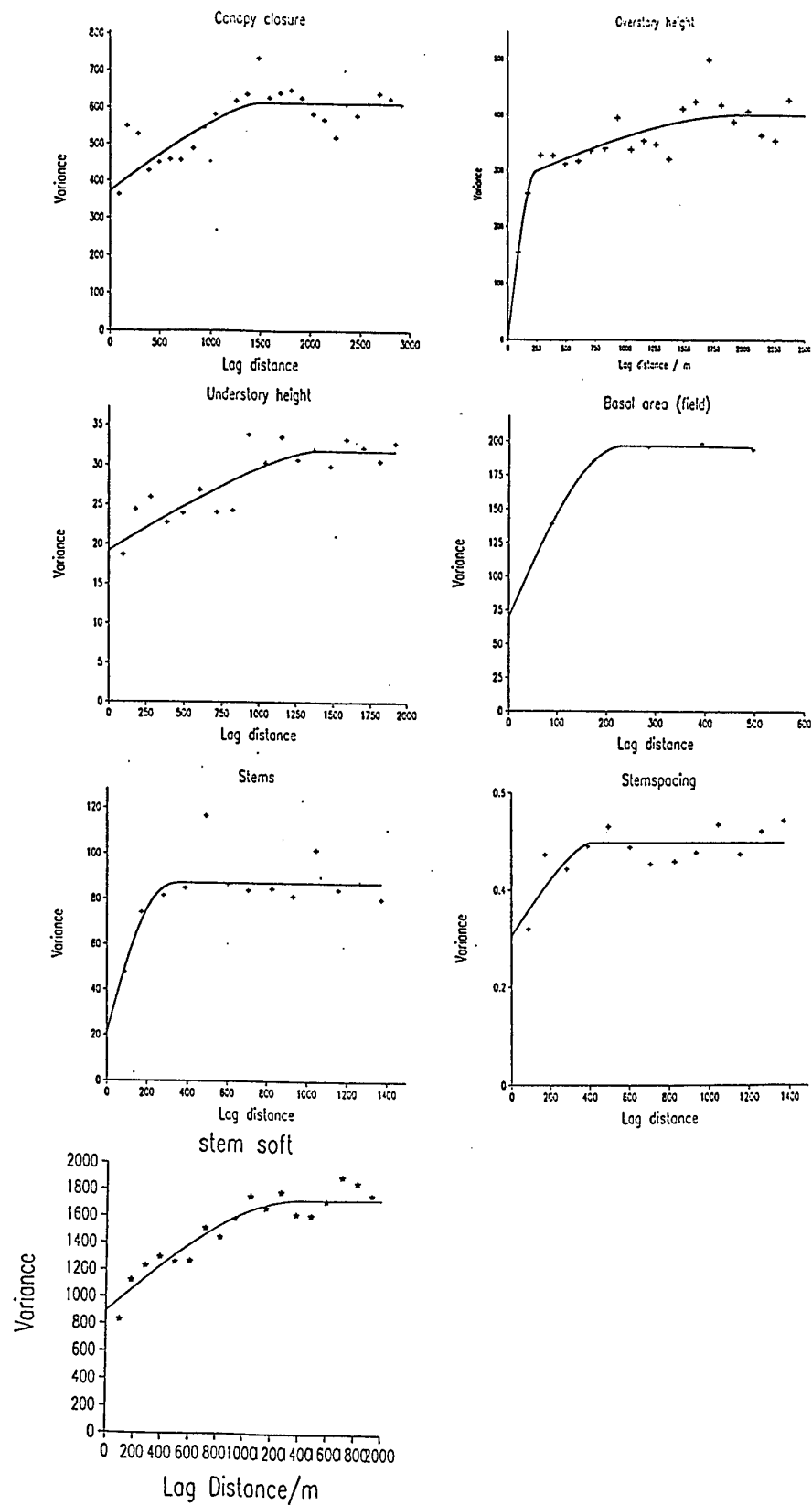
Figure 44: Experimental variograms and fitted models for Surveys 1 and 2.
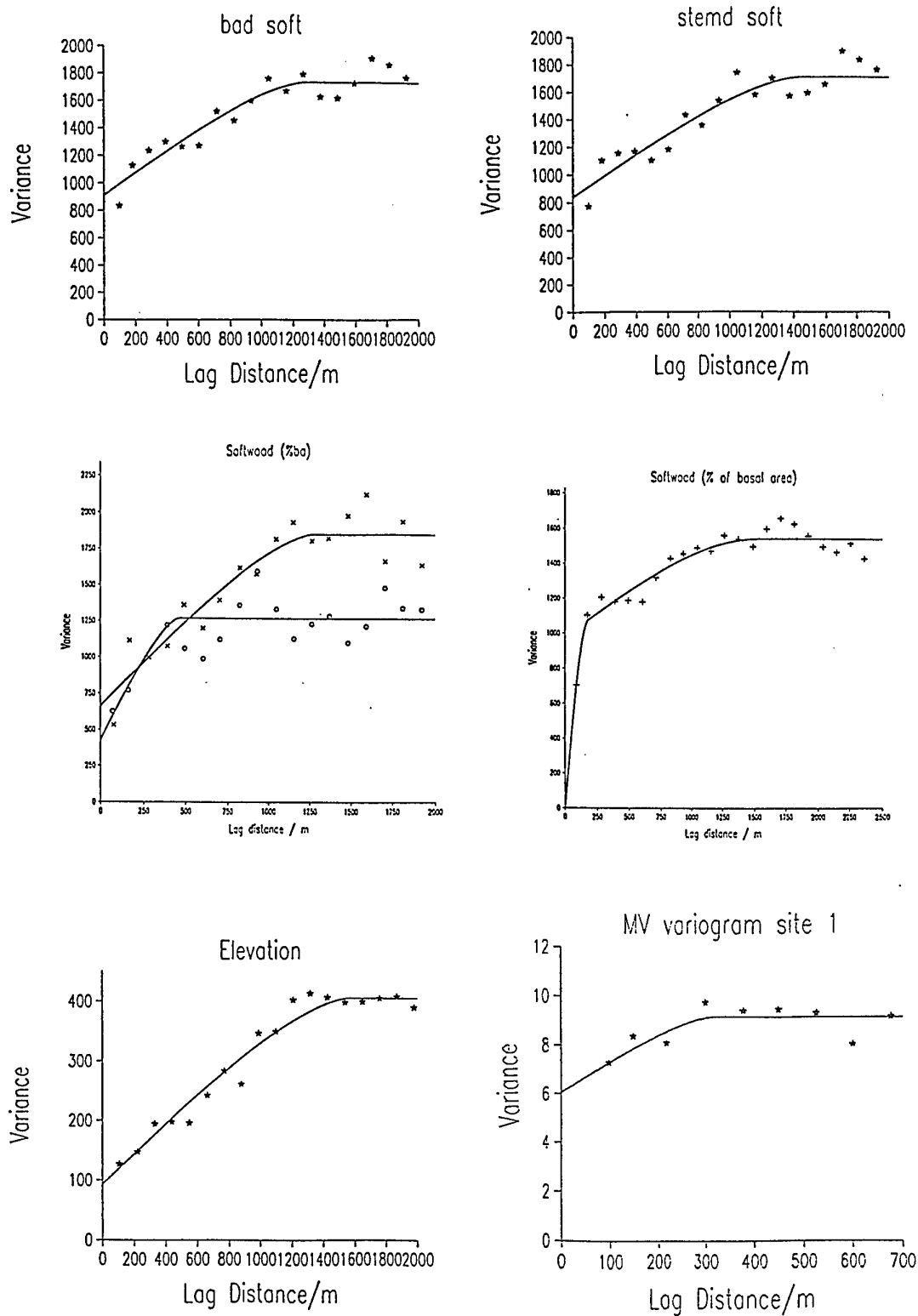
Figure 45: Experimental variograms and fitted model for Surveys 1 and 2.
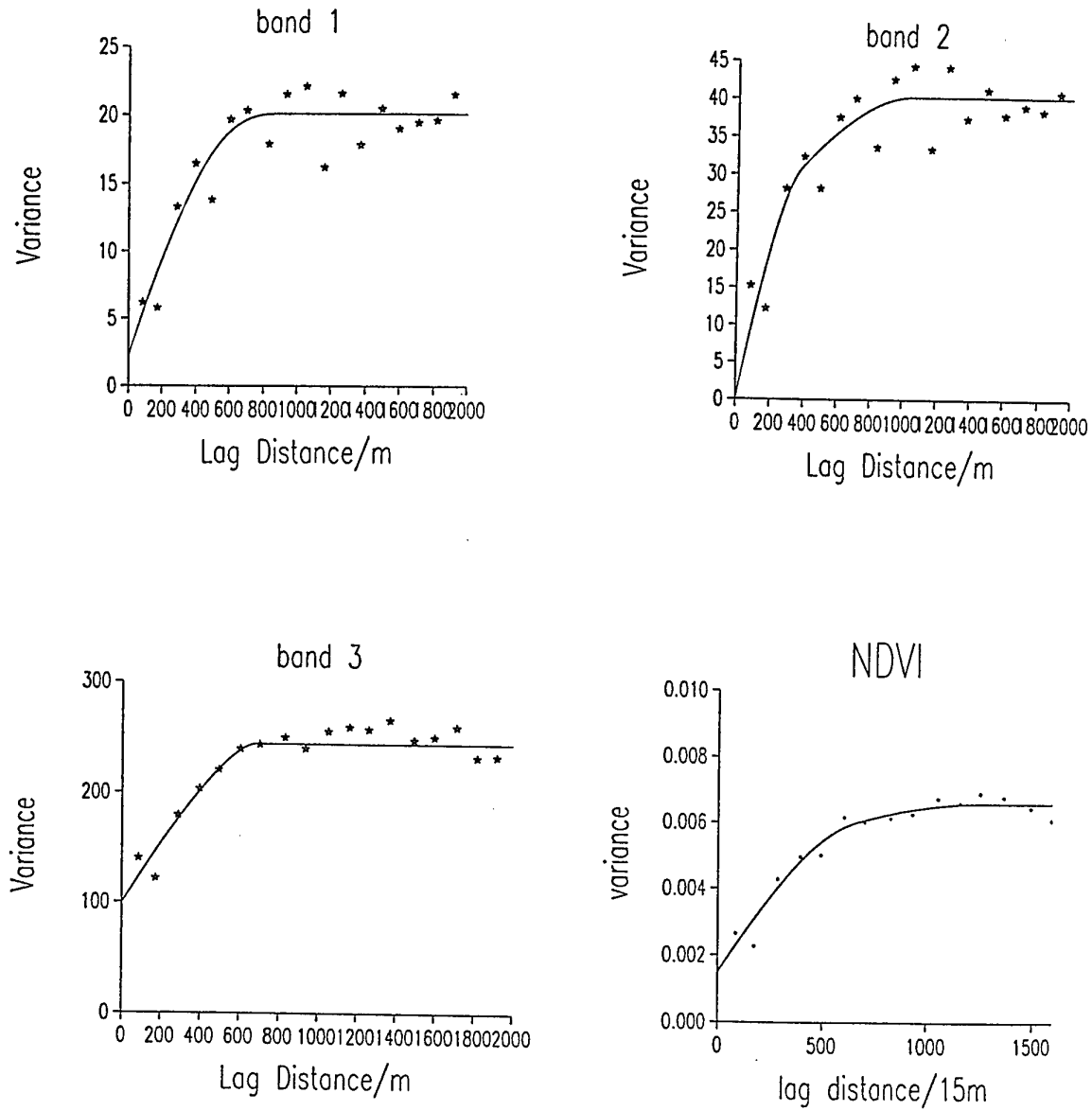
Figure 46: Experimental variograms and fitted models Surveys 1 and 2.

Cross variograms

The theory for computing cross variograms between two or more variables is given at the beginning of the report. Cross variograms were computed between the vegetation measures and the DNs from the three SPOT wavebands. Those selected and shown in Figures 47 to 50 show some relation between the variables. For band 1 (Red) there is a negative relation between maxcc, unstmn and stem, and a positive relation between stem spacing (Figure 47). The relations with the other variables is not clear. For band 2 (Green) there are clear negative relations with maxcc and stem, and a positive relation with stem spacing (Figure 48). For band 3 (NIR) there are positive relations between maxcc, ovstmax, stem and ba_f, and a negative relation with ba_so (Figure 49). Cross variograms with elevation are give in Figure 50. Overall their relations with the vegetation measures are weak.
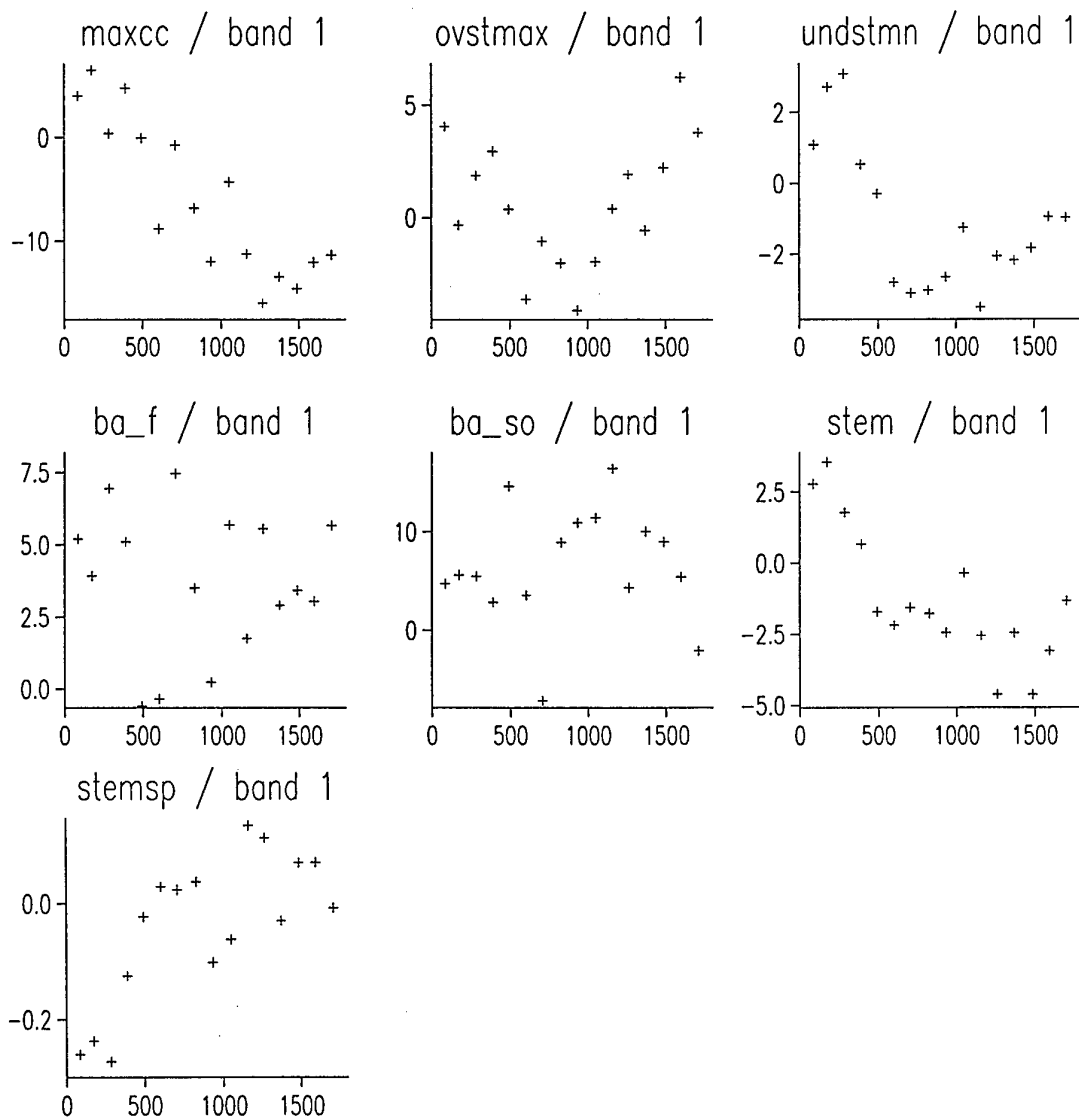
Figure 47: Cross experimental variograms between band 1 (Red) and selected vegetation measures for Surveys 1 and 2..
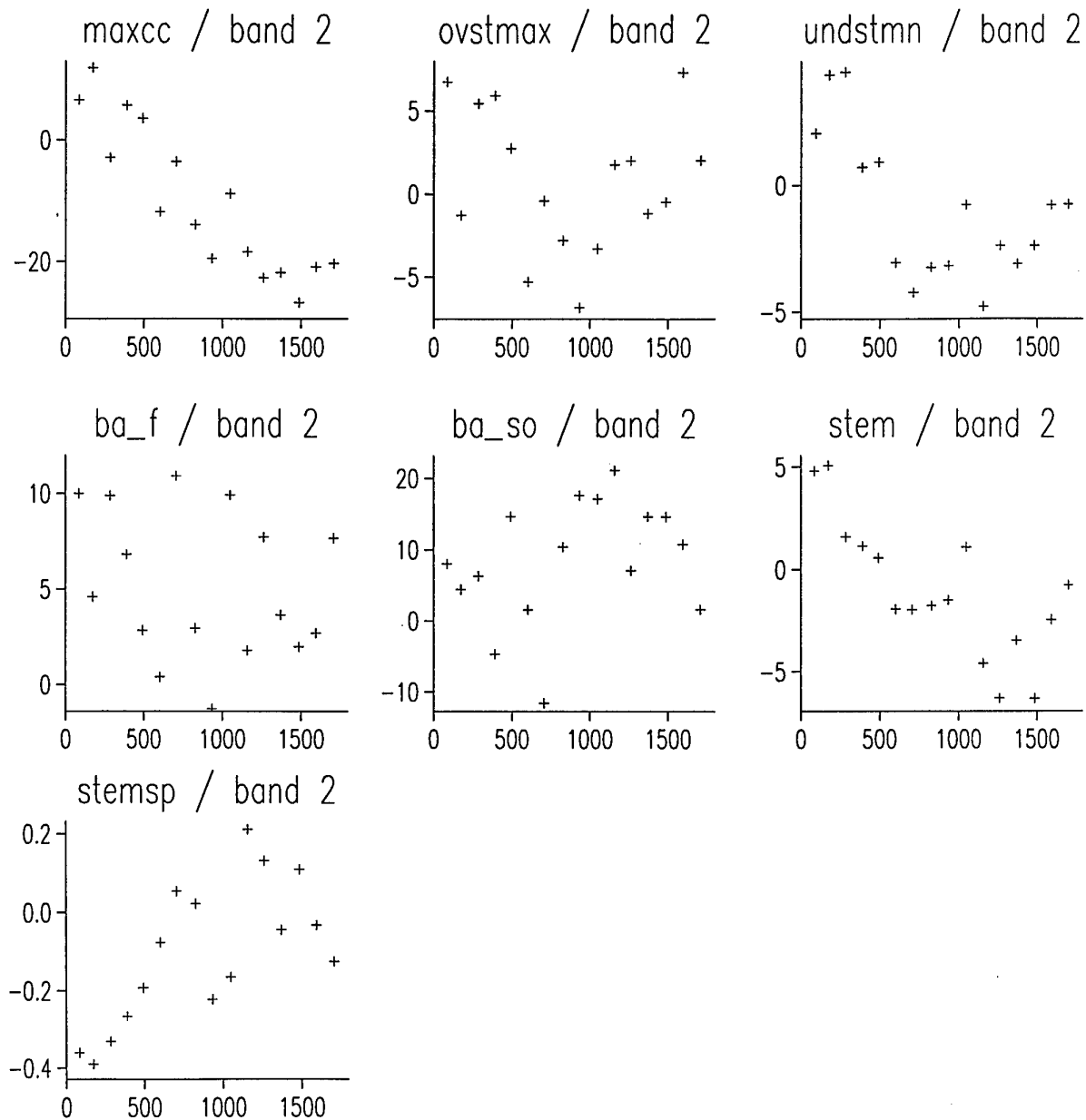
Figure 48: Cross experimental variograms between band 2 (Green) and selected vegetation measures for Surveys 1 and 2..
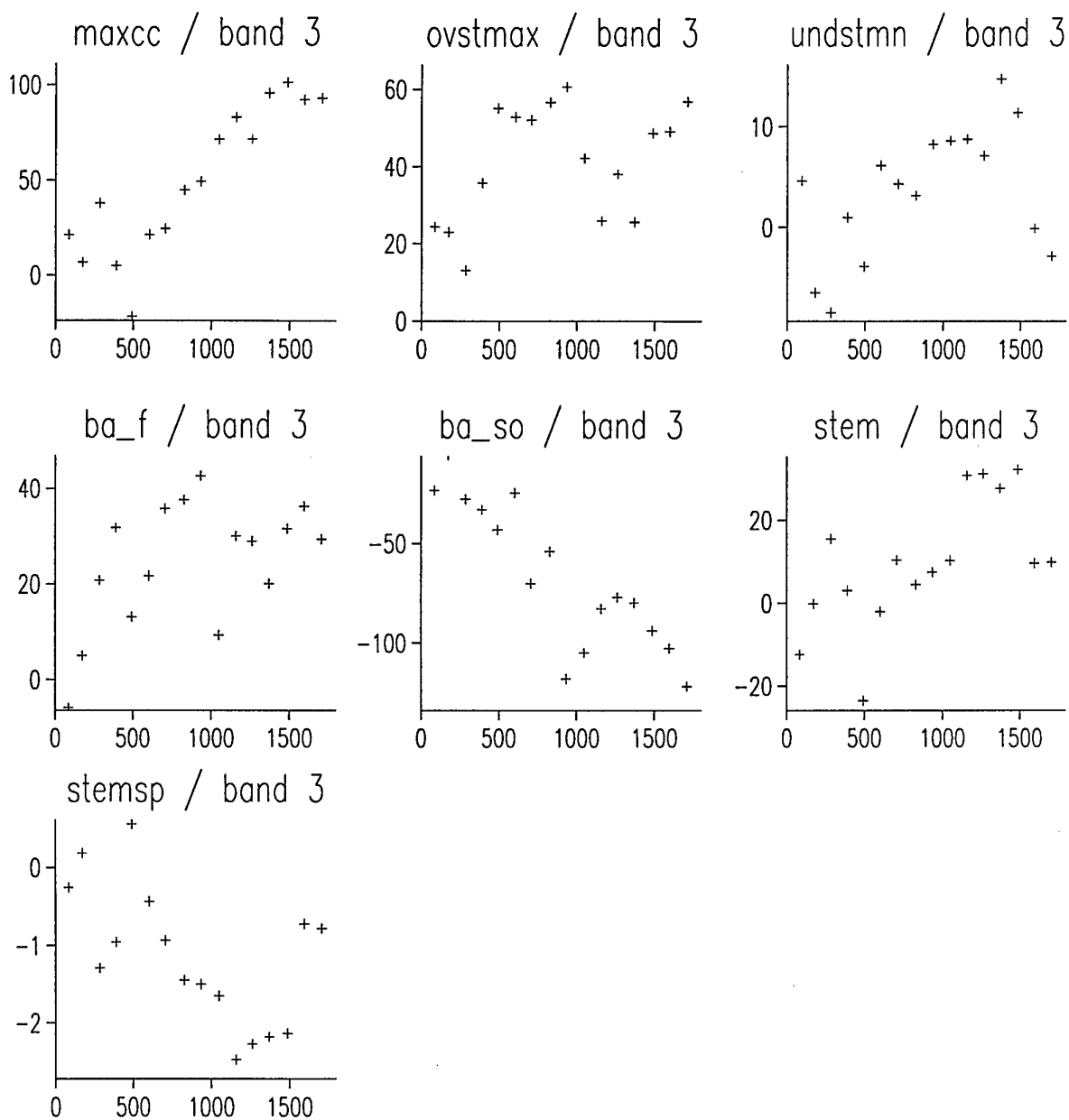
Figure 49: Cross experimental variograms between band 3 (NIR) and selected vegetation measures for Surveys 1 and 2..
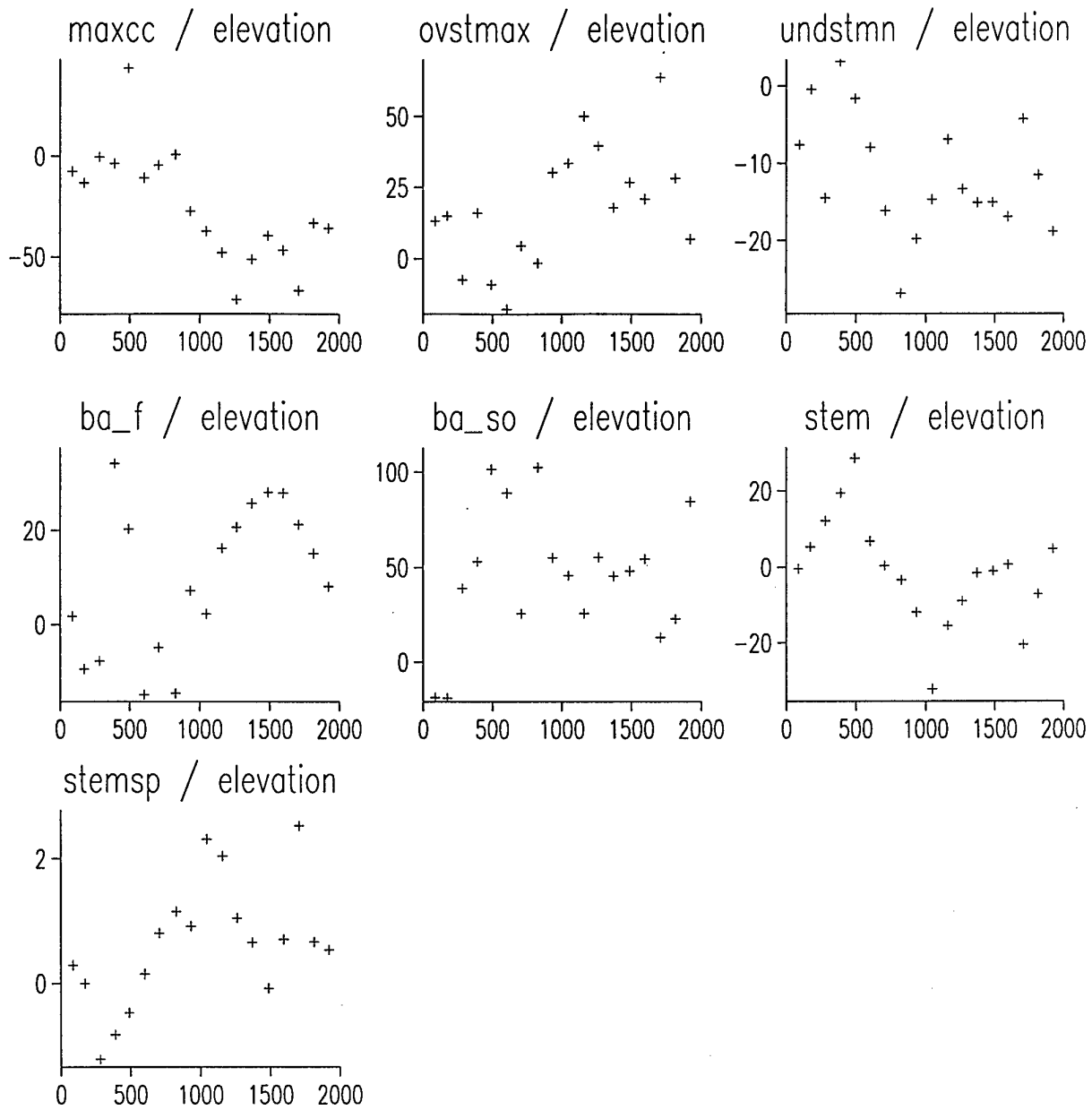
Figure 50: Cross experimental variograms between elevation and selected vegetation measures for Surveys 1 and 2..

The analysis of the qualitative data for Surveys 2 and 4

In addition to the measured values for the woodland areas, Surveys 2, 3 and 4 also described the vegetation in categories or classes. The distribution of the sites for all of the ground cover surveys is given in Figure 51, and that for Survey 4 alone in Figure 52. The sampling scheme for Survey 4 was along a series of transects with a sampling interval of 10 m. This survey was confined to a smaller area than the transects of Survey 3 which had a 50 m sampling interval.

In the original classification of these data there were several classes with few sites. Therefore, as for Survey 3 described in the previous final report (Contract N68171-97-C-9029), the number of classes was reduced. The original and new classes are given in Table 13. For Survey 2 there were 114 sampling points and for Survey 4 there were 321 points. Figure 53 shows the spatial distribution of the eight classes in relation to the sampling points for Survey 2 and Figure 54 shows their distribution for Survey 4. Some sites had a mixture of ground cover, for example grass/low bushes, and these were eliminated from the analysis. For Survey 2, 19 sites were excluded and so the variogram analyses were carried out using the remaining 95 sites. For Survey 4, 71 sites were excluded leaving 250 sites for the analysis. Table 14 summarises the contents of the classes.
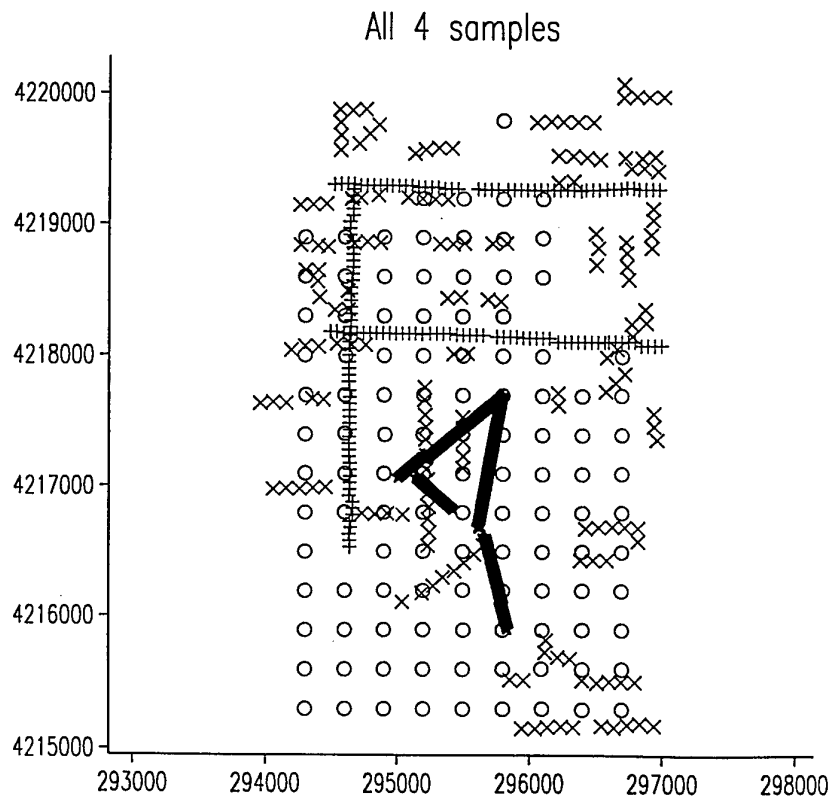
Figure 51: Map of sites for the four ground cover surveys.

Table 13: Reclassification of the classes of ground cover for sites Surveys 2 and 4.

Sample 2	Grass/Edge of Mixed	Sample 4	Forest (Wet/Dry) Forest Disturbed
Manmade		**Manmade works**	
Building/Asphalt		Asphalt	
Buildings	Grass/Houses	Asphalt/Grass	Forest/Grass
Campgrnd-like	Grass/Low Bushes	Asphalt/Grass/Soil	Forest/Road
Site	Grass/Rd/Bldg		Forest/Scrub
Gravel Parking	Grass/Road	Concrete	Forest/Tall Grass
Lot	Lake	roof-Asphalt	Grass/Asphalt
Powerline Grass	Maple/Pine		Grass/Asphalt/Cement
Private-Landfill	Oak/Holly	**Field**	
Road/Grass	Oak/Pine	Field	Grass/Conifer
	Pine/Maple		Grass/Dirt
Grass	Pine/Mix	**Grass**	Grass/Forest
Grass	Pine/Plantation	Grass	Grass/HW
	Marshy Wetland	Grass (Tall)	Grass/Soil
Grass Field	Private-Mix	Tall Grass	HW/Marsh
Grass Field	Private-Mixed		Marsh/HW
Tall Grass		**Hardwood**	Pine/Brush
		Hardwood	Pine/Grass
Oak		Forest (H)	Pine/Hard/Shrub
Oak			Pine/HW/Marsh
		Mixed Forest	Pine/Shrub
Hard Mix		Pine/Hardwood	Shrub/Scrub
Hard Mix		Pine/HW	ShrubScrub/Forest
Oak Mix		Forest (M)	Tall Grass/Field
Poplar			Wet Forest/HW
		Pine	
Mixed_For.		Pine	
Mixed_For.		Forest (P)	
Pine		**Forest**	
Pine		Forest	
Plantation			
Young Pine		**Shrub/Scrub/Wetland**	
Private-Pine		Shrub/Scrub/Wetland	
Wetland			
Wetland		**Excluded**	
Private-Wetland		Edge Field/Forest	
Wetland		Edge/Field	
w/Waterways		Field/Gravel Road	
		For Dist (M)	
Excluded		For/Tall Grass	
Grass/Cemetery			

Table 14: Summary of ground cover classes for sites Surveys 2 and 4.

Survey 2		Survey 4	
Ground Cover Class	**Number of samples**	**Ground Cover Class**	**Number of samples**
Manmade	11	Manmade works	20
Grass	16	Field	5
Grass field	3	Grass	71
Oak	3	Hardwood	24
Hard Mixed Forest	12	Mixed Forest	32
Mixed Forest	8	Pine	11
Pine	34	Forest	76
Wetland	8	Shrub/scrub/wetland	11
Excluded	19	Excluded	71
Total sites	**114**	**Total sites**	**321**
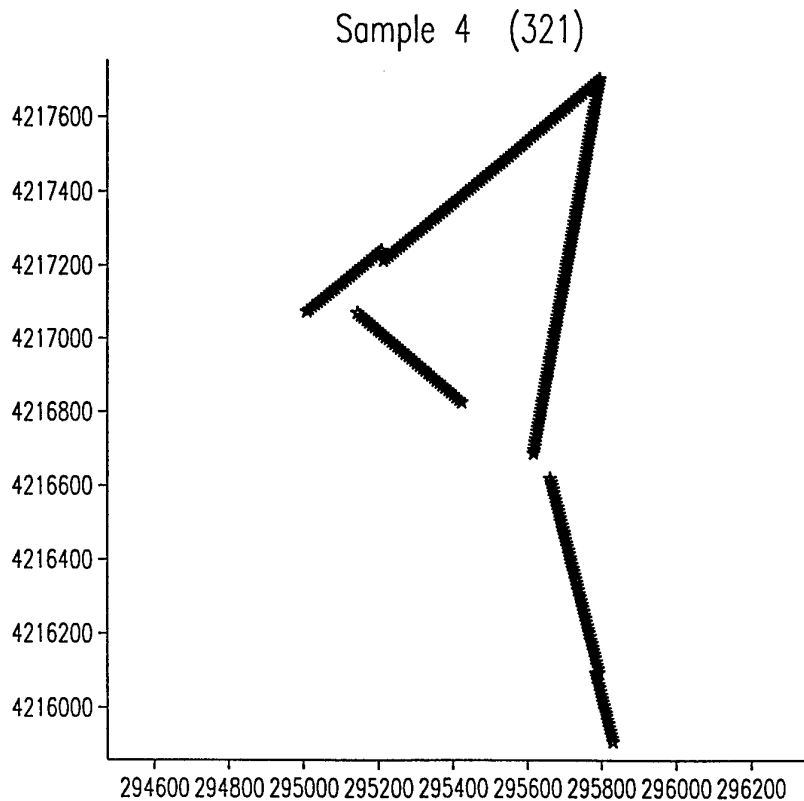
Figure 52: Map of sites for Survey 4.

Variogram analysis of categorical data for Survey 2

Experimental variograms were computed for each of the eight ground cover classes, Figure 55. The ones that show clear structure are for the categories: manmade, grass, oak, pine and wetland. Considering the small sample size the evident structure in these suggests that there are distinct areas of ground cover type that can be identified with relatively little sampling effort. The variogram for oak appears to have a nested structure. These variograms have not been modelled at present, but this could be done in the next phase of work. From the graphs the average range of spatial dependence is about 600 m. This fits in well with the long range component of the variation in NIR for the original part of the SPOT image analysed, Table 15.

The experimental multivariate variogram based on the classes was computed. This analysis summarises the average rate of change from one class of ground cover to another. Figure 56 shows the experimental variogram with the fitted model. The variogram has a large nugget variance because there were relatively few sites and the sample spacing of 300 m was large. The variation that has not been detected in the change from one type of ground cover to another is embraced by the nugget variance. The variogram model was a single structure with a range of spatial dependence of 575 m (Table 15). This corresponds closely with the long-range structure identified in the nested variogram of NIR computed from the original part of the SPOT image that was analysed. This was slightly larger than the area used for the wavelet analysis (Part II of this report). The variogram of this waveband was fitted by a nested spherical model with a short range component of 120 m and a long range component of 542 m (Table 15). It is evident that the spectral information is identifying the major changes in the different kinds of ground cover.

Table 15. Variogram model parameters for the wavebands in the original SPOT image and the qualitative information from Surveys 2 and 4.

Variables	Model type	Nugget variance	Sill c_1	Sill c_2	Range a_1 (m)	Range a_2 (m)
Red - average	Double spherical	0.4661	8.080	18.432	165.56	518.94
Green - average	Double spherical	2.026	16.568	28.437	224.32	650.48
NIR- average	Double spherical	0.0	151.39	118.87	120.56	542.22
NDVI- average	Double spherical	0.0	0.0343	0.0138	139.74	643.35
Ground cover 2	Circular	0.431	0.283		575.0	
Ground cover 4	Double spherical	0.112	0.307	0.328	67.0	689.0
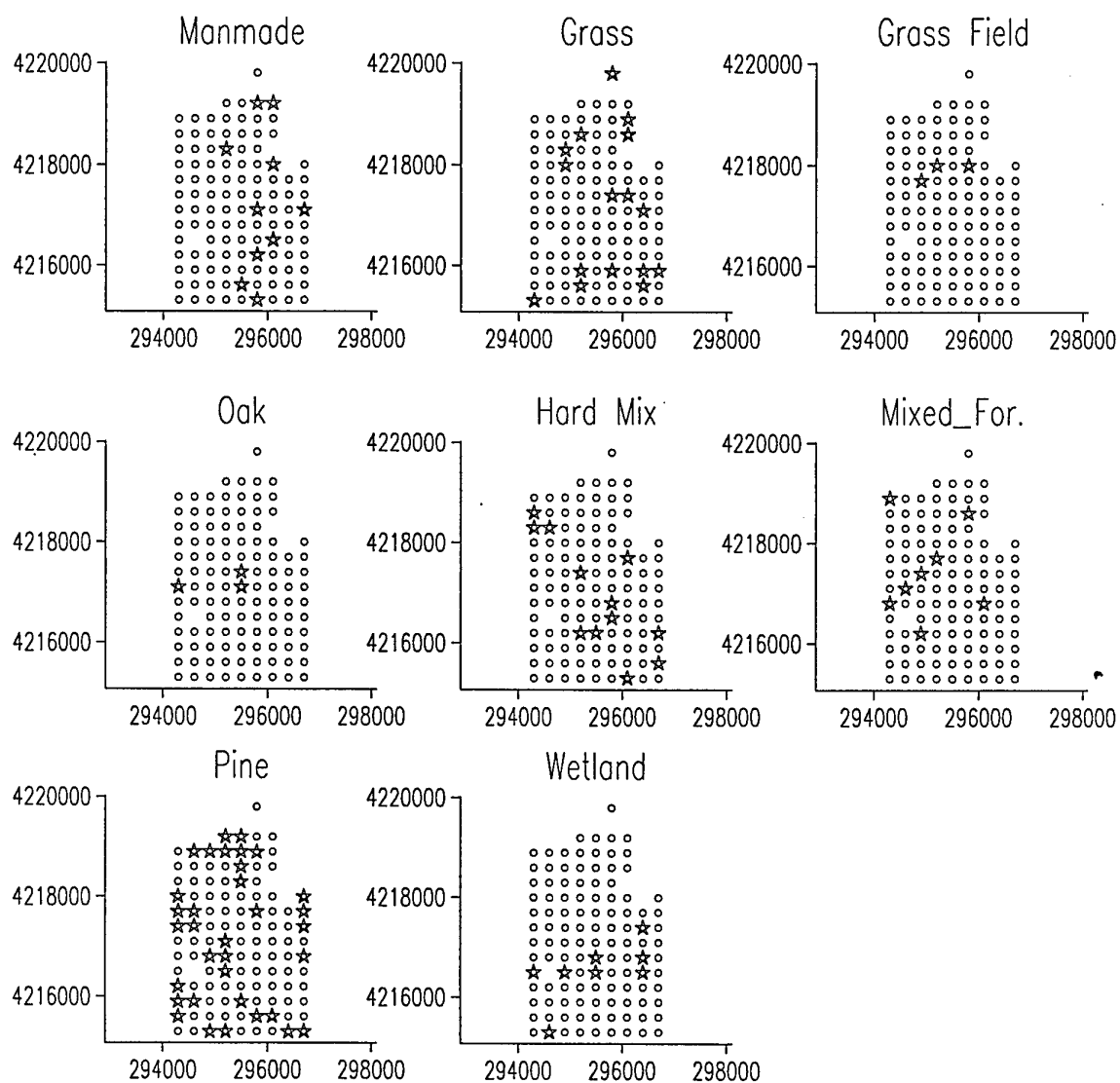
Figure 53: Distribution of sites for each category of ground cover for Survey 2.
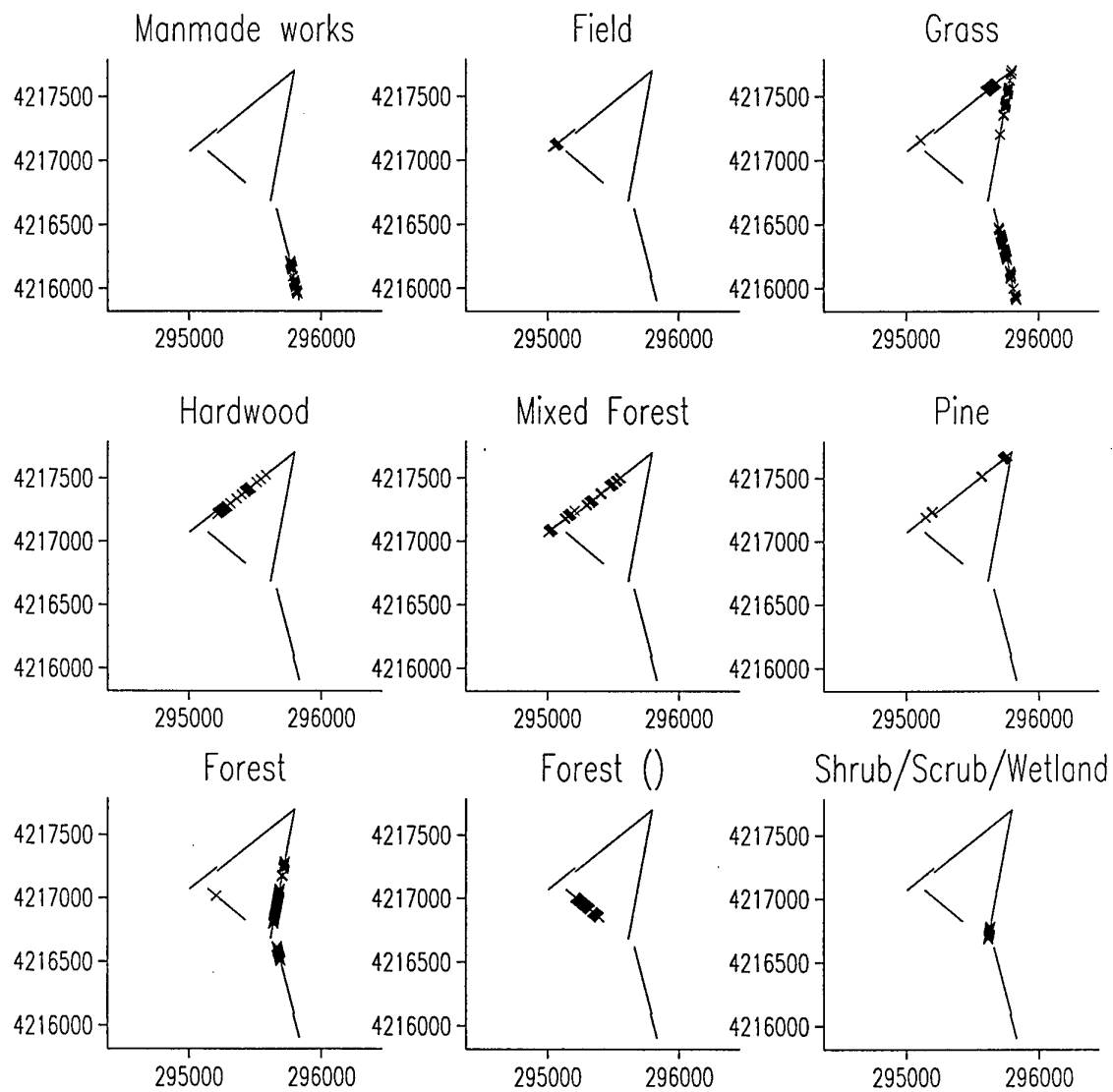
Figure 54: Distribution of sites for each category of ground cover for Survey 4.
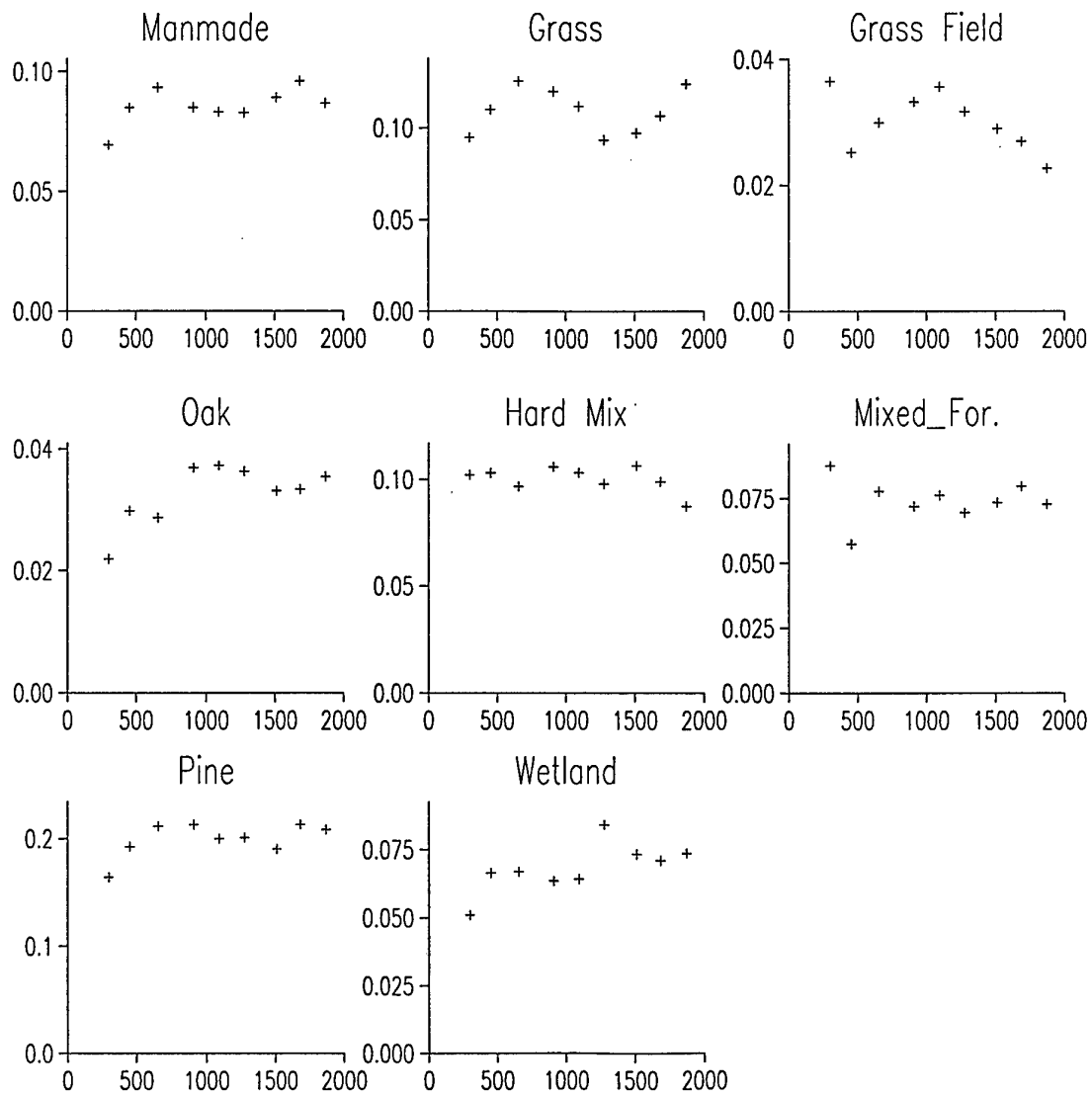
Figure 55: Experimental variograms of the ground cover classes for Survey 2.
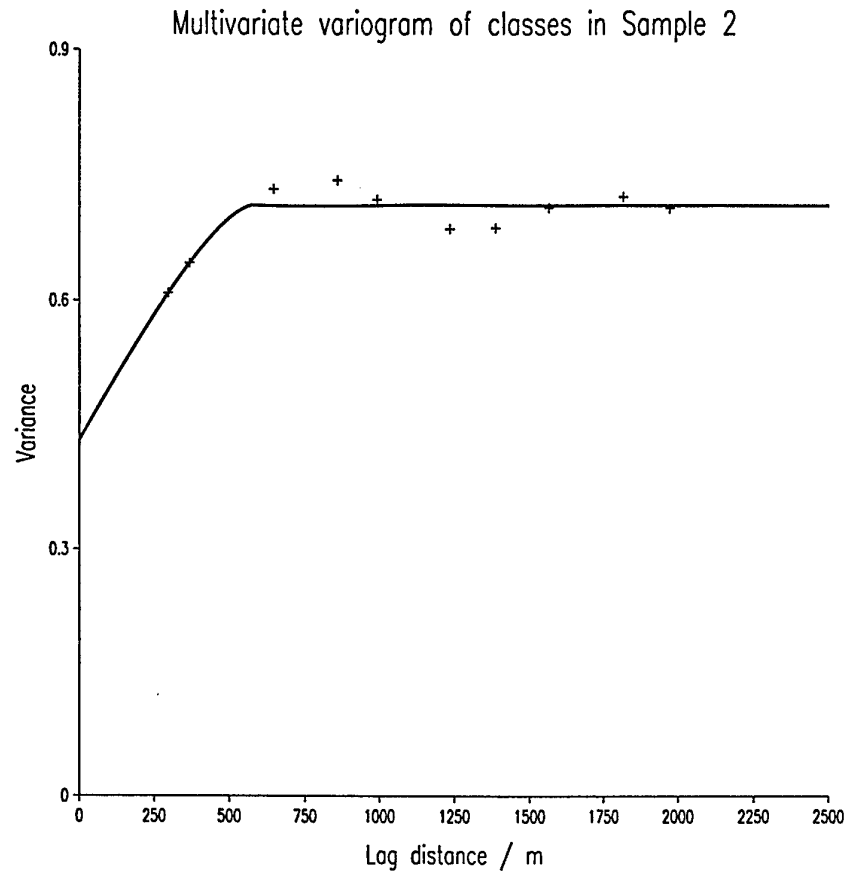
Figure 56: Experimental multivariate variogram (symbols) based on the ground cover classes for Survey 2 and the fitted model (solid line).

Cross variograms were computed as before between the ground cover classes and each of the three wavebands. Figures 57 to 59 show the cross variograms for Survey 2. Those for wavebands 1 and 2 are similar. For the Red waveband (1) manmade, grass, oak, hard mixed forest, mixed forest, pine and wetland show evidence of coregionalization with it. The strength of this cannot be judged at present until they have been modelled. The coregionalization for the Green waveband (2) is as above, except for grass. For NIR (3) the coregionalization is between oak, hard mixed forest, mixed forest and wetland. The relations for the two grass categories and pine are not strong.
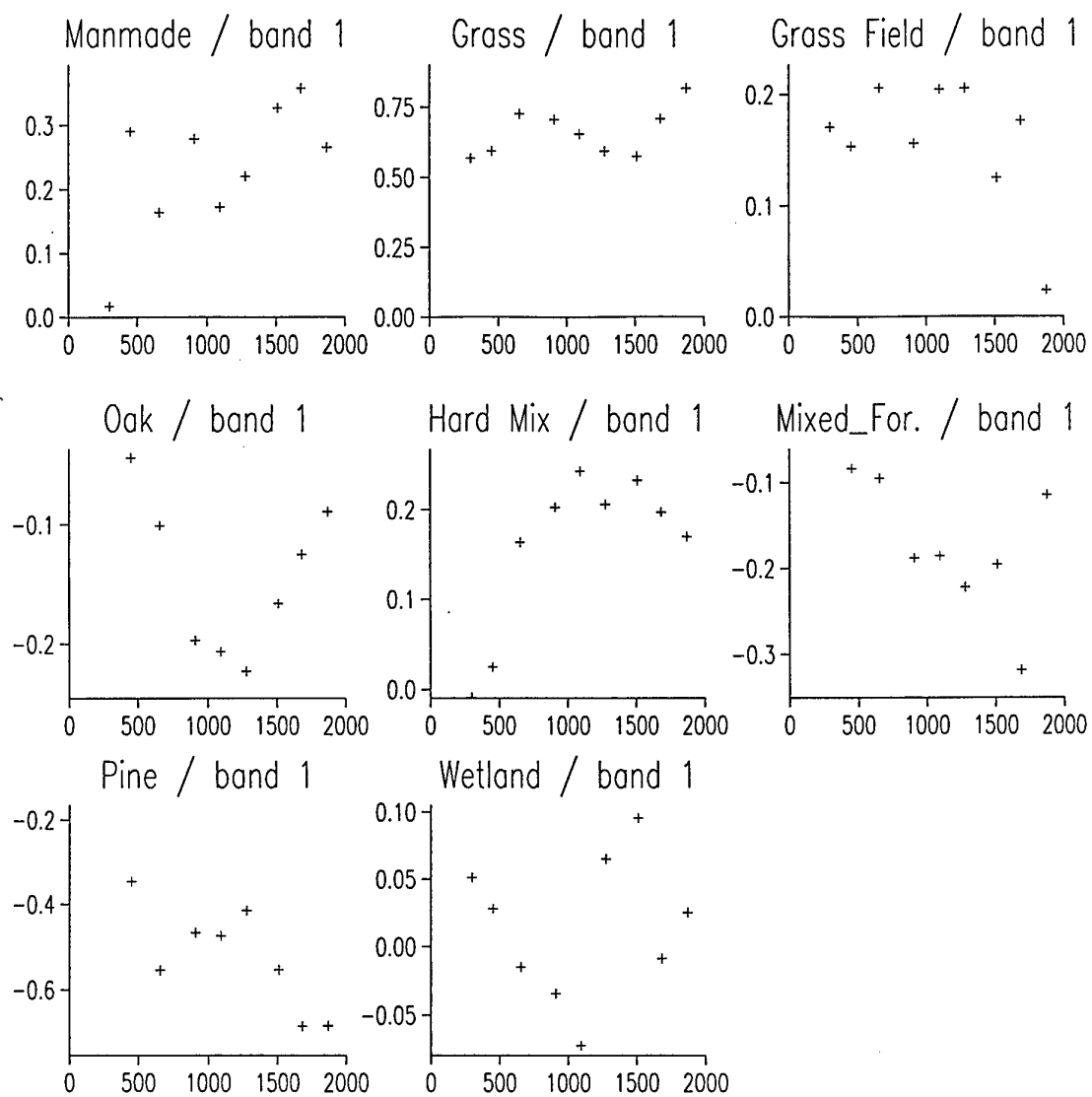
Figure 57: Cross experimental variograms between band 1 (Red) and the ground cover classes for Survey 2.
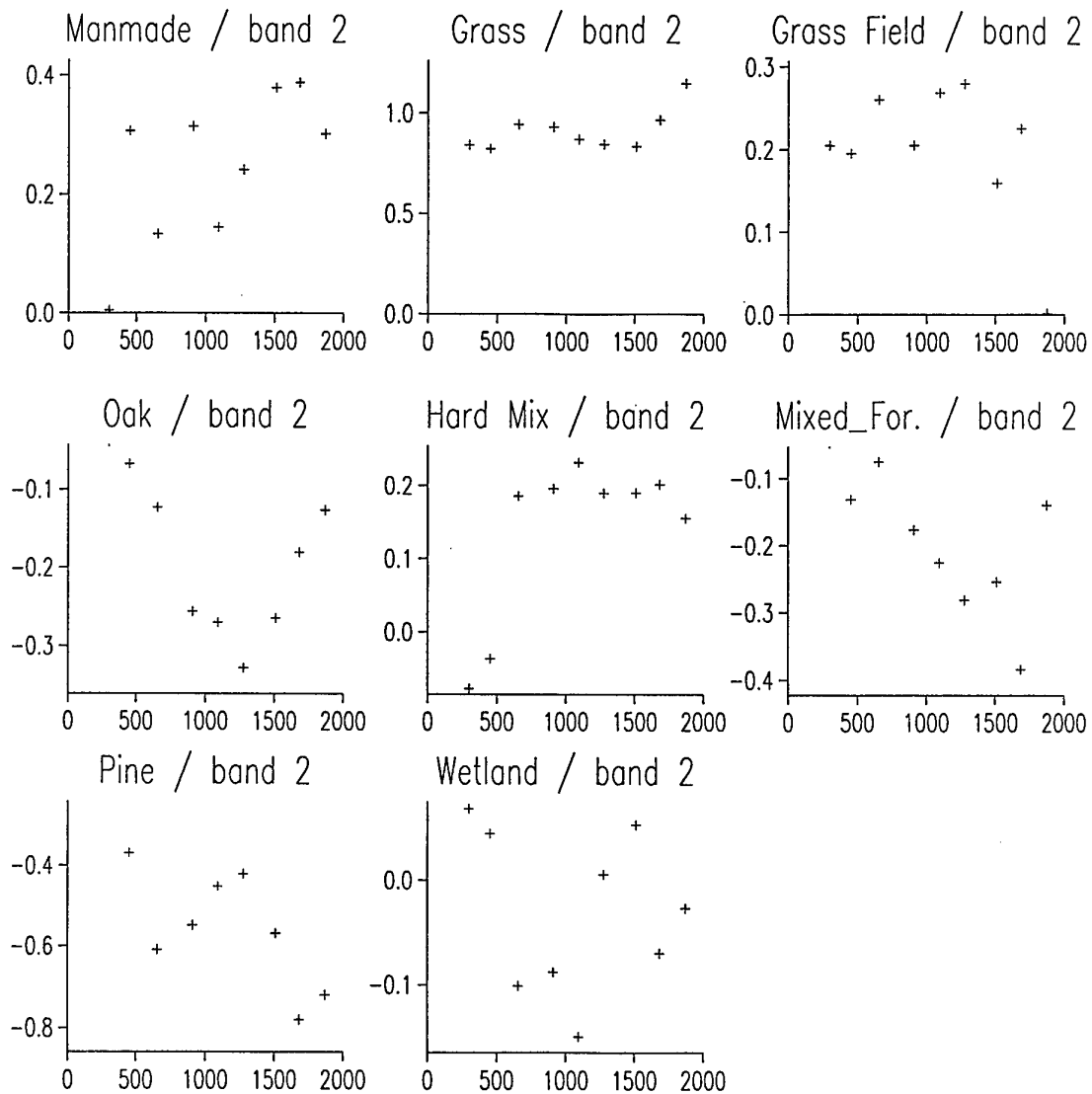
Figure 58: Cross experimental variograms between band 2 (Green) and the ground cover classes for Survey 2.

Figure 59: Cross experimental variograms between band 3 (NIR) and the ground cover classes for Survey 2.

Variogram analysis of categorical data for Survey 2

Experimental variograms were computed for each of the eight ground cover classes to a maximum lag of 400 m, Figure 60 and 1000 m, Figure 61. They are more erratic than the ones for Survey 2, which is surprising considering the large number of sampling points. However, the behaviour of the variograms probably reflects the fact that the categories of ground cover repeat themselves along the transects, this would cause the waviness that is apparent in many of them. The variograms all show clear structure, especially over a short distance of about 100 m. The average range of these variograms, based on where they start to flatten, is about 145 m. This relates closely to the short range component of the variation in NIR for the original part of the SPOT image analysed, Table 15. These variograms could be modelled in the next phase of the work.

The experimental multivariate variogram based on the classes was computed as before, Figure 62. The fitted model is the solid line the figure. The variogram was fitted best by a nested spherical model with a short-range structure of 67 m and long-range one of 689 m. However, the appearance of the experimental variogram suggests that the short- range component should be at about 150m to 175 m. Several attempts have been made to fit a better model, but the erratic nature of the experimental semivariances has prevented this. This variogram mirrors the form of that for NIR closely in spite of the fact that the model parameters are different for the short-range component.

Cross variograms were computed as before between the ground cover classes and each of the three wavebands. Figures 63 to 65 show the cross variograms for Survey 4. Those for the Red and Green wavebands are similar. The coregionalization appears to be weaker for this analysis, but this could be related to the complex nature of the individual variograms. The variables that show the strongest relation with wavebands 1 and 2 are manmade, field, grass, forest and wetland. For NIR (waveband 3) the strongest relations are with manmade, hardwood, mixed forest, pine, forest and wetland.

Cross variograms were also computed between the ground cover categories and elevation. The strongest relations are with field, mixed forest, forest and wetland. In the previous final report we commented on the fact that the patterns in the long-range component of the variation, in particular, appeared to have a strong relation with the physiography. These results appear to confirm this.

Figure 60: Experimental variograms of the ground cover classes for Survey 4 computed to a maximum lag of 400 m.
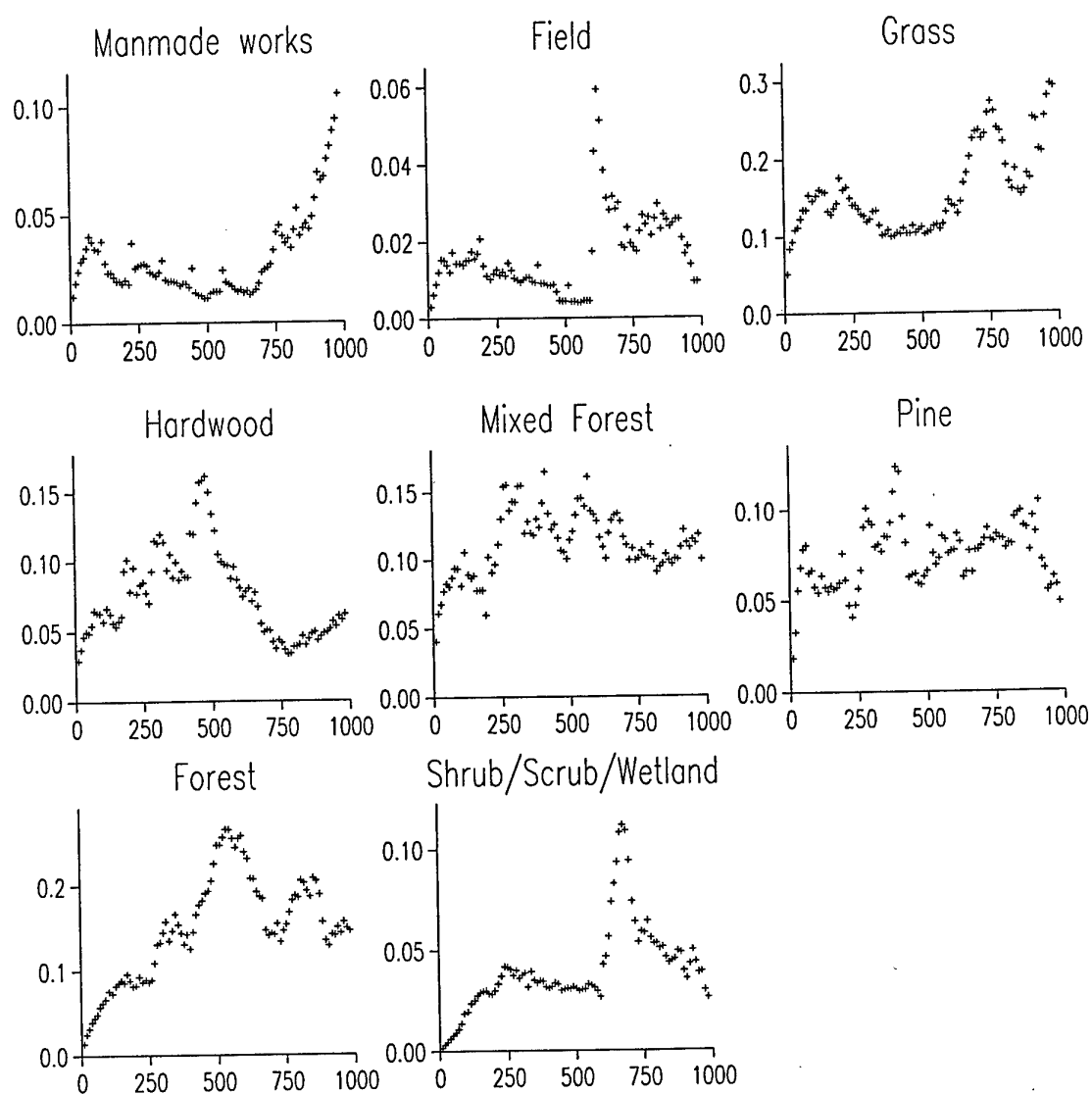
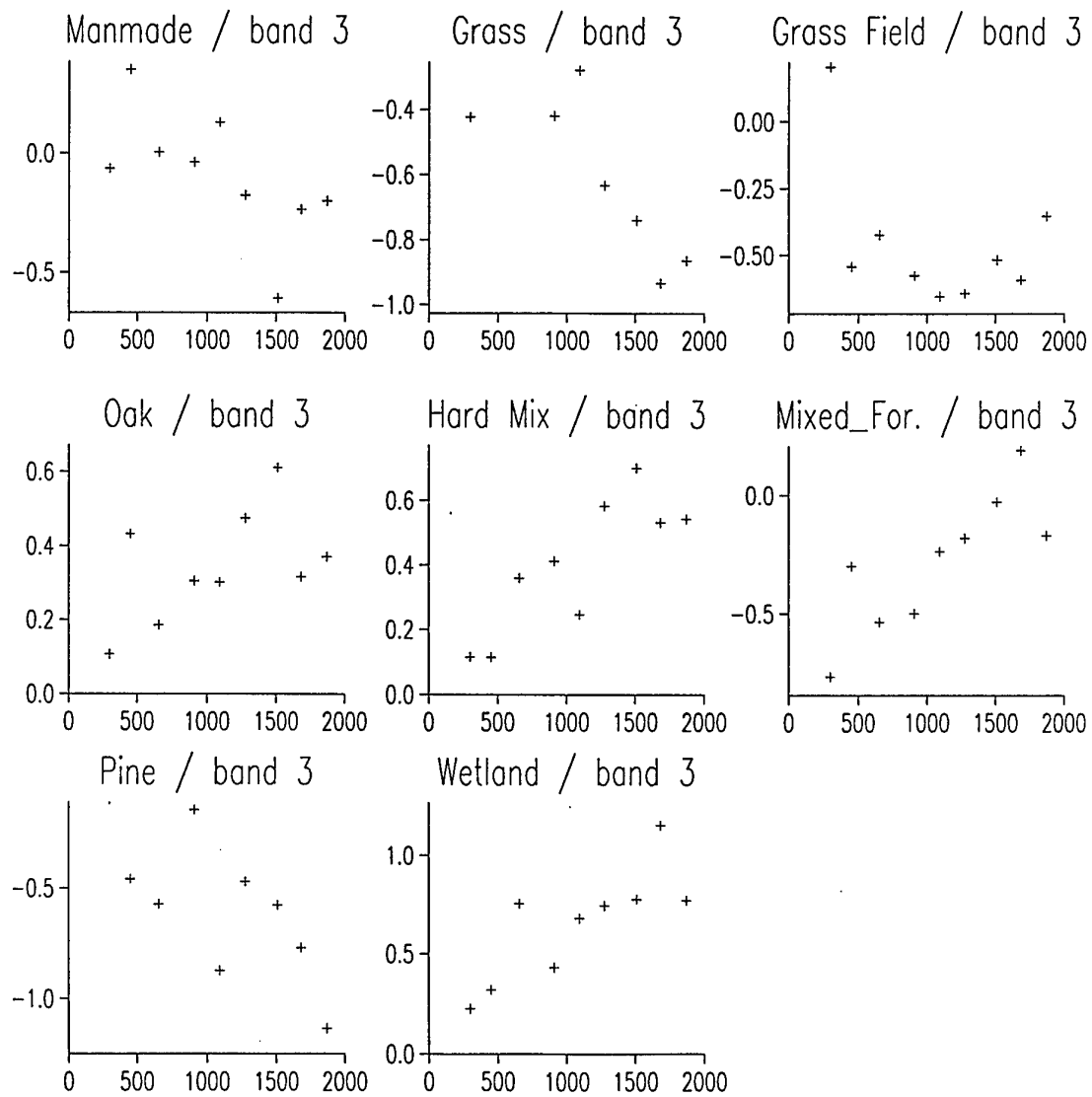**Figure 61:** Experimental variograms of the ground cover classes for Survey 4 computed to a maximum lag of 1000 m.

Summary of vegetation analysis

The results of the ground cover analyses suggest that there are distinct spatial patterns in the variation: a short-range one related to local changes in cover of about 150 m extent and a longer range one of about 550 m in extent. They relate to the patterns observed in the imagery, in particular for the NIR waveband.
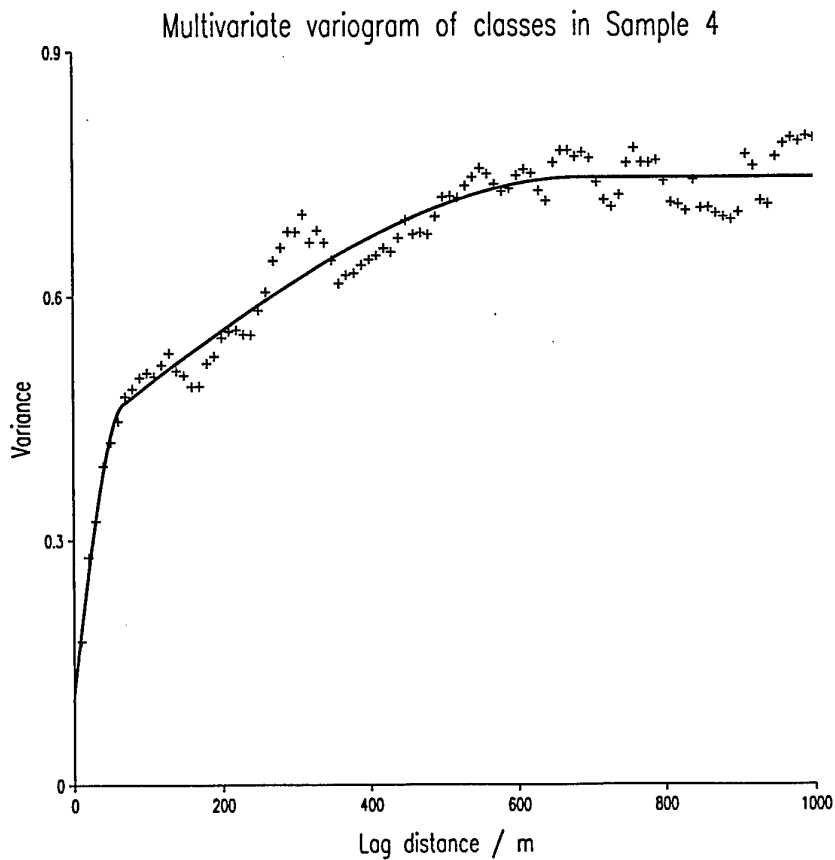
Figure 62: Experimental multivariate variogram (symbols) based on the ground cover classes for Survey 4 and the fitted model (solid line).
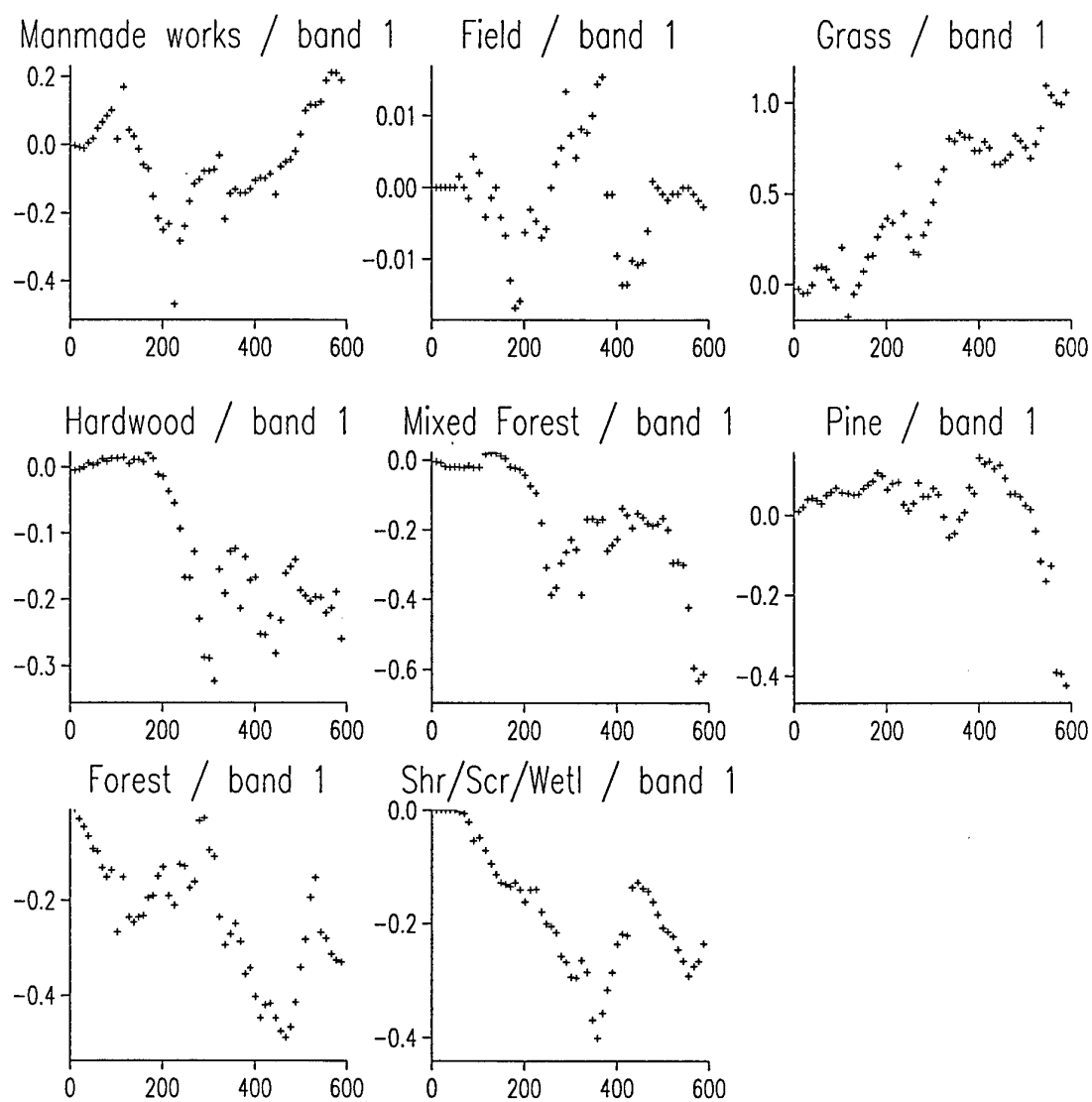
Figure 63: Cross experimental variograms between band 1 (Red) and the ground cover classes for Survey 4.
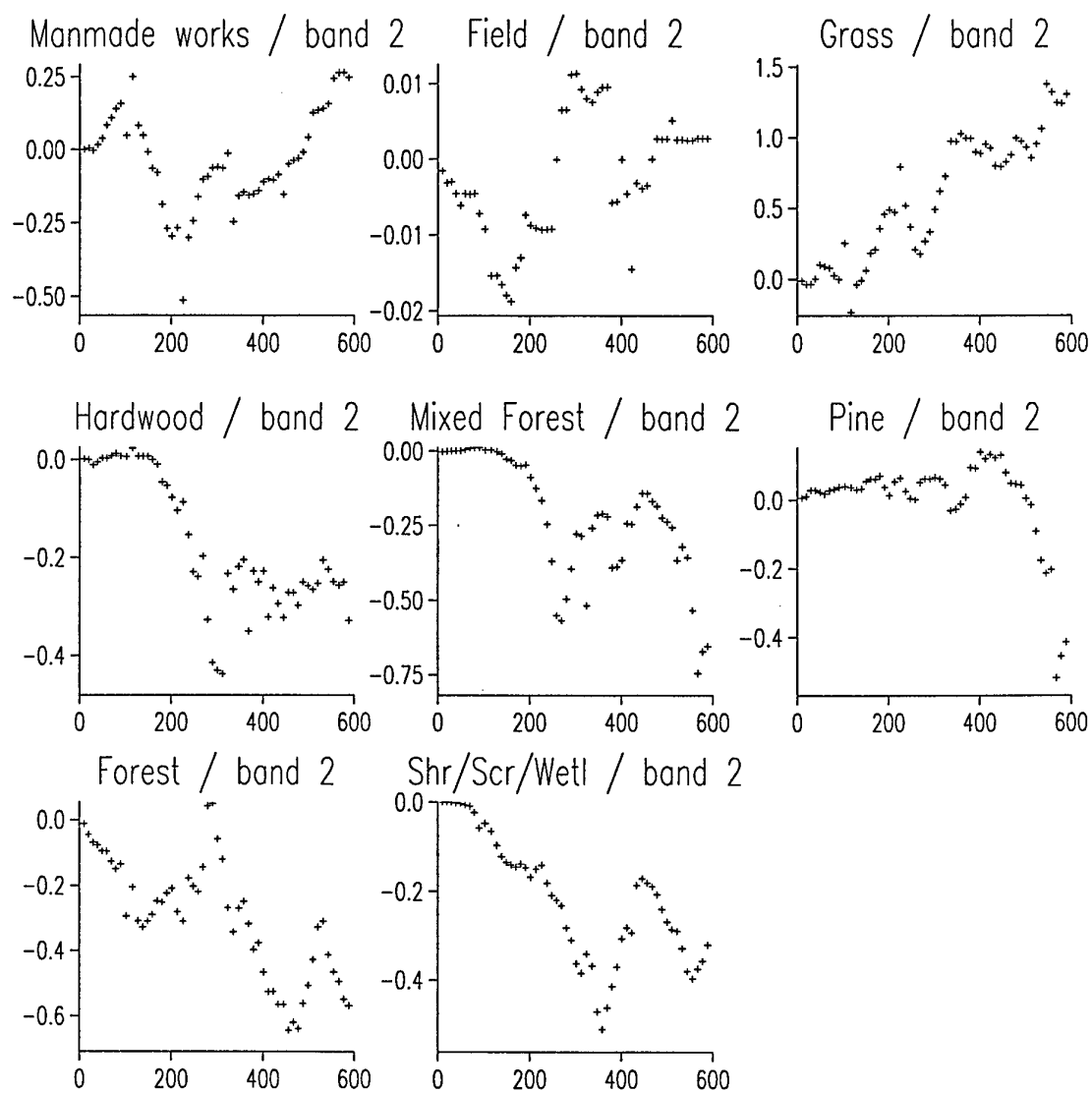
Figure 64: Cross experimental variograms between band 2 (Green) and the ground cover classes for Survey 4.
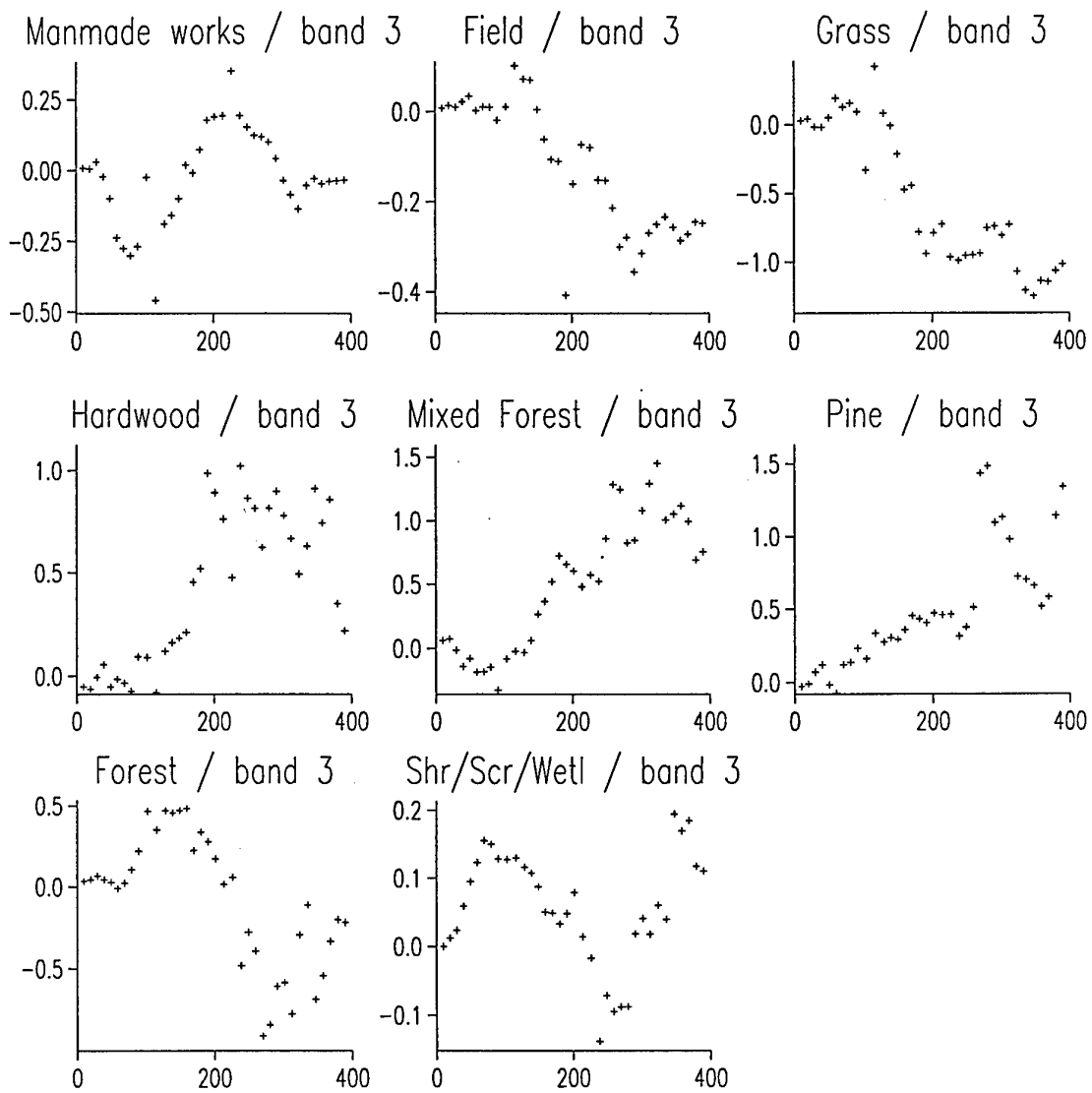
Figure 65: Cross experimental variograms between band 3 (NIR) and the ground cover classes for Survey 4.
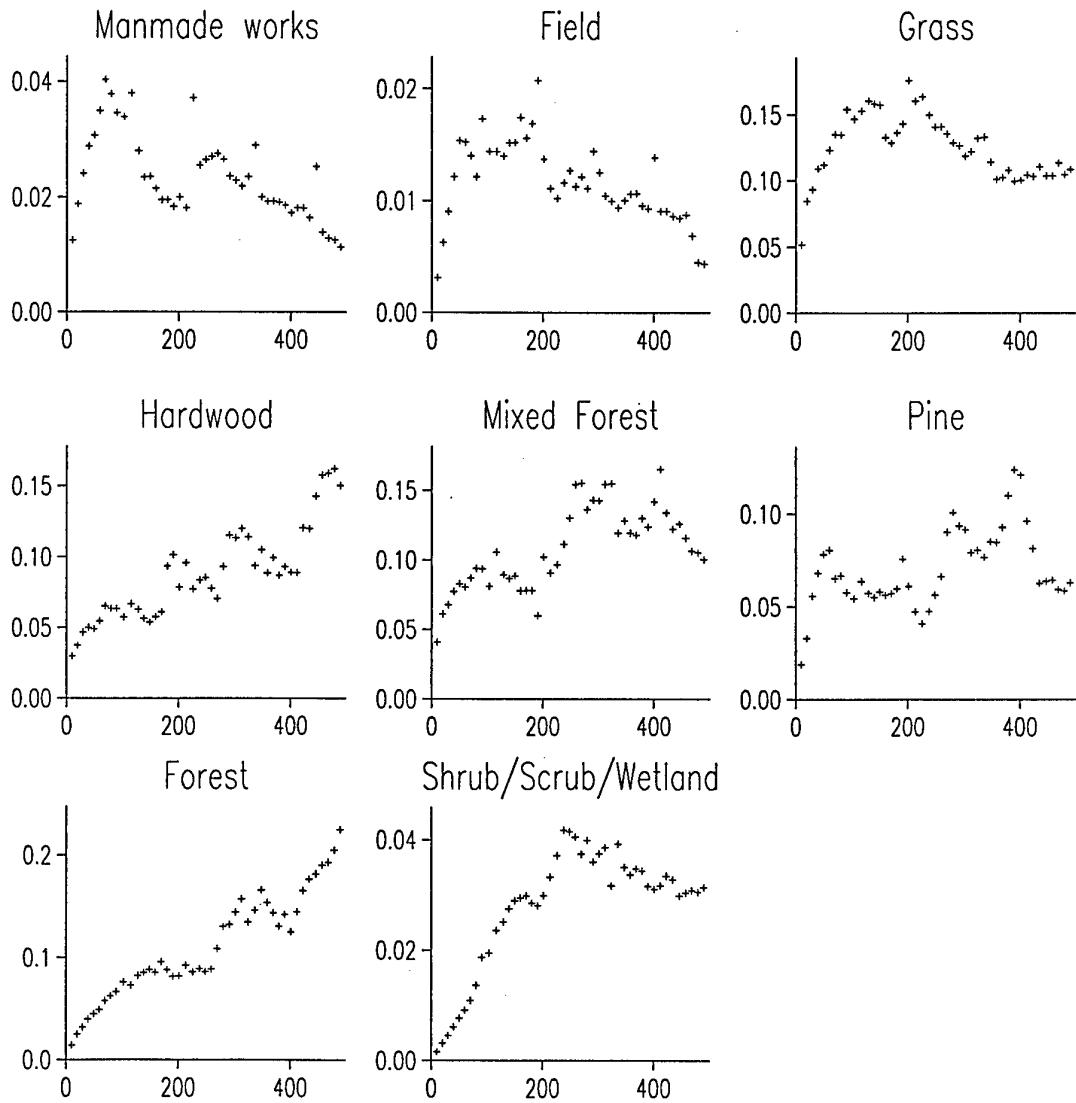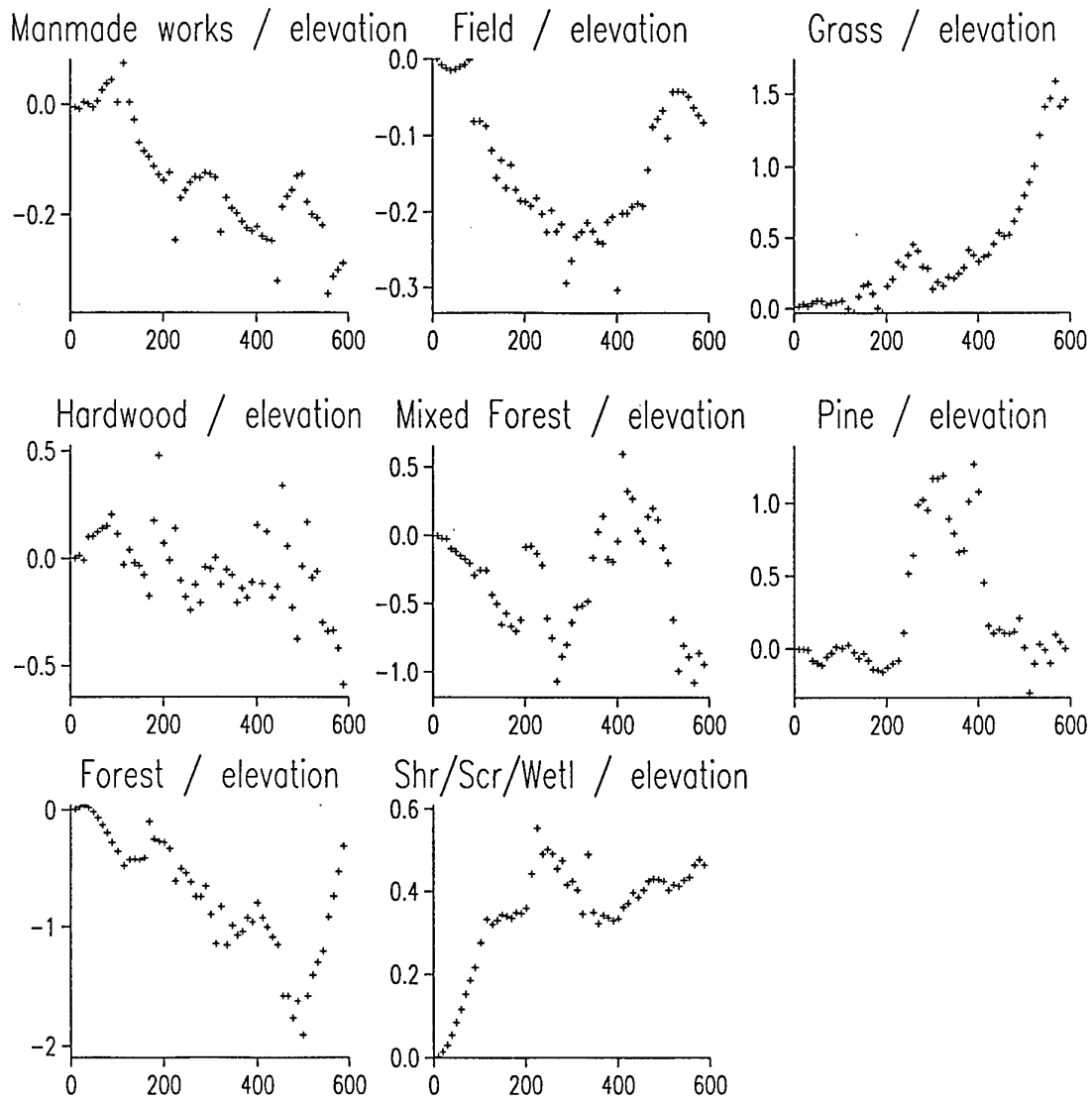
Figure 66: Cross experimental variograms between elevation and the ground cover classes for Survey 4.

Digital Elevation Analysis

Digital elevation information for A. P. Hill was provided for most of the area of the SPOT image that we have been working with. Part of the southwestern corner is missing because this are is beyond the confines of the base. The data were on a 5 m grid. Table 16 gives the summary statistics of the elevation data. Variograms were computed along the rows and columns of the grid and the average variogram was also estimated. Figure 67 shows the variograms. They all have a concave upward slope near to the origin which suggest that local trend or drift might be present. This is common for elevation data.

Table 16: Summary statistics for Elevation

	Elevation
Number of observations	26878
Minimum	155.0
Maximum	232.0
Mean	198.15
Variance	234.88
Standard deviation	15.33
Skewness	-0.5499

To assess whether the local trend could be removed by a coarser sampling interval the data were sampled to produce a 20 m grid. This corresponded with the information from the SPOT image with a pixel size of 20 m by 20 m. The variograms from these data now show no evidence of local trend, but there is evidence of regional trend, i.e. the variograms start to rise after an initial sill has been reached at about a lag distance of 800 m, Figure 68. The amount of trend present was determined by fitting linear, quadratic and cubic functions to the coordinates of these data. The linear function accounted for 17% of the trend, the quadratic 22% and the cubic 31%. Variograms were computed from the residuals to these trend functions. Figure 69 shows the variograms computed from the residuals of the linear trend. They show clearly that the regional trend has been removed. The variograms computed from the residuals of the quadratic trend, Figure 70, are similar, as are those for the cubic residuals, Figure 71. The variogram that is most different is the one for the columns in Figure 71 (cubic). This emphasises the possibility of some periodicity in the N-S direction. Table 17 gives the parameters of the models fitted to the average variograms. The model for the raw data was fitted to a lag of 600 m only because thereon the variogram continues to

rise. A single pentaspherical model provided the best fit. The model has a range of 578 m which relates closely to the long-range component in the image. The variograms of the residuals were all fitted best by nested spherical models, Table 17. Their ranges do not correspond as closely with image data as the vegetation does. The short-range component of about 220 m is similar to that of the Green waveband (2) and the long-range one of about 1000 m is similar to that fitted to the rows of NDVI.

Table 17. Variogram model parameters for elevation on a 20 m grid for A. P. Hill.

Variables	Model type	Nugget variance	Sill c_1	Sill c_2	Range a_1 (m)	Range a_2 (m)
Raw elevation data	Pentaspherical	0	162.1		578.0	
Residuals from linear trend	Double spherical	0	19.7	8.9	235.0	927.0
Residuals from quadratic trend	Double spherical	0	18.7	14.1	220.0	906.0
Residuals from Cubic trend	Double spherical	0	26.4	9.5	263.2	1363.0

The other aspect of these variograms is that there is more variation along the columns than the rows. This was also detected in the variograms of the SPOT data. Since the directional variation results in different sill heights we did not correct for it as this kind of anisotropy (zonal) requires stratification. Figure 72 shows that the two directional variograms overlap near to the origin which is the important point for kriging. It means that the kriged estimates will not be affected by the directional difference at the longer lag distances.
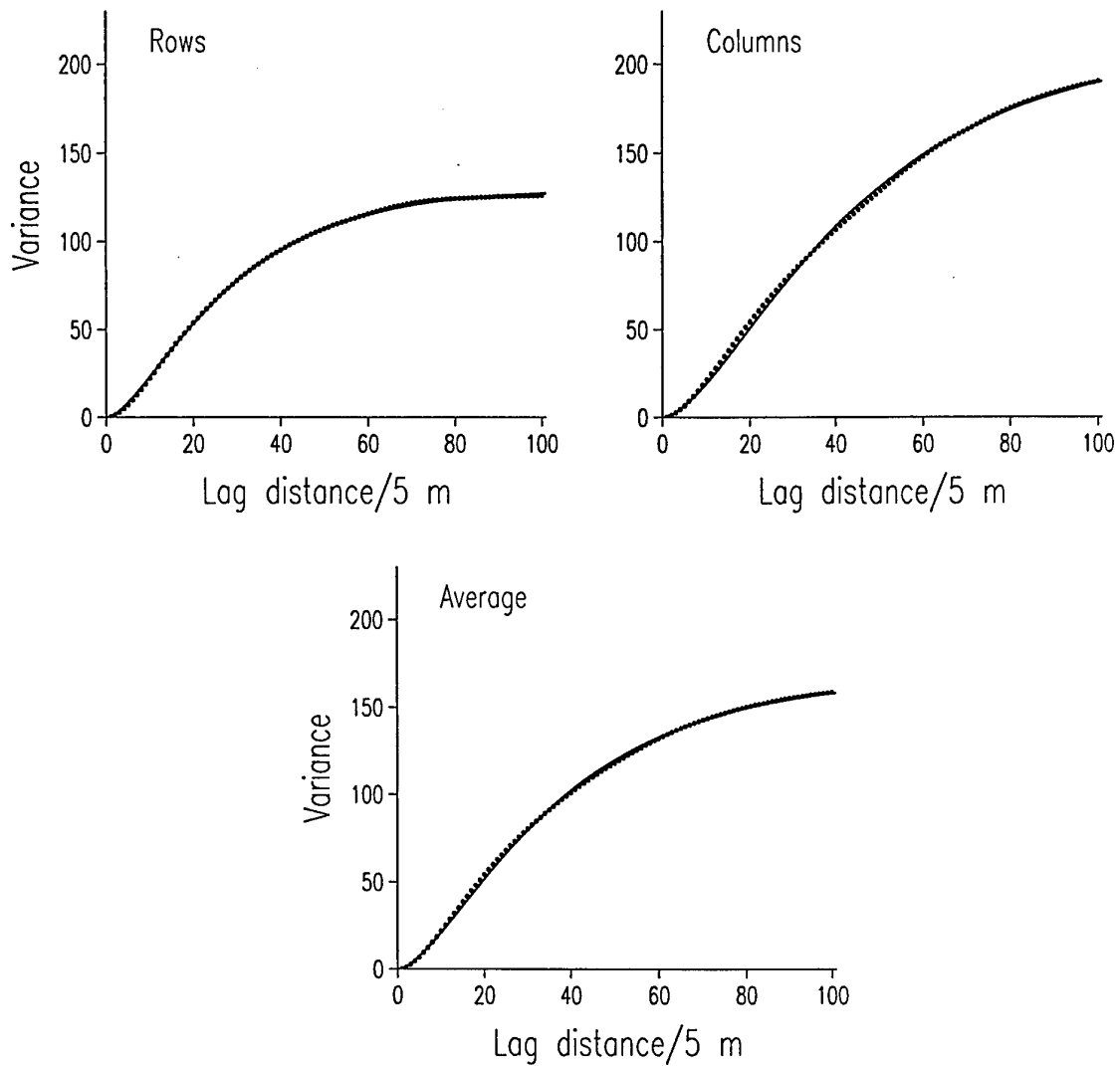
Figure 67: Experimental variograms of elevation for the rows and columns of a 5 m grid, and the average variogram of these for A. P. Hill.
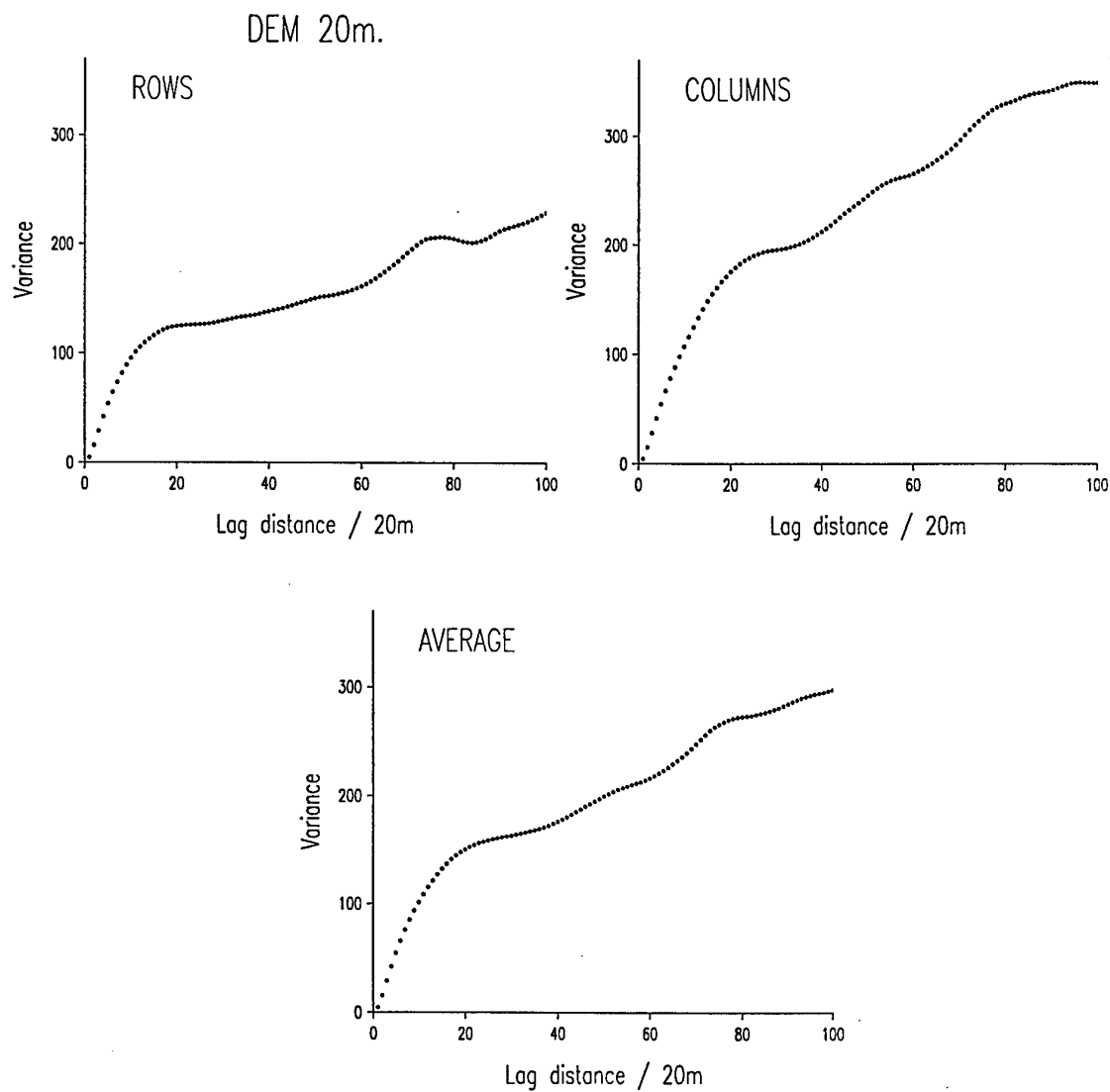
Figure 68: Experimental variograms of elevation for the rows and columns of a 20 m grid, and the average variogram of these for A. P. Hill.
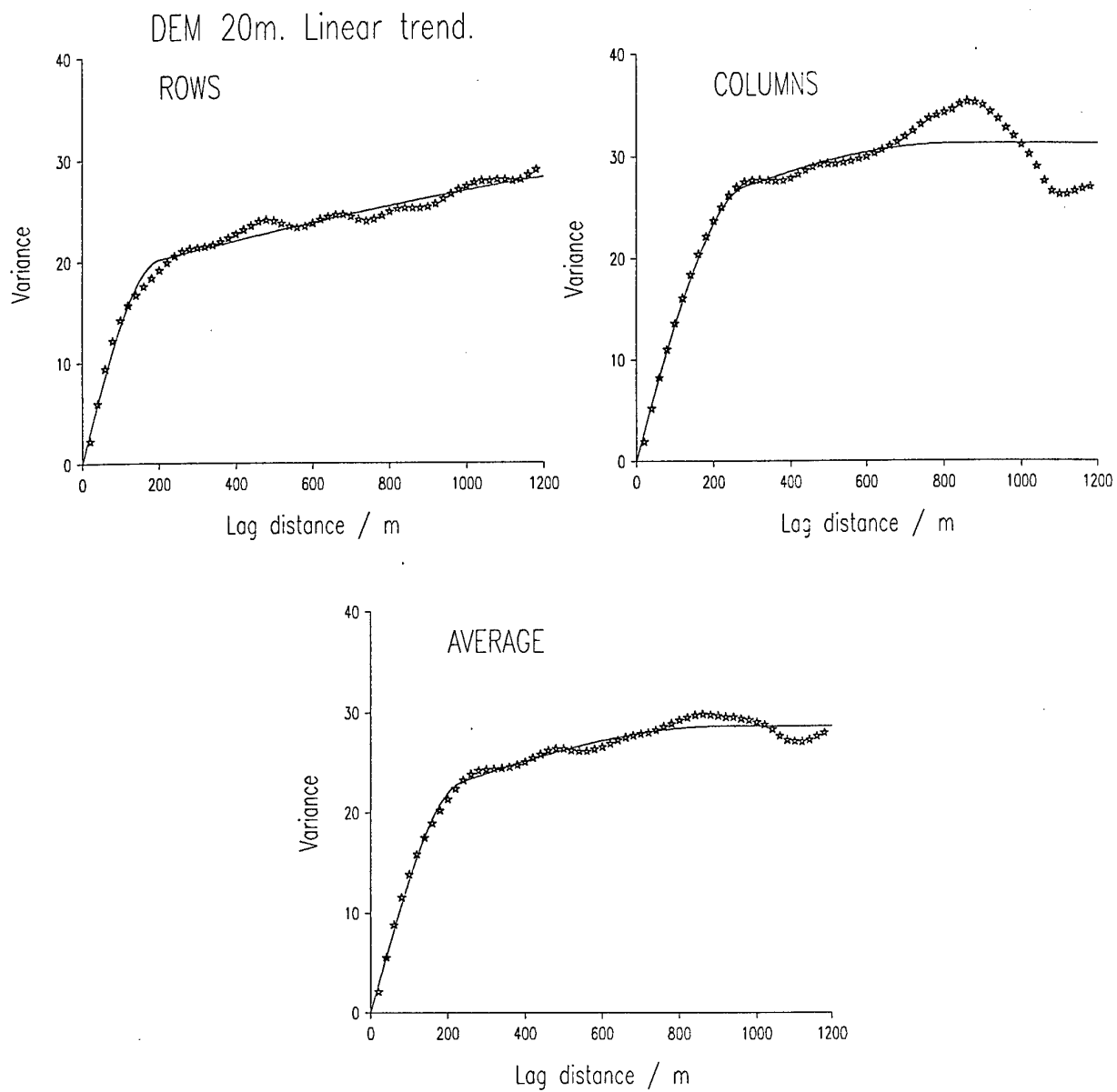
Figure 69: Experimental variograms of elevation for the rows and columns of a 20 m grid, and the average variogram of these computed from the residuals of a linear trend, and the fitted models (solid lines).
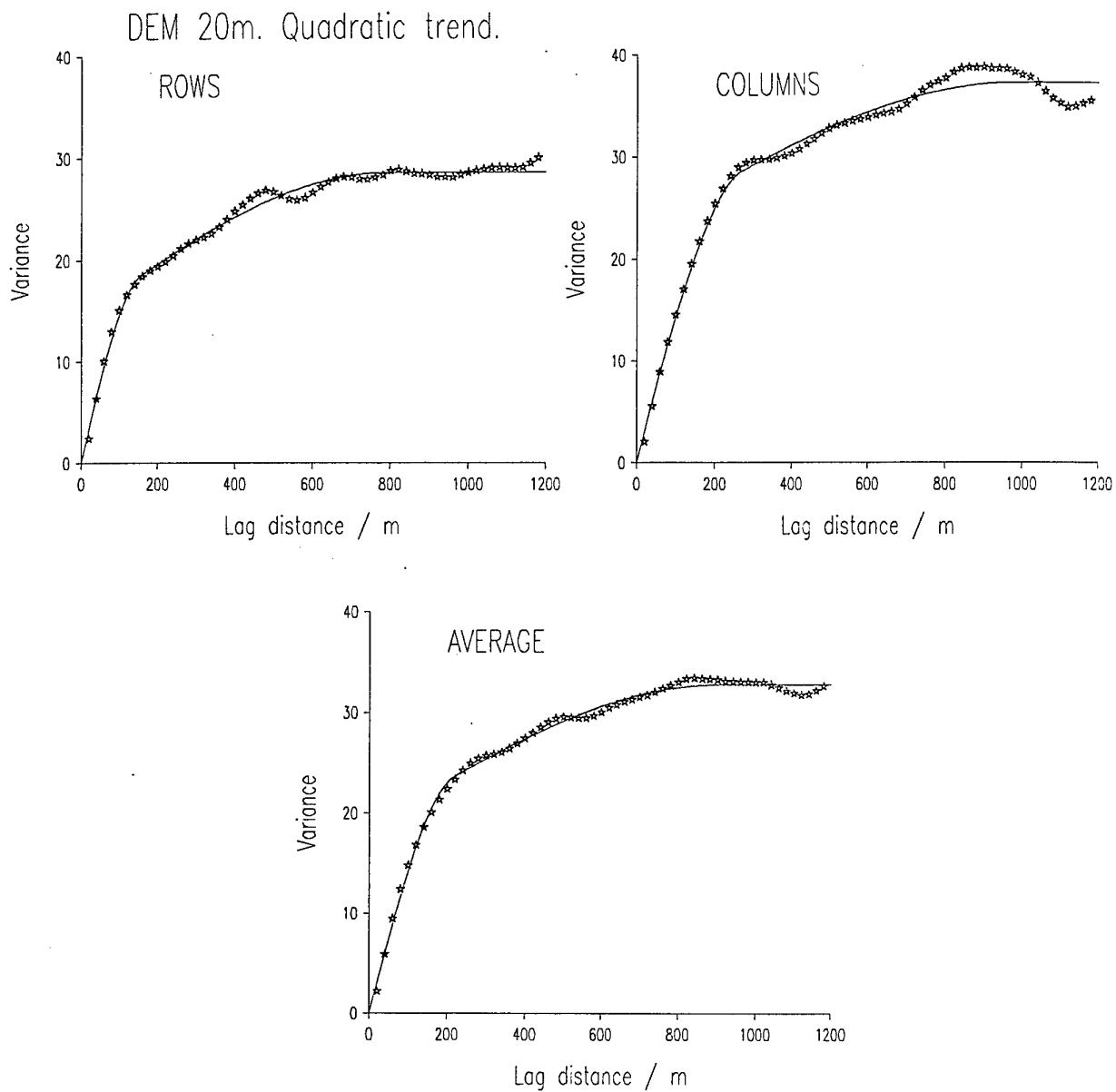
Figure 70: Experimental variograms of elevation for the rows and columns of a 20 m grid, and the average variogram of these computed from the residuals of a quadratic trend, and the fitted models (solid lines).
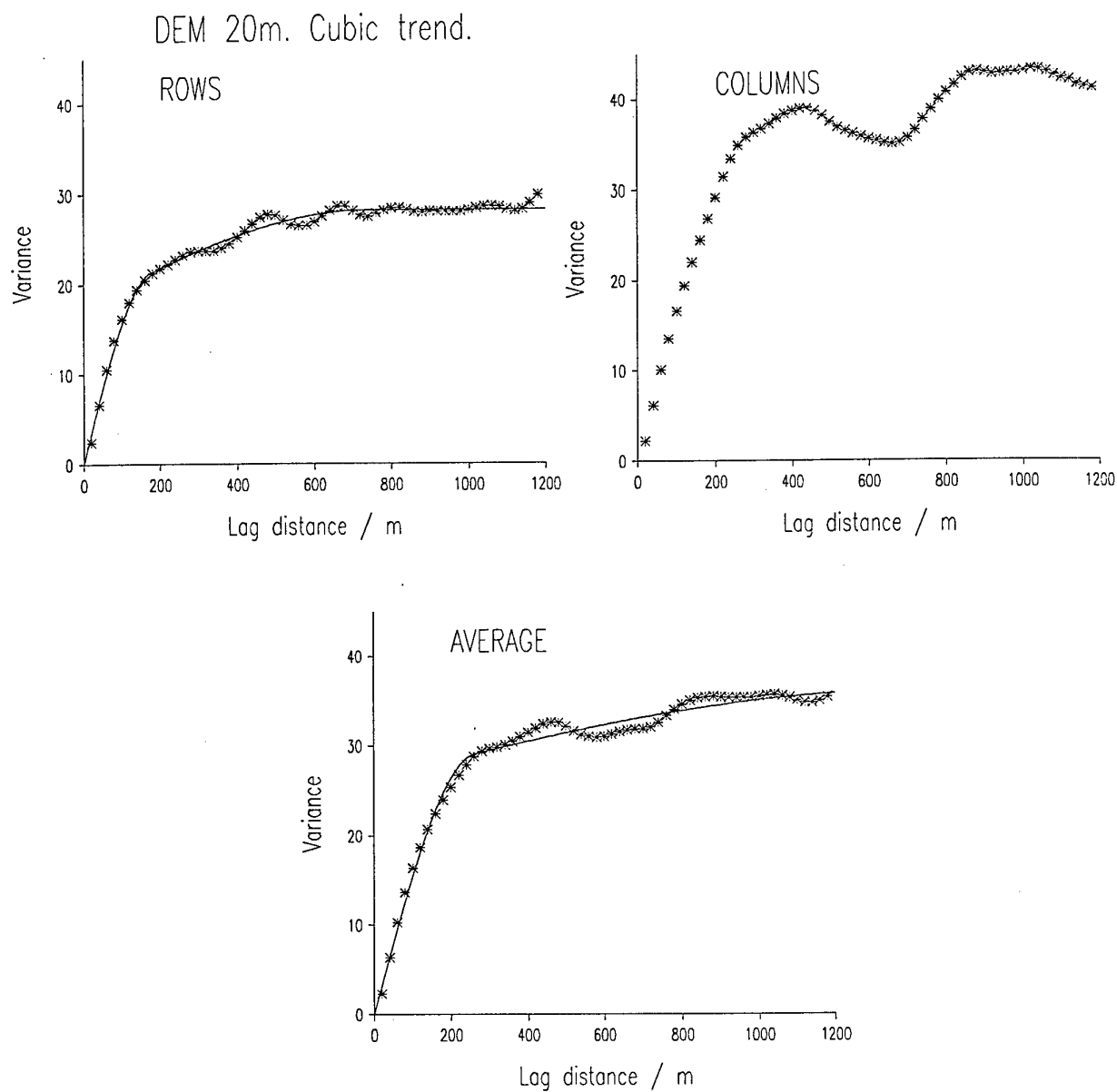
Figure 71: Experimental variograms of elevation for the rows and columns of a 20 m grid, and the average variogram of these computed from the residuals of a cubic trend, and the fitted models (solid lines).
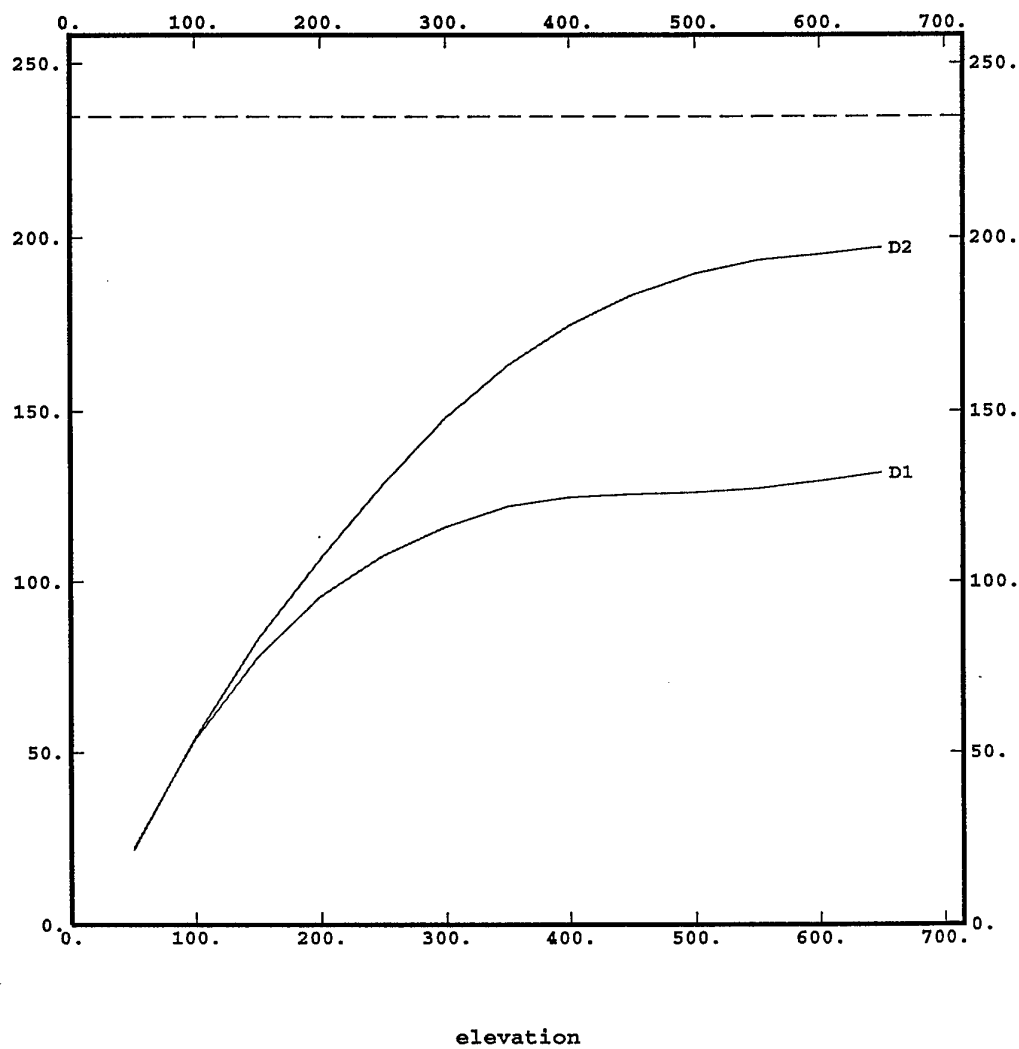
Figure 72: Experimental variograms of elevation for the rows and columns of a 20 m grid for A. P. Hill: D1 is from the rows and D2 is from the columns.

We decided to do the factorial kriging on the raw data and on the residuals from the quadratic trend. Figure 73 shows the experimental variogram and the model fitted to the average variogram of the quadratic residuals. Figures 74 and 75 show the kriged maps of the raw elevation data and that computed using the residuals from the quadratic trend, respectively. They are very similar, but the one for the residuals shows slightly more detail. The trend function that has been removed varies very smoothly and this has reduced the apparent variation in Figure 73. The strange pattern in the southwestern corner is the result of missing data in this region.

Figures 76 and 77 show the maps of the long-range component of the variation for the raw data and that from the quadratic residuals. The patterns that are evident are similar. It is interesting to compare these Figures with Figure 80, the long range component of NIR. The large valley that extends from the SW then E and then changes direction to the N E corresponds with the yellow area in Figure 80. The tributary valley that extends N from the major valley at about Easting 295500 (Figure 77) is also evident in Figure 80 as the orange area. The other valley system to the NW which runs in and E to W direction is also evident in both Figures 77 and 80. The reddish areas on the map of the long range component for NIR were interpreted as higher ground in a previous report and this is confirmed now in the maps of the DEM.

Figures 78 and 79 show the maps of the short range component of the variation for the raw data and that from the quadratic residuals. The patterns are almost identical. These correspond to the local variation in relief that is evident on the ordnance map for this area. The intricacy of the valley systems and general dissection is very clear in these maps. Again it is interesting to compare these with the short range component of NIR, Figure 81. A similar degree of detail and spatial scale is evident in all of the short-range maps.

If trend is present in data it should be removed for a geostatistical analysis. In this case it has affected the form of the variograms, but it appears to have had little effect on the spatial patterns observed after kriging both raw and residual data.

The relation between elevation and NIR was mentioned above. This was examined further by computing the cross variogram between them. Figure 80 shows the autovariograms for elevation and NIR together with their cross variogram. The outer dotted lines on the cross variogram show the hull of perfect correlation. It shows that although there is a relation between the image information and elevation it is weak. Visually it is more convincing. This result will be explored further in the next phase of work when we shall analyse a smaller part of the image.
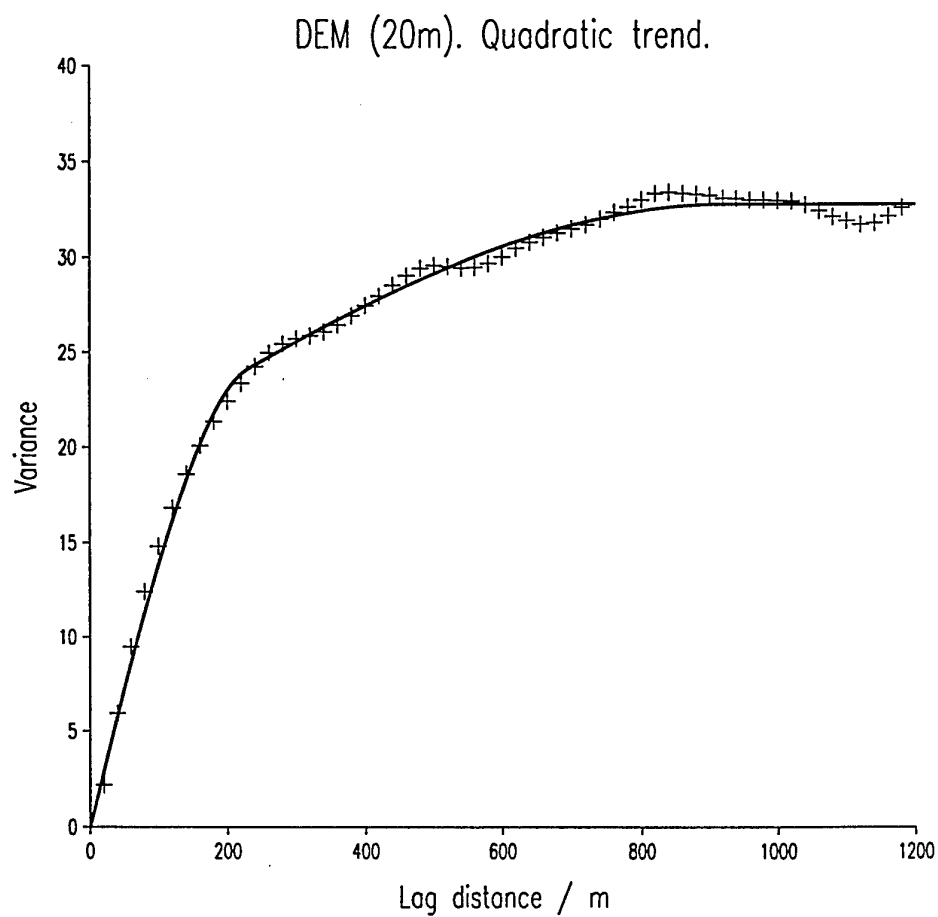
Figure 73: Average experimental variogram of elevation for the 20 m grid computed from the residuals of a quadratic trend, and the fitted models (solid line).
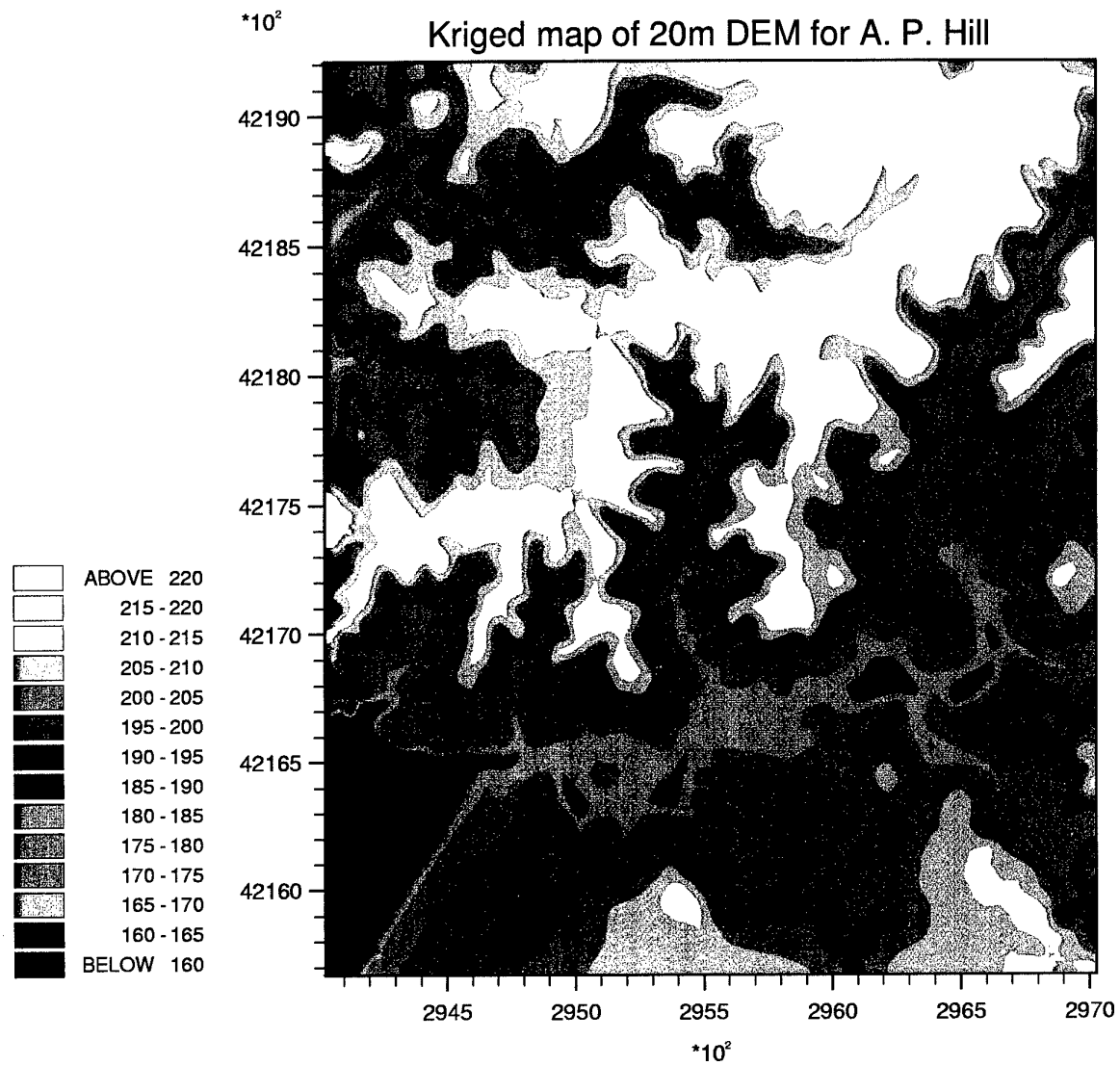
Figure 74: Kriged map of the raw elevation data on the 20 m grid for A. P. Hill.
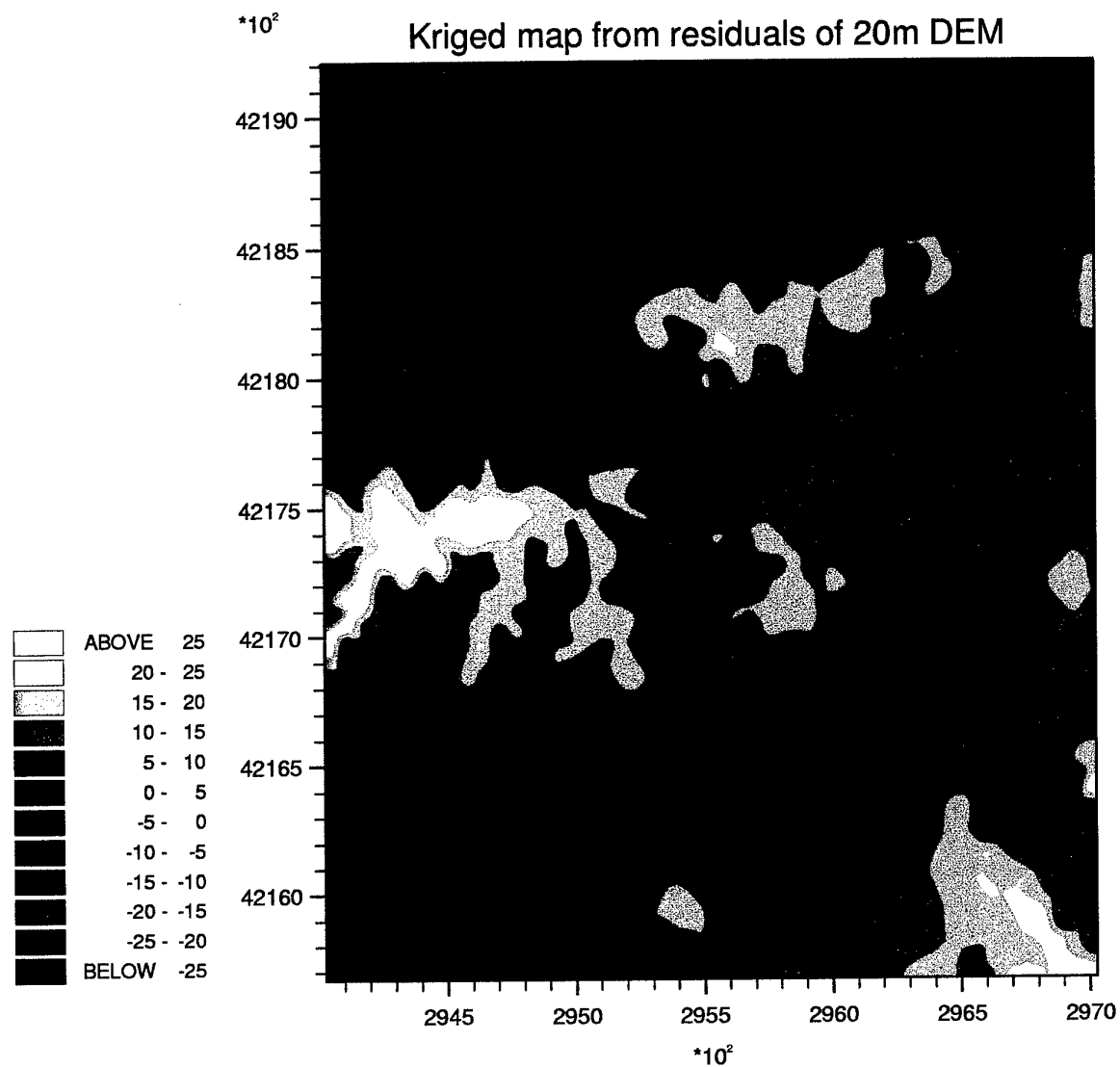
Figure 75: Kriged map of the residuals from a quadratic trend of elevation on the 20 m grid A. P. Hill.
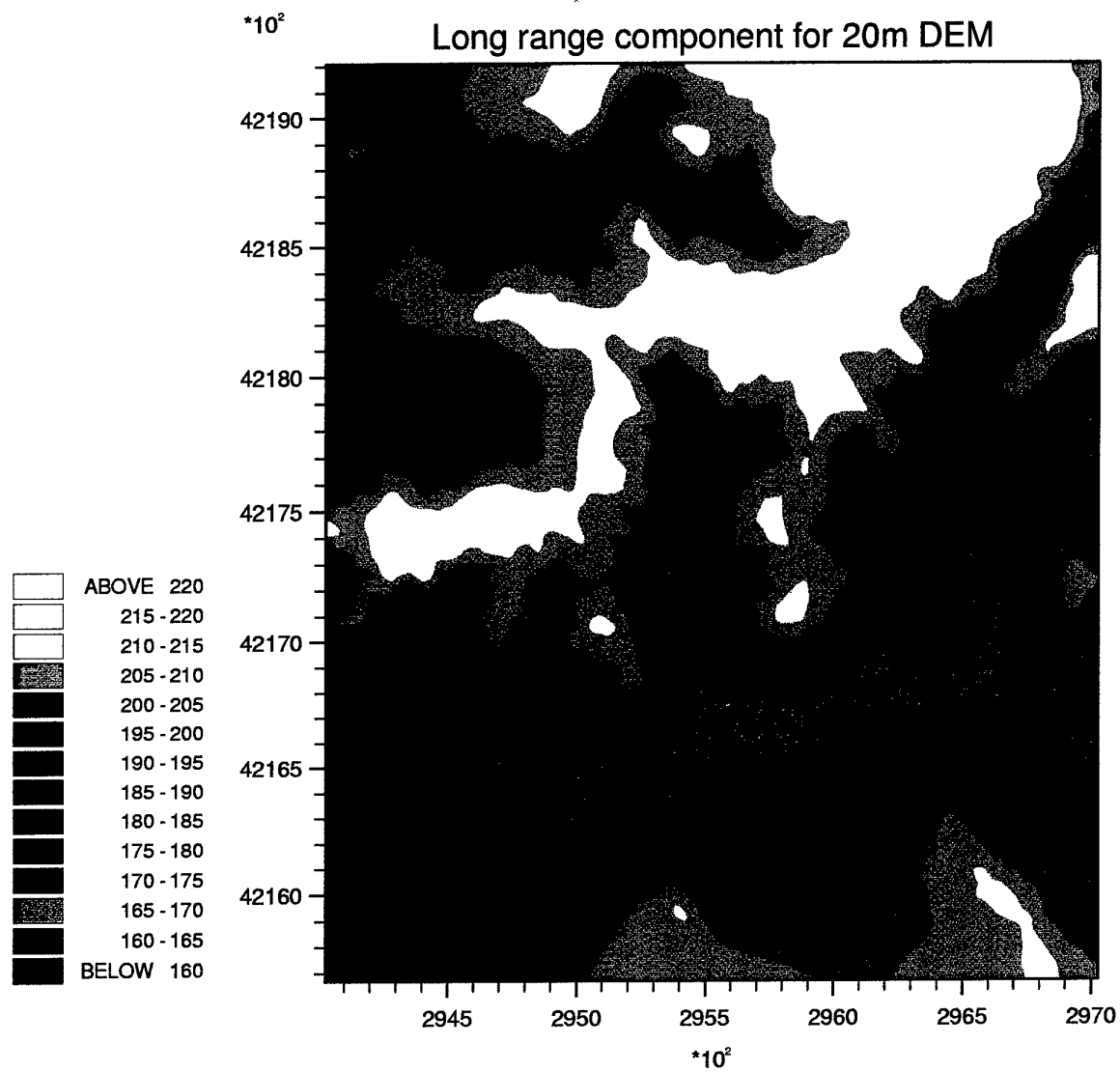
Figure 76: Kriged map of the long range component of the variation for the raw elevation data on the 20 m grid for A. P. Hill.
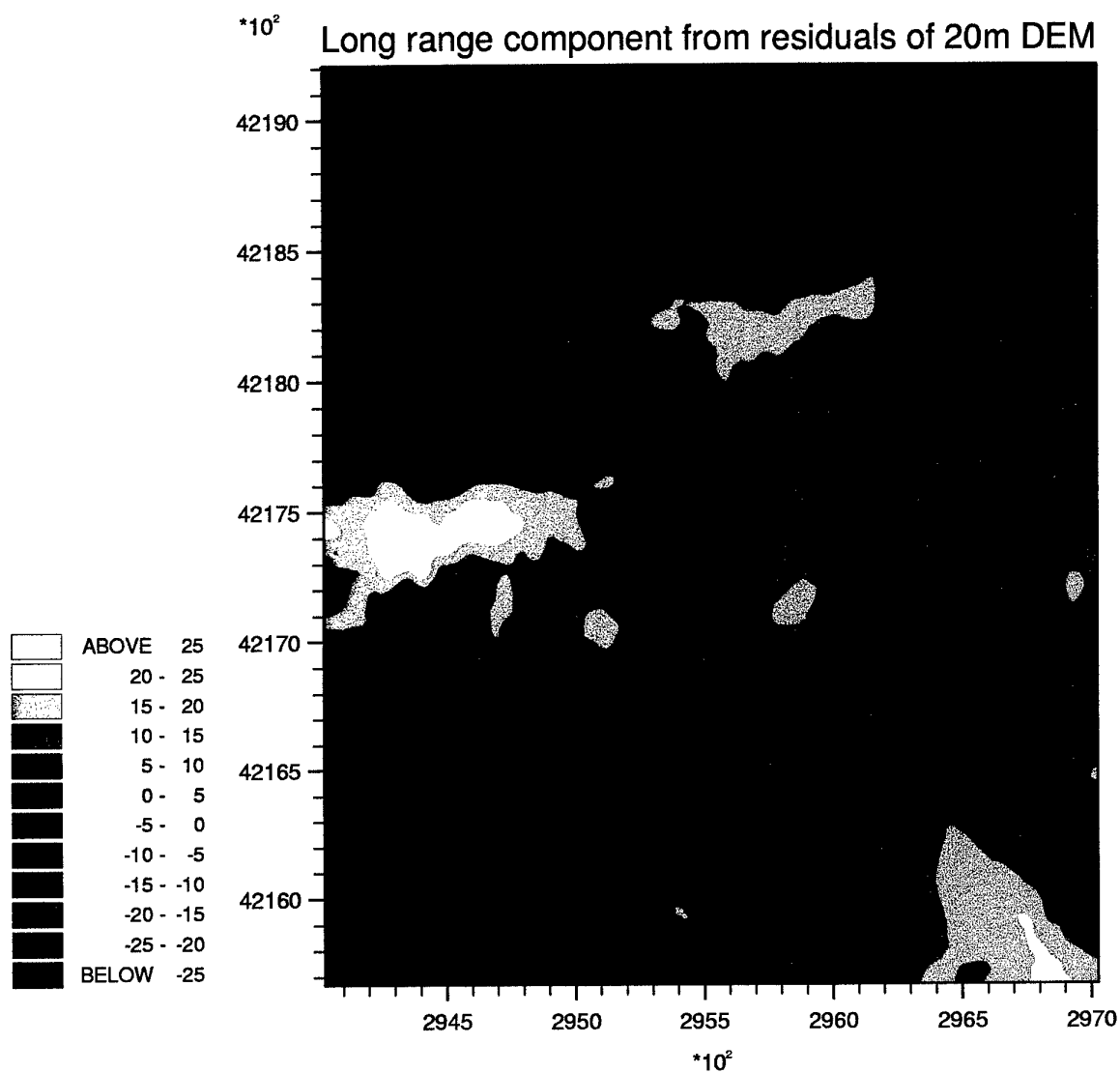
Figure 77: Kriged map of the long range component of the variation for the residuals from a quadratic trend of elevation on the 20 m grid A. P. Hill.
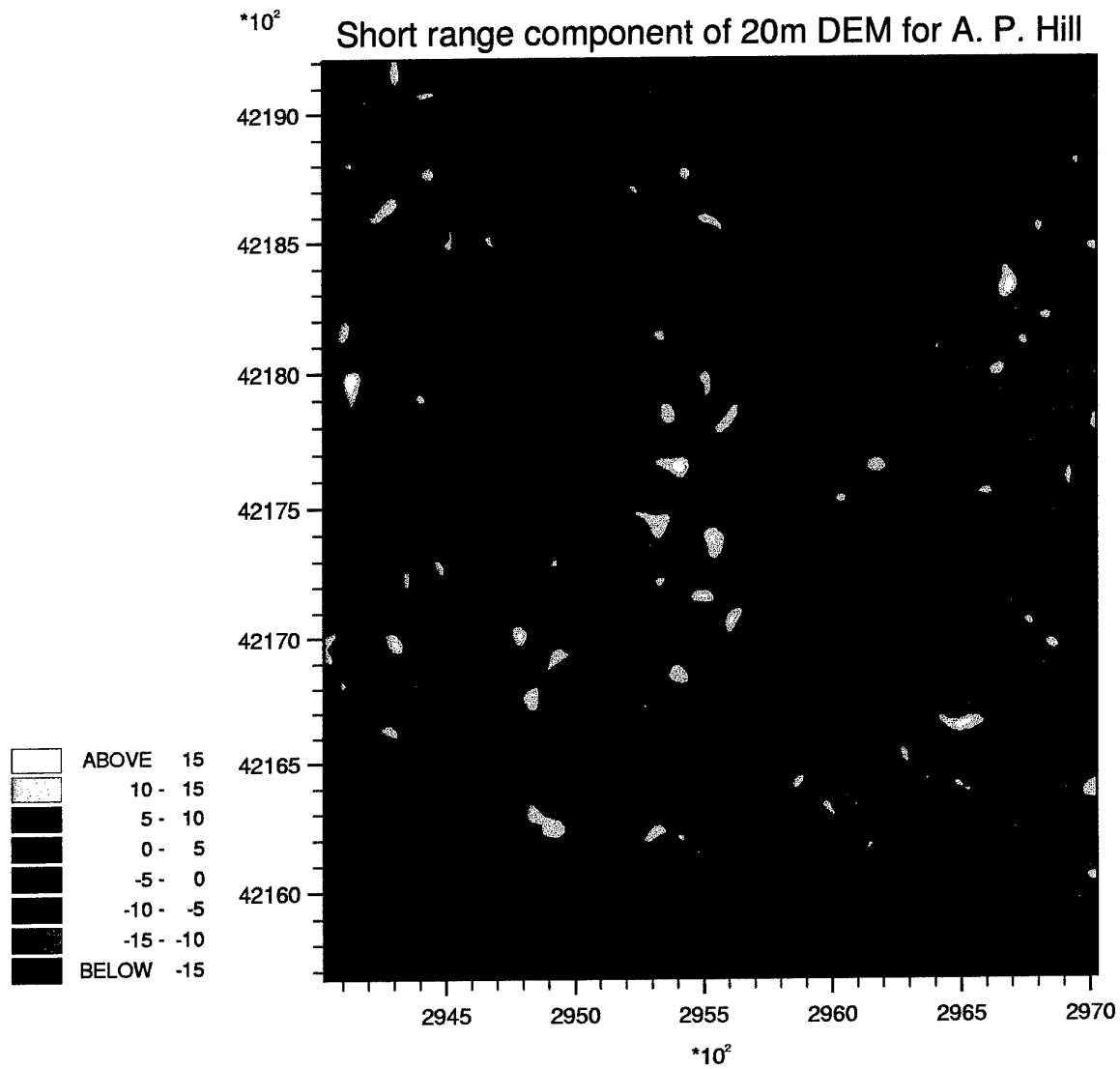
Figure 78: Kriged map of the short range component of the variation for the raw elevation data on the 20 m grid for A. P. Hill.
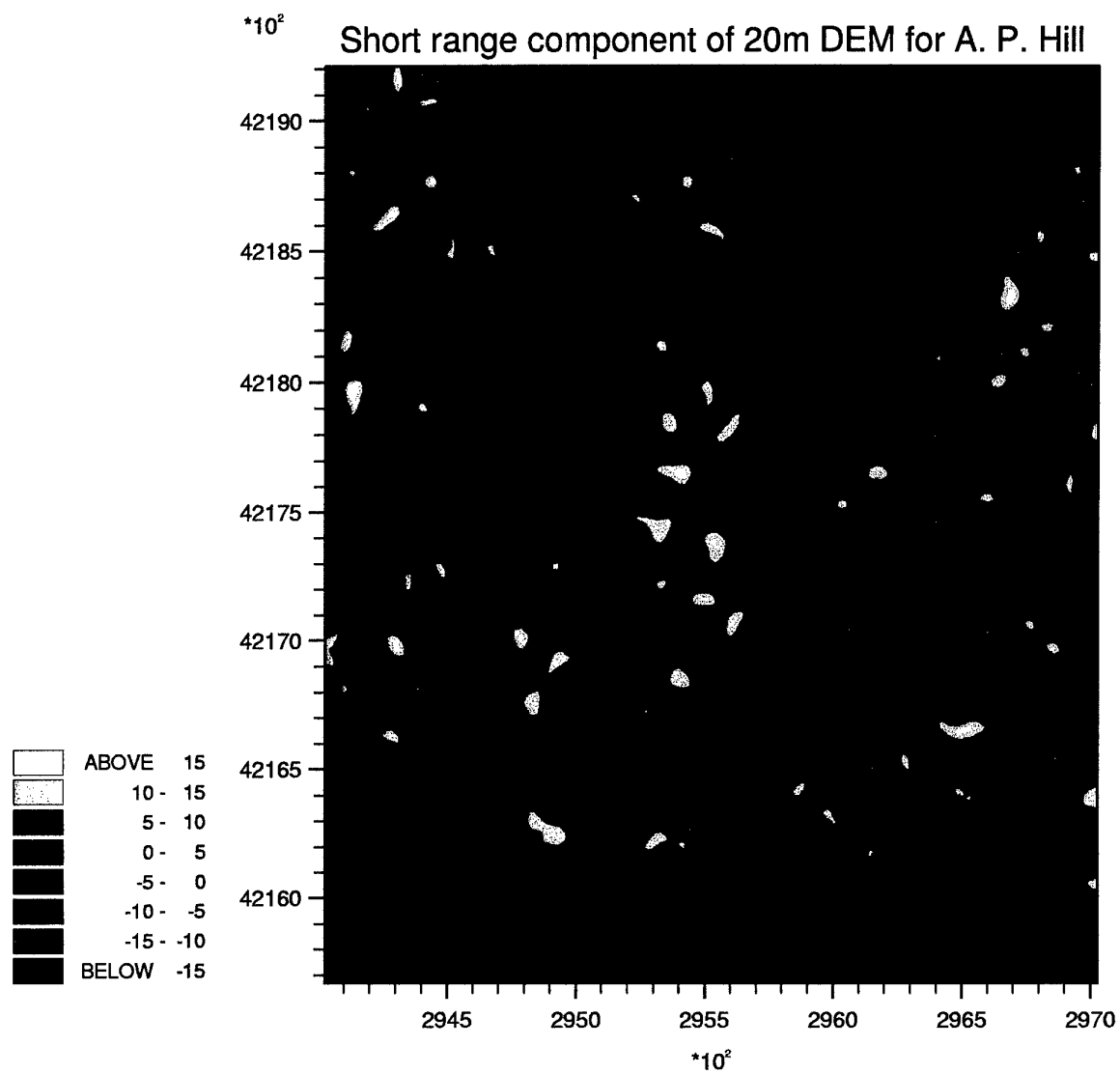
Figure 79: Kriged map of the short range component of the variation for the residuals from a quadratic trend of elevation on the 20 m grid A. P. Hill.

Long-range kriged estimates for NIR
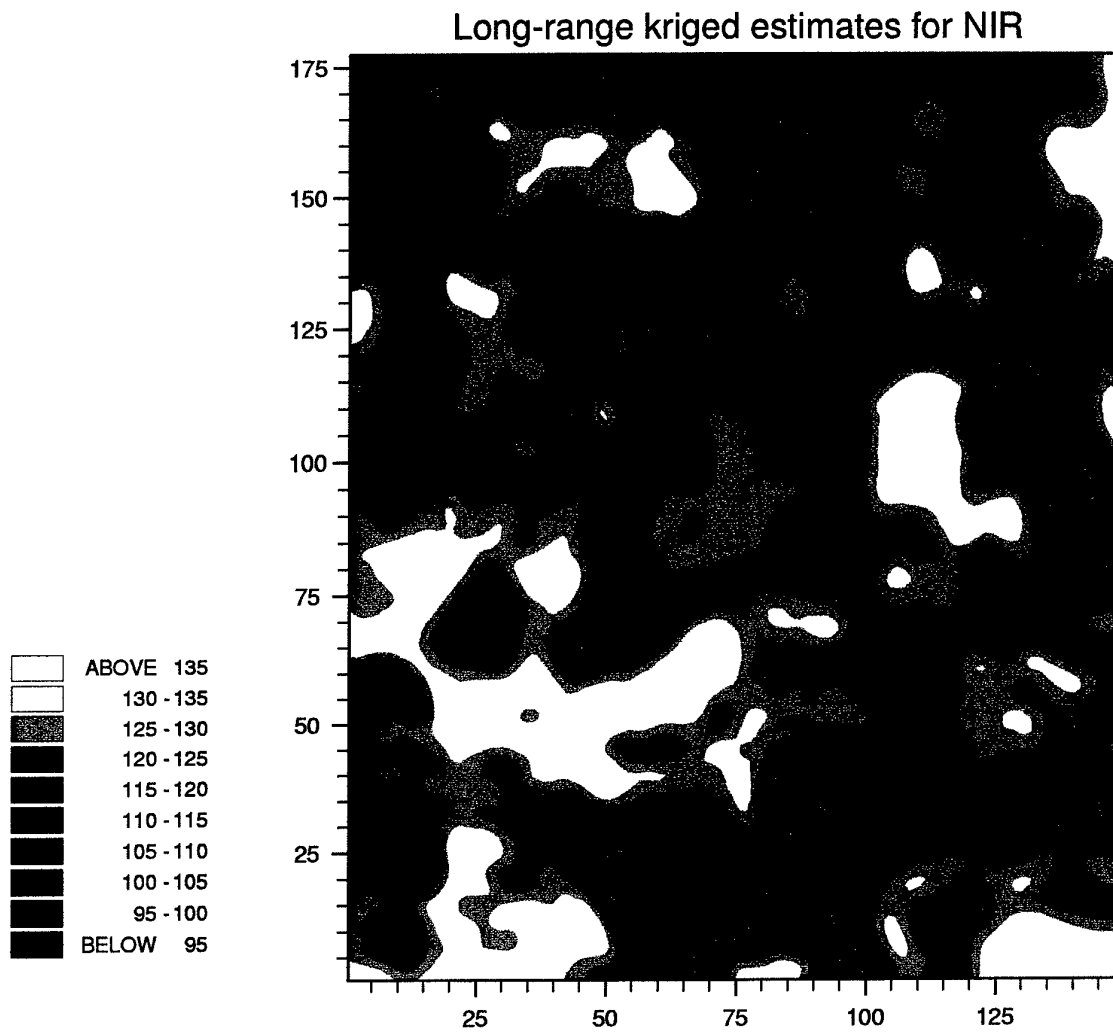
Figure 80: Kriged map of the long range component of the variation for NIR.
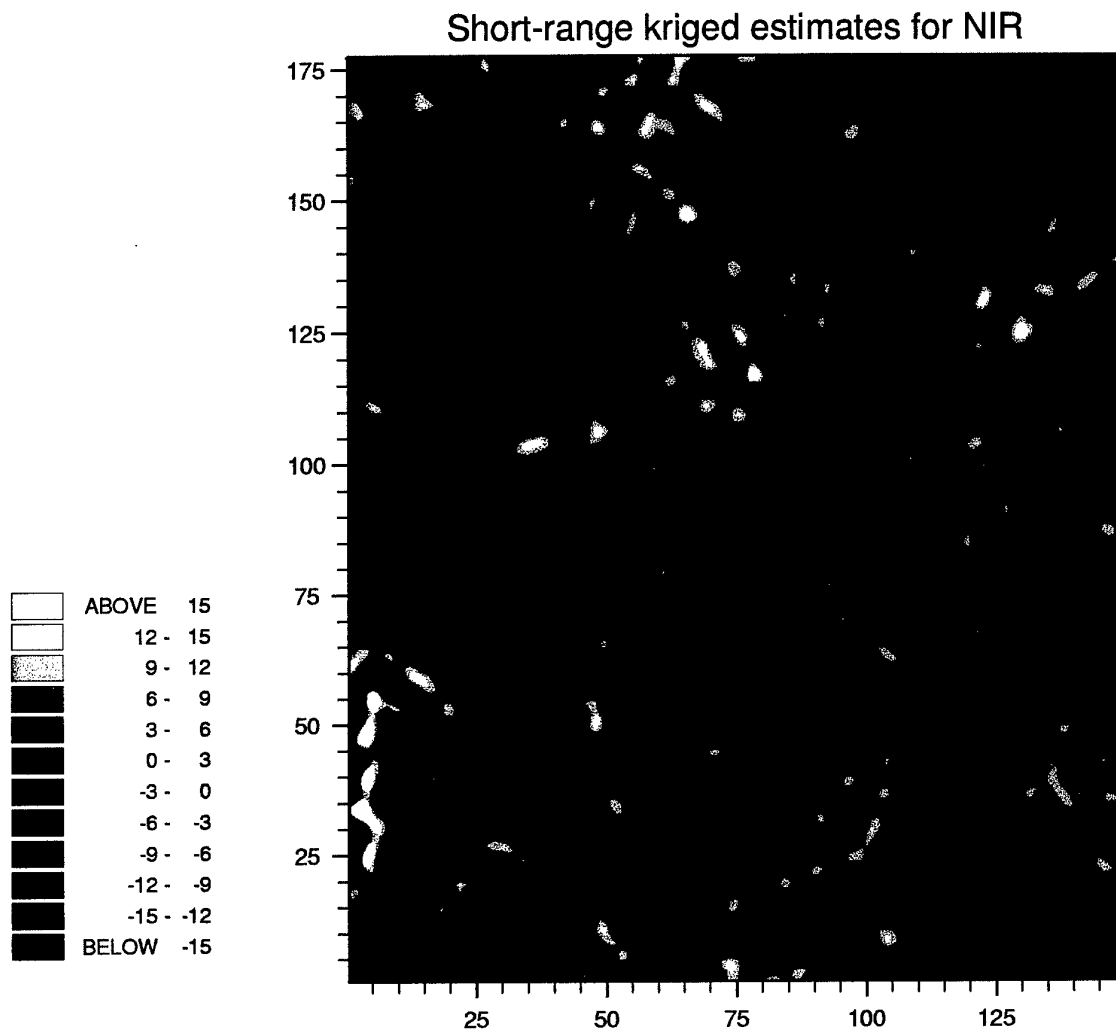
Figure 81: Kriged map of the short range component of the variation for NIR.
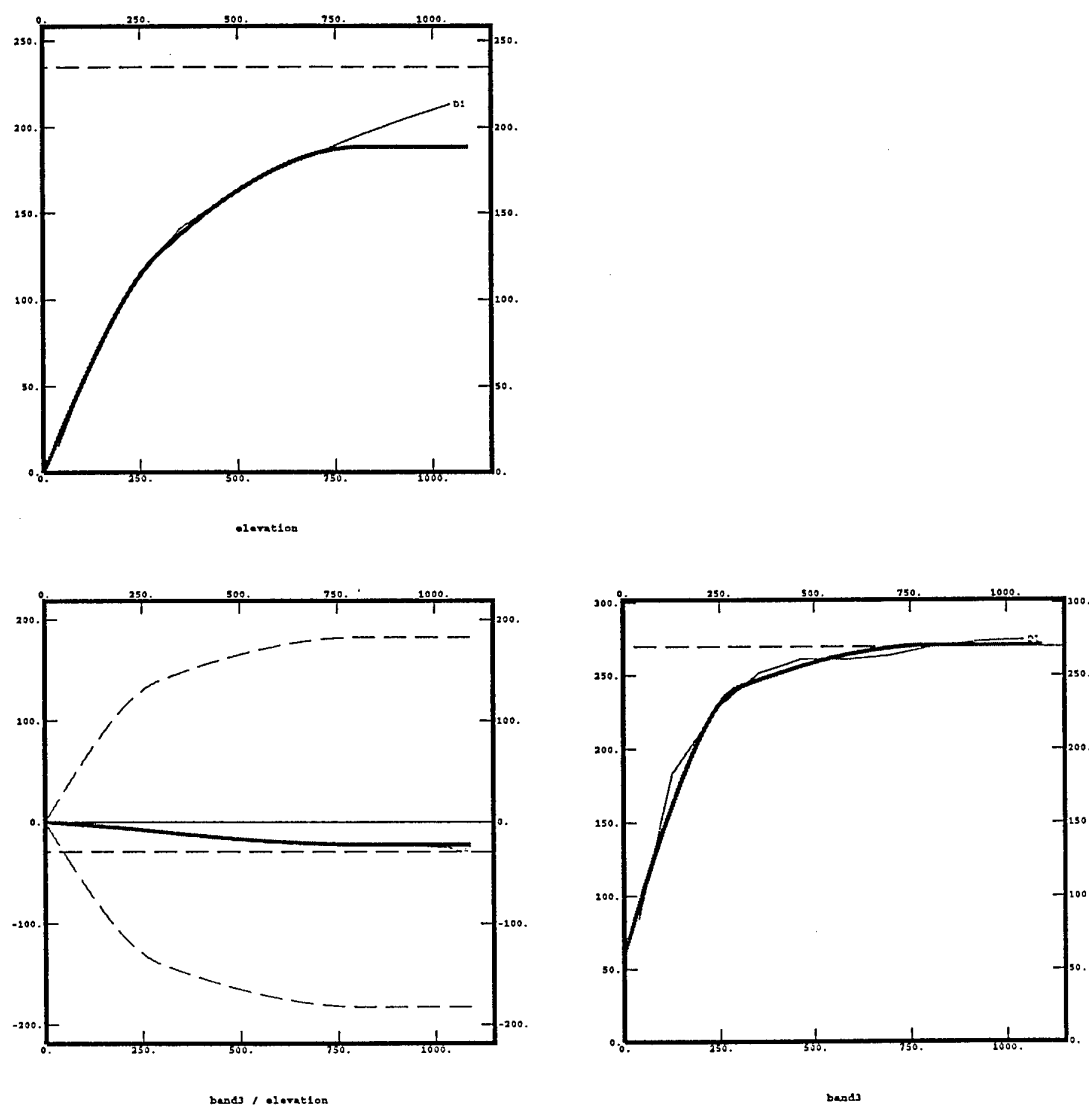
Figure 82: Auto- and cross-variograms of elevation and NIR for A. P. Hill.

Acknowlededgments

I thank Johan Stendahl for help with the analysis of the vegetation and elevation data, Ruth Kerry for help with some of the analysis and assembling the second report, and Robert Henderson for help in assembling the final report.

References

Daubechies, I 1988. Orthonormal bases of compactly supported wavelets. *Communications in Pure and Applied Mathematics*, **41**, 909-996.

Daubechies, I. 1992. *Ten Lectures on Wavlets*. Society for Industrial and Applied Mathematices (SAIM), Philadephia.

Kumar, P. and Foufoula-Georgio, E. 1994. Wavelet analysis in geophysics: An introduction. In: *Wavelets in Geophysics* (eds. E. Foufoula-Georgiou and P. Kumar), Academic Press, New York, pp. 1-42

Mallat, S. 1998. *A Wavelet Tour of Signal Processing*, Academic Press.

Oliver, M A., Webster, R and Slocum, K. 1999. Image filtering by kriging analysis. In: G. Goméz Hernandéz, A. Soares and R, Friodevaux (eds.), *geoENV II - Geostatistics for Environmental Applications*, Kluwer Academic Publishers, Dordrecht, pp. 549-560.

Oliver, M A., Webster, R and Slocum, K. 1999. Filtering SPOT imagery by factorial kriging. *International Journal of Remote Sensing*, (proofs completed).

Strang, G. 1989. Wavelets and dilation equations: A brief introduction. *SIAM Review, Journal of Mathematics*, **31**, 614-627.

IMAGE FILTERING BY KRIGING ANALYSIS

M. A. OLIVER, R. WEBSTER AND K. SLOCUM

Department of Soil Science, The University of Reading,
Whiteknights, Reading RG6 6DW, UK.

Statistics Department, Rothamsted Experimental Station,
Harpenden, Hertfordshire AL5 2JQ, UK.

AND

US Topographic Engineering Center, 7701 Telegraph Road,
Alexandria, VA 22315-3864, USA.

Abstract. Digital images contain so much information that it is difficult to identify and interpret spatial structures that they might contain. We have investigated kriging analysis to reveal structure in imagery and to estimate its spatial scales separately. We applied the analysis to part of a SPOT image of a dissected landscape in the south eastern United States. Variograms for the three wavebands in the imagery and the normalized difference vegetation index (NDVI) showed variation on two distinct spatial scales, which we modelled with a nested (double) exponential function, with effective ranges of 140 to 300 m and 2340 to 3400 m. By kriging analysis we estimated the separate contributions of the short- and long-range spatial components. The maps of the short-range components seem to represent a patchiness in the ground cover, whereas the long-range component seems to reflect the coarser pattern imposed by the gross physiography. The paper is illustrated with the results of analysing the NDVI.

1. Introduction

Satellite imagery provides complete cover of information over large tracts of terrain. That from SPOT records radiation from the Earth's surface in three wavebands, green, red and near infra red, at 20-m intervals with pixels that are nominally 20 m × 20 m. Figure 1 is an example. The spatial pattern is evidently complex. To make sense of it we need to separate what is meaningful from that with no significance. This distinction between

'signal' and 'noise' is a function of the the spatial scales that we wish to resolve. We want a separation driven by the data themselves rather than one imposed by the investigator, especially in the early stages when the aim is to understand the pattern. If there is variation at different spatial scales then we might want to isolate the spatial components to aid interpretion and to design ground surveys.

Geostatistics is being used increasingly to analyse remote imagery (e.g. Woodcock et al., 1988; Webster et al., 1989; van der Meer, 1993, and Wen and Sinding-Larsen, 1997). Ordinary kriging has enabled investigators to smooth images by removing some of the short-range variation, and in particular nugget variance, to produce simpler and more intelligible pictures. However, this has meant that the short-range variation has been treated as if it were unimportant, or noise. What is regarded as noise at one scale may be the signal at another, and we need a means of changing the emphasis. Matheron (1982) recognized the need, and developed a procedure that he called 'kriging analysis'. It treats the variation at each evident scale in turn as the signal, and separates it from variation at all other scales, which is treated as noise. Kriging analysis depends on identifying the distinct spatial scales in the spatial covariance function or the variogram. Once these have been modelled they can be used as separate components with which to krige.

We have explored the application of kriging analysis to part of a SPOT image of Columbus, Georgia. We detected two markedly distinct scales of spatial variation in the variograms of all three wavebands and in the normalized difference vegetation index (NDVI). We modelled these with nested functions which we used with the pixel data to filter the image and map the short- and long-range spatial components independently.

2. Theory and method

2.1 NESTED VARIATION

A spatial random process can be a combination of several constituent random processes one nested within another and acting at different characteristic spatial scales. If the constituent processes are independent of one another then the whole is their sum. In these circumstances the variogram of $Z(\mathbf{x})$ is itself a nested combination of two or more, say S, individual variograms:

$$\gamma(\mathbf{h}) = \gamma^1(\mathbf{h}) + \gamma^2(\mathbf{h}) + \cdots + \gamma^S(\mathbf{h}) , \qquad (1)$$

where the superscripts refer to the separate variograms. If we assume that the processes are uncorrelated then we can represent Equation (1) by the

sum of S basic variograms:

$$\gamma(\mathbf{h}) = \sum_{k=1}^{S} b^k g^k(\mathbf{h}) , \qquad (2)$$

where $g^k(\mathbf{h})$ is the kth basic variogram function, and b^k is a coefficient that measures the relative contribution of the variance of $g^k(\mathbf{h})$ to the sum. The nested variogram comprises the S variograms with different coefficents b^k, Figure 2. This is our linear model of regionalization. It represents the real world in which factors such as relief, geology, tree-throw, fauna, and man's divisions into fields and farms, operate on their own characteristic spatial scale(s), and each with its particular form and parameters, b^k, for $k = 1, 2, \ldots, S$.

2.2. KRIGING ANALYSIS

In ordinary kriging $Z(\mathbf{x})$ is estimated in a single operation from the data and the variogram, $\gamma(\mathbf{h})$. For kriging analysis $Z(\mathbf{x})$ itself is regarded as the sum of S orthogonal random functions, corresponding with the components of the variogram, $b^k g^k(\mathbf{h})$, in Equation (2). Provided $Z(\mathbf{x})$ is second-order stationary this sum can be represented as

$$Z(\mathbf{x}) = \sum_{k=1}^{S} Z^k(\mathbf{x}) + \mu , \qquad (3)$$

in which μ is the mean of the process. Each $Z^k(\mathbf{x})$ has expectation 0, and the squared differences are

$$\frac{1}{2}\mathrm{E}\left[\{Z^k(\mathbf{x}) - Z^k(\mathbf{x}+\mathbf{h})\}\{Z^{k'}(\mathbf{x}) - Z^{k'}(\mathbf{x}+\mathbf{h})\}\right] = b^k g^k(\mathbf{h}) \text{ if } k = k'$$
$$= 0 \text{ otherwise} . \qquad (4)$$

It is possible that the last component, $Z^S(\mathbf{x})$, is intrinsic only, so that $g^S(\mathbf{h})$ in Equation (2) is unbounded with intensity b^S. For two components, as in the images we have been examining, Equation (3) reduces to

$$Z(\mathbf{x}) = Z^1(\mathbf{x}) + Z^2(\mathbf{x}) + \mu . \qquad (5)$$

Relation (4) expresses the mutual independence of the S random functions $Z^k(\mathbf{x})$. With this assumption, the nested model (2) is easily retrieved from relation (3).

Each spatial component $Z^k(\mathbf{x})$ can be estimated as a linear combination of the observations $z(\mathbf{x}_i), i = 1, 2, \ldots, N$:

$$\widehat{Z}^k(\mathbf{x}_0) = \sum_{i=1}^{N} \lambda_i^k z(\mathbf{x}_i) . \qquad (6)$$

In practice N is replaced by n, where $n \ll N$ is the number of observations near to x_0. The λ_i^k are the weights assigned to the observations. They must sum to 0, not 1 as in ordinary kriging, to ensure that the estimate is unbiased and to accord with Equation (3). Subject to this condition they are chosen so that the estimation variance is minimal. This leads to the kriging system:

$$\sum_{j=1}^n \lambda_j^k \gamma(x_i, x_j) - \psi^k = b^k g^k(x_i, x_0) \quad \text{for all} \quad i = 1,2,\ldots,n$$

$$\sum_{j=1}^n \lambda_j^k = 0 .$$

(7)

This system is solved to find the weights, λ_j^k, which are then inserted into Equation (6). The quantity ψ^k is the Lagrange multiplier for the kth component. In this way we can extract from the data each of the correlation structures identified in the experimental variogram separately. If the variogram has two distinct spatial structures they can be estimated separately, and represented as two surfaces or maps that describe the variation at these resolutions (see Figures 4 and 5).

In many instances data contain long-range trend. This need not complicate the analysis because the kriging is usually done in fairly small moving neighbourhoods centred on x_0, as above. From a theoretical point of view it is necessary only that $Z(x)$ is locally stationary, or *quasi-stationary*. Equation (3) may then be rewritten as

$$Z(x) = \sum_{k=1}^S Z^k(x) + \mu(x) ,$$

(8)

where $\mu(x)$ is a local mean, which can be considered as a long-range spatial component. Matheron (1982) showed that this relation is also verified in terms of estimators, i.e.

$$\widehat{Z}(x) = \sum_{k=1}^S \widehat{Z}^k(x) + \widehat{\mu}(x) .$$

(9)

To krige a second-order stationary component at a place x_0 we start with the linear combination of the observations $z(x_j)$:

$$\widehat{\mu}(x_0) = \sum_{j=1}^n \lambda_j z(x_j) .$$

(10)

The weights are obtained by solving the kriging system:

$$\sum_{j=1}^n \lambda_j \gamma(x_i, x_j) - \psi = 0 \quad \text{for all} \quad i = 1,2,\ldots,n ,$$

$$\sum_{j=1}^n \lambda_j = 1 .$$

(11)

Estimation of the long-range component, i.e. the local mean $\mu(x)$ and the spatial component with the largest range, can be affected by the size of the moving neighbourhood, see Galli *et al.* (1984). To estimate a spatial component with a given range, the distance across the neighbourhood should be at least equal to that range. Frequently when the sampling density and the range are large there are so many data within the chosen neighbourhood that only a small proportion of them is retained. If all were retained then (a) instabilities would be likely when inverting the large variance matrices, and (b) only the nearest ones would contribute to the estimate because they would screen the more distant data. The latter means that the neighbourhood actually used is smaller than the neighbourhood specified and the range of the estimated spatial component is smaller than the range apparent from the structural analysis. To avoid these we adopted the procedure proposed by Jaquet (1989) and used by Goovaerts and Webster (1994). It simply involves adding an estimate of the local mean to the long-range spatial component estimated from the solution of system (7).

3. Analysis and Results

We obtained the data from SPOT as digital numbers in the three wavebands, geometrically corrected. The digital numbers in channels 2 and 3 were positively skewed, and we transformed them to logarithms to stabilize their variances in all subsequent analyses. We computed the normalized difference vegetation index (NDVI), D, from the digital numbers in the red (R) and near infra red (I) wavebands by

$$D = (I - R)/(I + R) .$$

(12)

The pixel map shown as Figure 1 is that of the NDVI. We concentrate on the NDVI because it combines the information in the reflectance from the ground cover most meaningfully and illustrates the technique. Some spatial structure is evident: there is a patch of black in the North central part of the map, and there are patches of medium grey, pale grey and white elsewhere. In other places what might be a coarse patchiness is masked by short-range fluctuation. There is some slight striation from North to South, which we

M. OLIVER ET AL.

3.1. IDENTIFYING NESTED SPATIAL STRUCTURES

We computed experimental variograms for the separate wavebands and for the NDVI from the pixel values by the usual formula:

$$\hat{\gamma}(\mathbf{h}) = \frac{1}{2m(\mathbf{h})} \sum_{i=1}^{m(\mathbf{h})} \{z(\mathbf{x}_i) - z(\mathbf{x}_i + \mathbf{h})\}^2, \qquad (13)$$

where the $z(\mathbf{x}_i)$ and $z(\mathbf{x}_i + \mathbf{h})$ are the observed pixel values at $\mathbf{x}_i$ and $\mathbf{x}_i + \mathbf{h}$ separated by $\mathbf{h}$, and $m(\mathbf{h})$ is the number of pairs of pixels at that lag. None of the experimental variograms showed evidence of anisotropy, but they all seemed to be nested. The model that fitted them best in the least squares sense was a double exponential without nugget variance:

$$\gamma(h) = c_1\{1 - \exp(-h/a_1)\} + c_2\{1 - \exp(-h/a_2)\}, \qquad (14)$$

in which $h = |\mathbf{h}|$ is the lag in distance only, c_1 and c_2 are the sills of the short-range and long-range components respectively, and a_1 and a_2 are the corresponding distance parameters.

The values of the parameters for each waveband and NDVI are given in Table 1. Figure 2 shows the average variogram for NDVI and its decomposed form to illustrate the two components of the nested variation, i.e. the long- and short-range components. Their distance parameters are 5 and 56 pixels, which correspond to correlation ranges of approximately 15 and 170 pixels, i.e. 300 m and 3400 m.

TABLE 1. Variogram model parameters for the three channels and NDVI

Channel	c_1	c_2	a_1	a_2
	variance		pixels	
1	40.84	42.71	3.26	38.87
2	0.0262	0.0845	3.23	53.36
3	0.0115	0.0400	2.33	51.92
NDVI	0.00428	0.00725	5.06	55.80

The variograms for channels 2 and 3 are of the common logarithms of the digital numbers, that for channel 1 is for the digital numbers themselves.
The distance parameters of the variograms can be multiplied by 3 to obtain the approximate correlation ranges.

3.2. ORDINARY KRIGING

We applied ordinary kriging first to estimate the NDVI using the model in Table 1 and the pixel values. We kriged on to a square grid that was
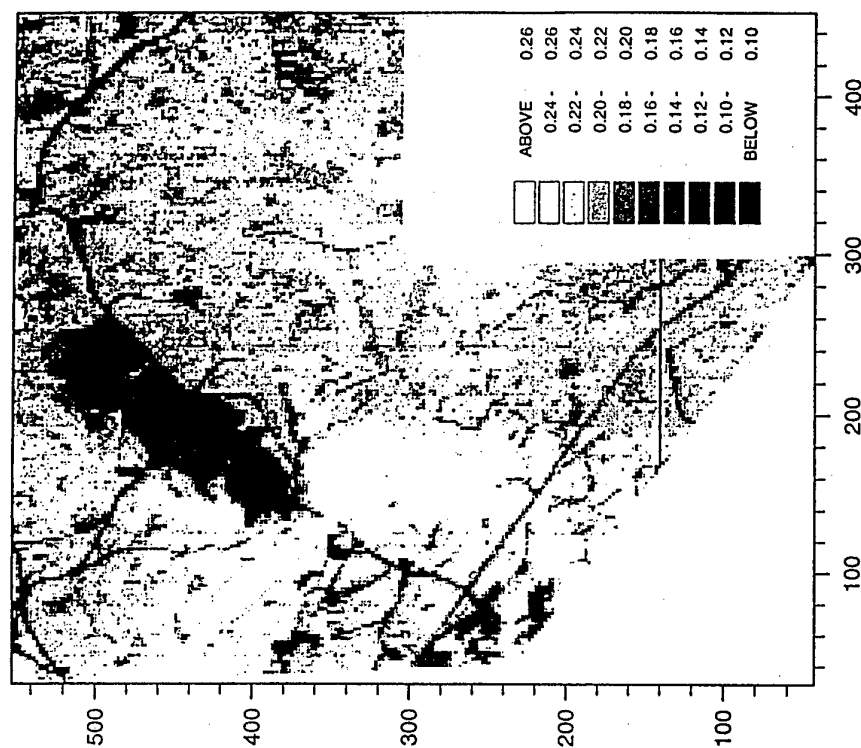
Figure 1. Pixel map of NDVI for part of Fort Benning

offset by 0.5 of a pixel in both the North–South and East–West dimensions; this avoided estimating at the pixels' centroids, which would have simply returned the pixel values. The result is shown in Figure 3 in which the 'contour' intervals are the same as in the pixel map (Figure 1). Comparison of the two maps shows that ordinary kriging has smoothed some of the local fluctuation. Nevertheless, the two scales of variation, the short-range
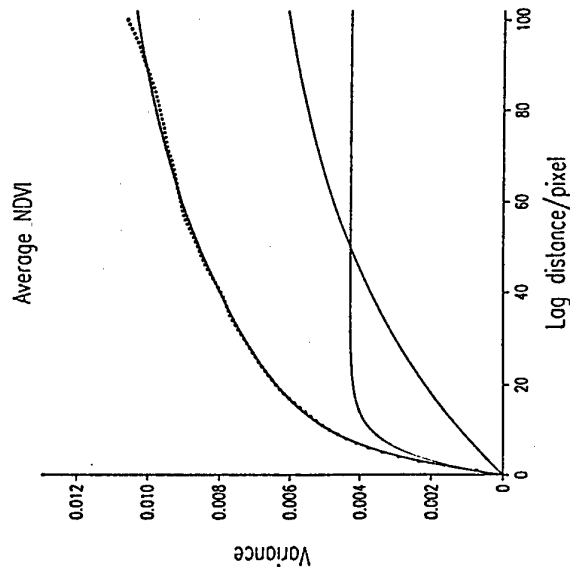
Figure 2. Experimental variogram (symbols) and the fitted model (solid line) of NDVI for the study area in Fort Benning. The variogram has also been decomposed into the long- and short-range components, and these are shown by the lower solid lines.

fluctuation nested inside that with the longer range, as represented in the variogram, are clearly visible. The longer range pattern seems to be largely that related to the physiography: white and pale grey areas are the low-lying poorly drained parts, and the darker grey ones are the uplands with better drainage. The black areas are those that reflected most light; they include the large area in the North central part of the map which has been cleared of vegetation.

3.3. KRIGING ANALYSIS

3.3.1. *Long-range variation*

When the long-range component is kriged separately by solving the system (7) with $k = 2$ and system (11) the broader structures become clearer, as in Figure 4. The short-range variation is filtered out as if it were noise, and the coarse pattern that remains shows the extent of the dominant classes of ground cover, such as evergreen woodland, mixed deciduous and evergreen woodland, and marsh. The pale grey and white areas on Figure 4 represent the wet land, and the intermediate and darker greys and black represent the drier land that reflects more light, as before. The striations
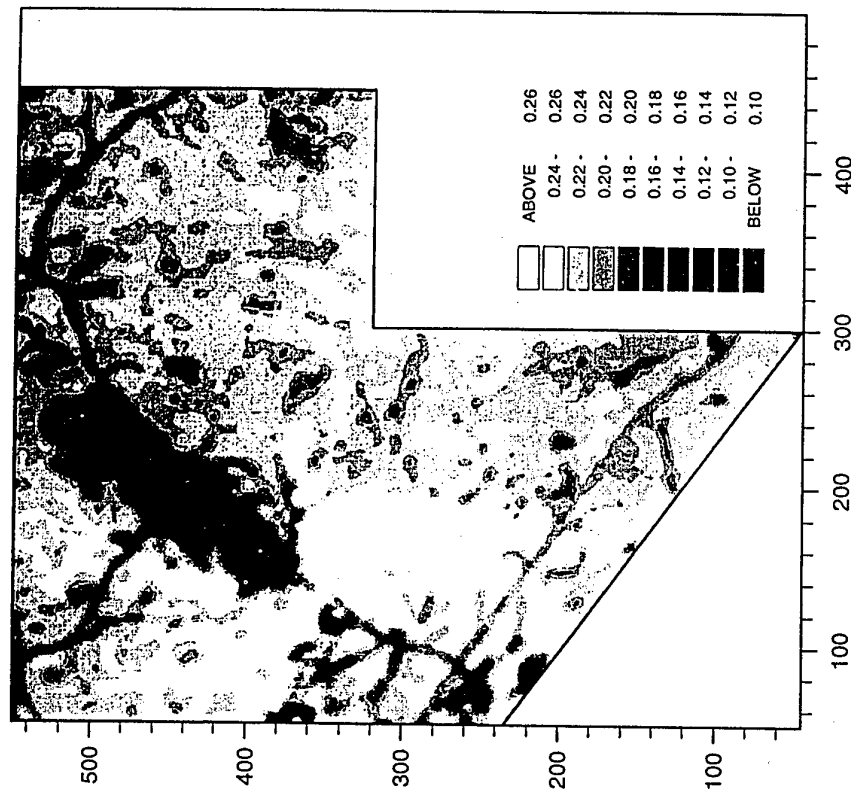
Figure 3. Map of ordinary kriged estimates of NDVI for part of Fort Benning

from North to South in the pixel map (Figure 1) still appear as a weak alignment in the pattern.

3.3.2. *Short-range variation*

The map of the short-range component, obtained by solving system (7) with $k = 1$, shows the local detail and the roads (Figure 5). The intricate

Figure 5. Map of short-range kriged estimates of NDVI after filtering for part of Fort Benning

them to the system of sensing on the SPOT.

4. Summary and conclusions

Kriging analysis of the NDVI in the SPOT image revealed variation on two distinct spatial scales. A short-range component, with an effective range of

Figure 4. Map of long-range kriged estimates of NDVI after filtering for part of Fort Benning

pattern seems to arise from a patchiness in the vegetation. The ground reconnaissance survey suggested changes in canopy, closure, species, height and stem diameter at this scale. McKenna Hill appears as the large black patch in Figure 3 with an intricate pattern associated with eroded gullies and soil deposited from them. The alignments from North to South are more evident in this map than in Figure 4, and as above, we attribute

about 300 m, that seems to derive from the variation in the local topography and its associated vegetation as assessed by ground survey. Kriging this component shows the intense pattern of variation. This scale of variation is less evident in the ordinary kriged map than the long-range component, suggesting that the latter obscured the short-range component which has the smaller variance. The scale of the long-range component is an order of magnitude greater with an effective range of 3.4 km. The latter is almost certainly determined by the gross physiography and the main elements of the vegetation associations: evergreen, deciduous, and mixed woodlands, and wetland.

5. Acknowledgement

6. References

Galli, A., Gerdil-Neuillet, F. and Dadou, C. (1984) Factorial kriging analysis: a substitute to spectral analysis of magnetic data. In: G. Verly, M. David, A. Journel and A. Marechal (eds), *Geostatistics for Natural Resources Characterization*, D. Reidel, Dordrecht, pp. 543–557.

Goovaerts, P. and Webster, R. (1994) Scale-dependent correlation between topsoil copper and cobalt concentrations in Scotland. *European Journal of Soil Science*, **45**, 79–95.

Jaquet, O. (1989) Factorial kriging analysis applied to geological data from petroleum exploration. *Mathematical Geology*, **21**, 683–691.

Matheron, G. (1982) *Pour une analyse krigeante de données régionalisées.* Note N-732, Centre de Géostatistique, Ecole des Mines de Paris, Fontainebleau.

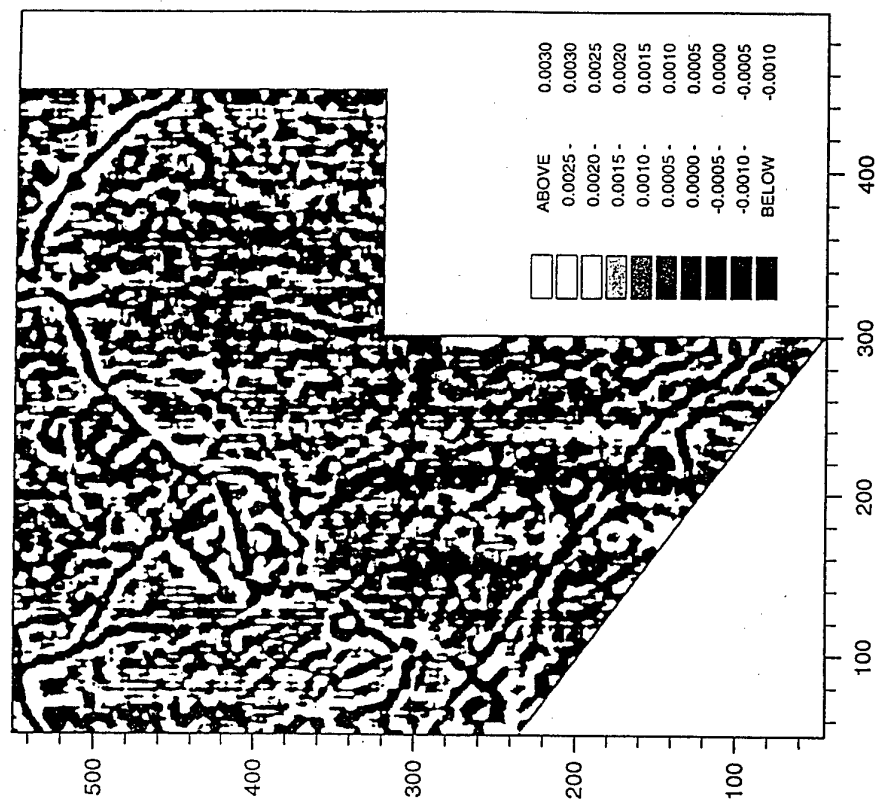Van Der Meer, F. (1993) Classification of high spectral resolution imagery using an indicator kriging based technique. In: A. Soares (ed.), *Geostatistics Tróia '92, Volume 2*, Kluwer Academic Publishers, Dordrecht, pp. 829–840.

Webster, R., Curran, P. J. and Munden, J. W. (1989) Spatial correlation in reflected radiation from the ground and its implications for sampling and mapping by ground-based radiometry. *Remote Sensing of Environment*, **29**, 67–78.

Wen, R. and Sinding-Larsen, R. (1997) Image filtering by factorial kriging—sensitivity analysis and application to Gloria side-scan sonar images. *Mathematical Geology*, **29**, 433–468.

Woodcock, C. E., Strahler, A. H. and Jupp, D. L. B. (1988) The use of variograms in remote sensing II. Real digital images. *Remote Sensing of Environment*, **25**, 349–379.

Appendix II

Wavelets and Kriging for Filtering and Data Reconstruction

M. A. OLIVER[1], E. BOSCH[2] and K. SLOCUM[2]

[1]*Department of Soil Science, The University of Reading, Whiteknights, Reading RG6 6DW, UK,*
[2]*US Topograhic Engineering Center, 7701 Telegraph Road, Alexandria, Virginia 22310-3864, U. S. A.*

Abstract

Wavelet analysis operates locally and can describe a wide range of frequencies simultaneously and filter them by multi-resolution analysis. Kriging analysis also filters spatial variation at different resolutions. We compare the effectiveness of wavelets and factorial kriging for exploring nested variation in a SPOT image. In addition both wavelets and kriging can be used to restore image data after compression. We compare the reliability of the restorations from the two approaches.

The near infrared (NIR) waveband of part of a SPOT image covering Fort A. P. Hill in Virginia was used for these analyses. The region is on the dissected Piedmont area of the eastern United States. An area of 128 by 128 pixels was selected from the scene for analysis. The experimental variogram was computed and modelled by a nested spherical function with correlation structures of about 6.5 pixels and 21 pixels. The variogram and factorial kriging separated the two main spatial features present. The low-frequency component from the wavelet analysis contained the spatial structure. The long-range component became evident as the resolution decreased. The high-frequency components removed only the uncorrelated variation and we could not retrieve the short-range component.

The image was sampled so that one in every four pixels was retained, one in every 16 and one in every 64. Using the variogram model for the full set of data values were estimated at the former data points by ordinary kriging. The low-frequency wavelet transform for these resolutions was inverted so that the missing values were restored. The restored values from both analyses were compared with the original values and the mean squared differences (MSD) computed. For all resolutions the MSD was smaller for the wavelet reconstruction. However, the MSD proved somewhat misleading when frequency distributions of the errors were compared. They suggested that wavelets are more able to deal with the local fluctuations present in the image and with local non-stationarity than kriging, but that for the majority of points the kriged estimates have a smaller error.

The paper will be illustrated with maps of the results, and we shall suggest improvements for restoring images by kriging.

```
◆C **** PROGRAM TO COMPUTE VARIOGRAMS FOR SQUARES OF VARIOUS SIZES
C
C **** R WEBSTER     ROTHAMSTED
C        Latest version 22 July 1999
C
C       This program was written as part of US project
C       and may be handed over to TEC.
C
C       Program reads data on a grid with X and Y coordinates
C          and converts them to an array for the selected variate
C          with implied coordinates.
C
C       It tiles the grid into non-overlapping squares of
C          given side.   Any points to the bottom or right
C          of the grid left over play no role.
C
        DIMENSION ZK(190,189), ZA(30), GRID(30,30)
C **** ZK( , ) will hold grid of data.
        character*72 TITLE(2)
        character*72 INFILE, OP12, IN11, FDAT
        data MAXROW, MAXCOL/190,189/
        data IN,INDAT,LP/10,11,12/
        PRINT * ,  'WHAT IS THE NAME OF THE STEERING FILE ?'
        READ (5,'(A)') INFILE
        OPEN (INDAT,FILE=INFILE,STATUS='OLD')
        print * , 'WHAT IS THE NAME OF THE DATA FILE ? '
        read (5,'(a)') IN11
        open (IN,file=IN11,status='OLD')
        PRINT *,'WHAT DO YOU WANT TO CALL THE MAIN OUTPUT FILE ?'
        READ (5,'(A)') OP12
        OPEN (LP,FILE=OP12,STATUS='NEW')
C        PRINT *,'WHAT DO YOU WANT TO CALL THE SECOND RESULTS FILE ?'
C        READ (5,'(A)') OP12
C        OPEN (LF8,FILE=OP12,STATUS='NEW')
        READ (INDAT,10) TITLE
        WRITE (LP,10) TITLE
C        WRITE (LF8,12) TITLE
    10 FORMAT (A)
        NVAR  = int(CYNPUT(INDAT)+0.1)
        NSEL  = int(CYNPUT(INDAT)+0.1)
        MSIDE = int(CYNPUT(INDAT)+0.1)
        MAXLAG= int(CYNPUT(INDAT)+0.1)
        ZMIS  = CYNPUT(INDAT)
        ILOG  = int(CYNPUT(INDAT)+0.1)
        if (ILOG.eq.1) SHIFT=CYNPUT(INDAT)
C ****  NVAR is number of variates in file.
C       NSEL is the one selected for analysis.
C       MSIDE is the side of the square within which
C                averages are computed.
C       MAXLAG is the maximum lag distance of variograms
C       ZMIS is the value used for missing or blank.
C       ILOG = 1 to transform to log to base 10.
C       SHIFT is a value to be added to data to shift the origin
C             before taking logarithms.
C **** Set data grid to blank
C       if (ILOG.eq.1) ZMIS=log10(ZMIS)
        do 20 I=1,MAXROW
          do 20 J=1,MAXCOL
              ZK(I,J)=ZMIS-10000.0
    20 continue
C
        read (INDAT,10) FDAT
C **** Read the data.
    35 NC=0
```

```
      NROW=0
      NCOL=0
 36 NC=NC+1
      read (IN,FDAT,end=45) ICOL, IROW, (ZA(J), J=1,NVAR)
      if (ICOL.gt.MAXCOL) then
          write (LP,38) ICOL
          stop
      endif
      if (IROW.gt.MAXROW) then
          write (LP,39) IROW
          stop
      endif
 38   format (/10x,'ICOL exceeds array bound'//)
 39   format (/10x,'IROW exceeds array bound'//)
      if (NROW.lt.IROW) NROW=IROW
      if (NCOL.lt.ICOL) NCOL=ICOL
      ZL=ZA(NSEL)
      if (ILOG.eq.1) then
          if (ZL.gt.0.01) then
              ZL=log10(ZL+SHIFT)
          else
              ZL=ZMIS-100000.0
          endif
      endif
      ZK(IROW,ICOL)=ZL
      goto 36
 45 continue
      NC=NC-1
      write (LP,47) NC, NROW, NCOL
 47   format(// 10x, 'Number of data       ',i10/
    1          10x, 'Number of rows       ',i10/
    2          10x, 'Number of columns    ',i10/)
      if (ILOG.eq.1) write (LP, 51) SHIFT
 51 format (/10x,'DATA TRANSFORMED TO LOG TO BASE 10'/
    1          10x,'SHIFT ',F10.3/)
      ZMAX=-99999999
      ZMIN=999999999
      NN=NC
      ZBAR=0.0
      SSQ=0.0
      COUNT=0.0
      do 54 I=1,NROW
          do 53 J=1,NCOL
              ZZ=ZK(I,J)
              if (ZZ.le.ZMIS) goto 53
                  if (ZMAX.lt.ZZ) ZMAX=ZZ
                  if (ZMIN.gt.ZZ) ZMIN=ZZ
                  DIF=ZZ-ZBAR
                  COUNT=COUNT+1.0
                  ZBAR=ZBAR+DIF/COUNT
                  SSQ=SSQ+(1.0-1.0/COUNT)*DIF*DIF
 53       continue
 54 CONTINUE
      A3=0.0
      do 57 I=1,NROW
          do 56 J=1,NCOL
              ZZ=ZK(I,J)
              if (ZZ.le.ZMIS) goto 56
                  A3=A3+(ZZ-ZBAR)**3
 56       continue
 57 CONTINUE
      A2=SSQ/COUNT
      A3=(A3/COUNT)/(A2*sqrt(A2))
      VAR=SSQ/(COUNT-1.0)
```

```fortran
      STD=sqrt(VAR)
      write (LP, 58) COUNT, ZMIN, ZMAX, ZBAR, VAR, STD, A3
   58 format (//,10X, ' Count               ',f10.1/
     1           10x, ' Minimum             ',f10.4/
     1           10x, ' Maximum             ',f10.4/
     1           10x, ' Mean                ',f10.4/
     2           10x, ' Variance            ',f12.6/
     3           10x, ' Standard deviation  ',f10.4/
     4           10x, ' Skewness            ',f10.4/)
C
C **** Compute starting in top left corner of grid.
      NTILER=int(NROW/MSIDE)
      NTILEC=int(NCOL/MSIDE)
C
      do 300 IR=1,NTILER
          IRS=(IR-1)*MSIDE+1
          IRE=IR*MSIDE
          do 300 IC=1,NTILEC
              ICS=(IC-1)*MSIDE+1
              ICE=IC*MSIDE
              II=0
              do 210 I=IRS,IRE
                  JJ=0
                  II=II+1
                  do 210 J=ICS,ICE
                      JJ=JJ+1
                      GRID(II,JJ)=ZK(I,J)
  210         continue
C **** Data are now transferred into array GRID( , ) covering
C.        a small square of side MSIDE.
C         Initialize accumulators.
      do 220 I=1,MAXLAG
          WLAG(I)=0.0
          GAM(I)=0.0
          WT(I)=0.0
          SUM=0.0
          SSQ=0.0
          COUNT=0.0
  220 continue
      do 225 I=1,MSIDE
          do 225 J=1,MSIDE
              ZZ=GRID(I,J)
              if (ZZ.lt.ZMIS) goto 225
              COUNT=COUNT+1.0
              DIF=ZZ-SUM
              SUM=SUM+DIF/COUNT
              SSQ=SSQ+(1.0-1.0/COUNT)*DIF*DIF
  225 continue
      SSQ=SSQ/(COUNT-1.0)
      SDV=sqrt(SSQ)
      write (LP, 227) IRS, ICS, SUM, SSQ, SDV
  227 format (//5X, 'CORDINATES      ', I6,I6/
     1          5X, 'MEAN            ', F12.5/
     2          5X, 'VARIANCE        ', F12.5/
     3          5X, 'ST. DEVIATION ', F12.5/)
      write (LP,230)
  230 format (/2x, 'LAG   ANGLE     SEMIVARIANCE     COUNT'/)
      do 255 I=1,MSIDE
          do 255 J=1,MSIDE
              Z1=GRID(I,J)
              if (Z1.lt.ZMIS) goto 255
              do 245 K=1,MSIDE
                  do 245 L=1,MSIDE
                      Z2=GRID(K,L)
```

```
                    if (Z2.lt.ZMIS) goto 245
                    X1=float(I)
                    X2=float(K)
                    Y1=float(J)
                    Y2=float(L)
                    D=sqrt((X1-X2)**2+(Y1-Y2)**2)
                    LAG=int(D)+1
                    WLAG(LAG)=WLAG(LAG)+D
                    GAM(LAG)=LAG(LAG)+(Z1-Z2)**2
                    WT(LAG)=WT(LAG)+1.0
     245          continue
     255  continue
          ANGLE=0.0
          do 270 I=1,MAXLAG
              WLAG(I)=WLAG(I)/WT(I)
              GAM(I)=0.5*GAM(I)/WT(I)
              write (LP,275) WLAG(I),ANGLE,GAM(I),WT(I)
     270  continue
     275  format (2x,f7.2,f6.2,f12.5,f10.1)
     300  continue
          stop
          end
C
          FUNCTION CYNPUT(IN)
C **** READS A REAL NUMBER FROM AN 80-BYTE RECORD IN FREE FORMAT
          DIMENSION K(80),NUM(10)
          DATA NUM/1H0,1H1,1H2,1H3,1H4,1H5,1H6,1H7,1H8,1H9/
          DATA INOLD,N,IFL,NPLUS,MINUS,NDOT/0,81,0,1H+,1H-,1H./
          CYNPUT=-0.0
          IF(INOLD.EQ.IN.AND. N.LE.80) GOTO 20
        5 IF(IFL.NE.0) RETURN
          INOLD=IN
          READ(IN,10) (K(I),I=1,80)
       10 FORMAT(80A1)
       15 N=1
       20 IF(N.GT.80) GOTO 35
          DO 30 I=N,80
             II=K(I)
             DO 25 J=1,10
                IF(II.EQ.NUM(J)) GOTO 40
       25    CONTINUE
             IF(II.EQ.MINUS) GOTO 40
             IF(II.EQ.NDOT) GOTO 40
             IF(II.EQ.NPLUS) GOTO 40
       30 CONTINUE
       35 GOTO 5
       40 SIGN=1.0
          IF(II.EQ.MINUS) SIGN=-1.0
          IF(II.EQ.MINUS .OR. II.EQ.NPLUS) I=I+1
          IF(I.GT.80) GOTO 60
          DO 55 N=I,80
             NN=K(N)
             IF(NN.EQ.NDOT)GOTO 70
             DO 45 J=1,10
                KK=J-1
                IF(NN.EQ.NUM(J)) GOTO 50
       45    CONTINUE
             GOTO 65
       50    CYNPUT=10.0*CYNPUT+KK
       55 CONTINUE
       60 N=82
       65 CYNPUT=SIGN*CYNPUT
          RETURN
       70 I=N+1
```

```
          TENS=1.0
          IF(I.GT.80) GOTO 90
          DO 85 N=I,80
            NN=K(N)
            DO 75 J=1,10
              KK=J-1
              IF(NN.EQ.NUM(J)) GOTO 80
  75      CONTINUE
          GOTO 65
  80      TENS=TENS*0.1
          CYNPUT=CYNPUT+TENS*KK
  85 CONTINUE
  90 N=82
     GOTO 65
     END
```
♦♦C **** PROGRAM TO COMPUTE MOVING VARIANCES FOR SQUARES
C   OF VARIOUS SIZES
C **** R WEBSTER   ROTHAMSTED
C   Latest version 22 July 1999
C
C
C   This program was written as part of US project
C   and may be handed over to TEC.
C
C   Program reads data on a grid with X and Y coordinates
C   and converts them to an array for the selected variate
C   with implied coordinates.
C
```
      DIMENSION ZK(190,189), ZA(30), VM(190,189), AM(190,189)
```
C **** ZK(,) will hold grid of data.
```
      character*72 TITLE(2)
      character*72 INFILE, OP12, IN11, FDAT
      data MAXROW, MAXCOL/190,189/
      data IN,INDAT,LP/10,11,12/
      PRINT * ,  'WHAT IS THE NAME OF THE STEERING FILE ?'
      READ (5,'(A)') INFILE
      OPEN (INDAT,FILE=INFILE,STATUS='OLD')
      print * , 'WHAT IS THE NAME OF THE DATA FILE ? '
      read (5,'(a)') IN11
      open (IN,file=IN11,status='OLD')
      PRINT *,'WHAT DO YOU WANT TO CALL THE MAIN OUTPUT FILE ?'
      READ (5,'(A)') OP12
      OPEN (LP,FILE=OP12,STATUS='NEW')
```
C   PRINT *,'WHAT DO YOU WANT TO CALL THE SECOND RESULTS FILE ?'
C   READ (5,'(A)') OP12
C   OPEN (LF8,FILE=OP12,STATUS='NEW')
```
      READ (INDAT,10) TITLE
      WRITE (LP,10) TITLE
```
C   WRITE (LF8,12) TITLE
```
  10 FORMAT (A)
      NVAR  = int(CYNPUT(INDAT)+0.1)
      NSEL  = int(CYNPUT(INDAT)+0.1)
      MSIDE = int(CYNPUT(INDAT)+0.1)
      ZMIS  = CYNPUT(INDAT)
      ILOG  = int(CYNPUT(INDAT)+0.1)
      if (ILOG.eq.1) SHIFT=CYNPUT(INDAT)
```
C **** NVAR is number of variates in file.
C   NSEL is the one selected for analysis.
C   MSIDE is the side of the square within which
C   averages are computed.
C   ZMIS is the value used for missing or blank.
C   ILOG = 1 to transform to log to base 10.
C   SHIFT is a value to be added to data to shift the origin
C   before taking logarithms.
C **** Set data grid to blank